

SLAC - 333
UC - 34D
(T)

THE APPLICATION OF LIGHT-CONE QUANTIZATION
TO QUANTUM CHROMODYNAMICS
IN ONE-PLUS-ONE DIMENSIONS

Kent John Hornbostel

Stanford Linear Accelerator Center
Stanford University
Stanford, California 94309

December 1988

Prepared for the Department of Energy
under contract number DE-AC03-76SF00515

Printed in the United States of America. Available from the National Technical Information Service, U.S. Department of Commerce, 5285 Port Royal Road, Springfield, Virginia 22161. Price: Printed Copy A08, Microfiche A01.

THE APPLICATION OF LIGHT-CONE QUANTIZATION
TO QUANTUM CHROMODYNAMICS
IN ONE-PLUS-ONE DIMENSIONS

Kent John Hornbostel, Ph.D.
Stanford University, 1989

Formal and computational aspects of light cone quantization are studied by application to quantum chromodynamics (QCD) in one spatial plus one temporal dimension. This quantization scheme, which has been extensively applied to perturbative calculations, is shown to provide an intuitively appealing and numerically tractable approach to non-perturbative computations as well.

In the initial section, a light-cone quantization procedure is developed which incorporates fields on the boundaries. This allows for the consistent treatment of massless fermions and the construction of explicitly conserved momentum and charge operators.

The next section, which comprises the majority of this work, focuses on the numerical solution of the light-cone Schrodinger equation for bound states. The state space is constructed and the Hamiltonian is evaluated and diagonalized by computer for arbitrary number of colors, baryon number and coupling constant strength. As a result, the full spectrum of mesons and baryons and their associated wavefunctions are determined. These results are compared with those which exist from other approaches to test the reliability of the method. The program also provides a preliminary test for the feasibility of, and an opportunity to develop approximation schemes for, an attack on three-plus-one dimensional QCD.

Finally, analytic results are presented which include a discussion of integral equations for wavefunctions and their endpoint behavior. Solutions for hadronic masses and wavefunctions in the limits of both large and small quark mass are discussed.

Acknowledgements

It is a pleasure to recognize those who have contributed their ideas and encouragement to this work, in particular, to Hans-Christian Pauli and Gary McCartor, and to acknowledge the hospitality of the Max Planck Institute for Nuclear Physics, where this work began. I would also like to thank Professors Sid Drell, Michael Peskin, and Lenny Susskind for serving on my orals committee, and Dick Blankenbecler for this as well as for his continuing interest in this work and his unerring advice. Thanks especially to my friends and co-laborers from the third floor night shift, past and present, who made SLAC the place to be when there was no place else to go. Finally, I would like to express my gratitude to my advisor, Stan Brodsky, for his freely shared time and expertise, and even more for his unparalleled combination of enthusiasm and patience.

For Mom and Dad, Scott and Marc

Table of Contents

	page
Introduction	1
Chapter 1. Quantization	
1.1 Light-Cone Quantization	3
1.2 Long Range Fields and Conserved Charges	5
1.3 Quantization of Free Fermions	8
1.4 Quantization of $SU(N)_{1+1}$	15
1.5 Discrete Hamiltonian, Momentum and Boost Operators	29
1.6 Lorentz and Parity Properties of Wavefunctions	36
1.7 Chiral Anomaly	41
Chapter 2. Numerical Results	
2.1 Overview of Program	45
2.2 Spectra	48
2.3 Quark-Antiquark Valence Wavefunctions	63
2.4 Structure Functions	65
2.5 Valence Structure Functions	66
2.6 General Wavefunction Results	68

2.7 Higher-Fock Wavefunctions	82
2.8 Higher-Fock Wavefunctions at Weak Coupling	86
2.9 A Preliminary Look at Renormalization	89

Chapter 3. Analytic Results

3.1 Valence Meson Integral Equations	91
3.2 Valence Baryon Integral Equations	96
3.3 Meson Wavefunction Endpoint Behavior	98
3.4 Baryon Wavefunction Endpoint Behavior	100
3.5 Estimating Numerical Errors	102
3.6 Estimate of Necessary Resolution	106
3.7 Higher-Fock Equations: Endpoints and Errors	110
3.8 Heavy Quark Limit for Mesons	118
3.9 Heavy Quark Limit for Baryons	123
3.10 Massless Mesons and Baryons at Strong Coupling	127
3.11 Excited Meson States at Strong Coupling	134
3.12 Hadron Masses at Small Quark Mass	138
3.13 Comparison with Results from Bosonization	141
3.14 Matrix Elements for Small Quark Mass	145
Conclusions	151

Appendix A. Matrix Elements and Color Contractions	152
Appendix B. Evaluation of Integral in Section 3.3	157
References	159

List of Figures

	page
1. Surfaces Used to Define Charges.	6
2. Development of $N = 3$ Spectrum with Increasing K ; Weak Coupling. . .	49
3. Development of Spectrum with Increasing K ; Strong Coupling.	50
4. Development of $N = 3$ Spectrum with Coupling Constant λ	52
5. Lightest Meson and Baryon Mass versus Quark Mass for $N = 2, 3$ and 4.	54
6. Comparison of Lightest Meson Mass for $N = 2, 3$ and 4 with Lattice Calculation for $N = 2$	57
7. Comparison of Lightest Meson Mass for $N = 2, 3$ and 4 with Large- N Meson.	59
8. Lightest Meson Mass for $SU(2)$ and $U(2)$	62
9. Wavefunctions for First Five $N = 3$ Mesons in Valence Approximation.	64
10. Structure Functions for the Lightest $N = 3$ Meson and Baryon.	67
11. Structure Functions for the Valence and Four-Quark $N = 3$ Meson Wavefunctions at Weak Coupling.	69
12. Structure Functions for the Valence and Five-Quark $N = 3$ Baryon Wavefunctions at Weak Coupling.	70
13. Structure Functions for the Valence and Eight-Quark $N = 3$ Two-Baryon Wavefunctions at Weak Coupling.	71

14. Structure Functions for the Valence and Four-Quark $N = 3$ Meson Wavefunctions at Strong Coupling.	73
15. Structure Functions for the Valence and Five-Quark $N = 3$ Baryon Wavefunctions at Strong Coupling.	74
16. Structure Functions for the Valence and Eight-Quark $N = 3$ Two-Baryon Wavefunctions at Strong Coupling.	72
17. Contribution to Lightest $N = 3$ Meson Structure Function from Four-Quark Wavefunction.	75
18. Contribution to Lightest $N = 3$ Baryon Structure Function.	77
19. Contribution to Lightest Meson Structure Function from the Four-Quark Wavefunction as a Function of N	78
20. Contribution to Lightest $U(N)$ Meson Structure Function from the Four-Quark Wavefunction as a Function of N	79
21. Comparison of Single Meson Four-Quark Higher-Fock Wavefunction with Wavefunction of a Pair of Valence Mesons.	81
22. Dependence of $N = 2$ Meson Higher-Fock Wavefunction on Momentum K	85
23. Momentum Splitting from $q\bar{q}$ to $q\bar{q}q\bar{q}$ Fock States in Meson.	87
24. Momentum Splitting in $SU(3)$ Baryons.	88
25. Running Coupling Constant Defined by Holding Fixed the $N = 2, B = 0$ Meson Mass to $M^2/m^2 = 6$	91
26. Numerical Approximation of Principal-Value-Regulated Integral.	103

27. Extrapolation Fit to $SU(2)$ Lightest Meson Mass.	108
28. Typical Diagrams which Contribute to the Integral Equation for $\phi_2(x)$	113
29. Terms in the Integral Equation for ϕ_4 which Contribute to the Leading Small- x Behavior.	115
30. Leading Terms in Large- N Limit for the ϕ_4 Integral Equation.	116
31. Comparison of Lightest Meson Mass for $N = 2, 3,$ and 4 with Nonrelativistic Solutions.	123
32. Integration Contour.	157

List of Tables

	page
1. Four Quark Interactions in Hamiltonian.	32
2. Diagonal Interactions.	33
3. N-Dependent Spectrum.	55
4. Ratio of First Excited State to Lightest State; $N = 2, B = 0$	56
5. Magnitude of Higher-Fock in $SU(2)$ Meson as a Function of N	80
6. Magnitude of Higher-Fock Component in Lightest $SU(2)$ Meson Versus m/g	84
7. Number of States in Fock Space as a Function of the Invariant Cutoff.	90
8. Estimate of K Needed for Numerical Accuracy as a Function of Coupling Constant.	107
9. Estimate of Excited Meson Spectrum at Strong Coupling.	137
10. Suppression of the Valence Wavefunction Due to the Presence of Higher-Fock Components.	143
11. Small Quark Mass (from Bosonization) and Large Quark Mass Limits for Ratio of Meson to Baryon Mass for N from 2 to 4.	144
12. Measured Ratio of Meson to Baryon Mass for $N = 3$ and 4.	145

INTRODUCTION^[1]

Quantum Chromodynamics (*QCD*), a field theory of strong interactions based on the gauge group $SU(3)$, potentially describes all of hadronic and nuclear physics in terms of quarks and gluons as fundamental degrees of freedom. The short-distance structure of this theory, probed in processes involving large transfers of momentum, is relatively well understood. In this region, *QCD* is asymptotically free, and the effective interaction strength diminishes with increasing momentum. As a result, perturbative calculations become possible, and thus far have provided the best opportunities for experimental confrontation and confirmation. However, the most significant and intrinsically nonperturbative aspects of the theory, its predictions for the spectrum and wavefunctions of hadrons, as well as the mechanisms for confinement and jet hadronization, remain unsolved.

Lattice gauge theory, in which the Feynman path integral is evaluated on a discrete spacetime grid, provides an appropriate tool for such calculations. For strong coupling, it provides an appealing description of confinement. Numerical results in general have been consistent with experiment, if qualitative, and there is little doubt their accuracy will improve with increasing computing power.

Nevertheless, there is certainly room for the development of other methods. In this work, the general nonperturbative approach to field theory, “Discretized Light-Cone Quantization (DLCQ)”, introduced by Pauli and Brodsky in Ref. [2] is applied to $SU(N)$ gauge theories in one space and one time ($1+1$) dimensions as an initial step in that direction. In addition to this numerical approach, analytic solutions in the limits of both strong and weak coupling are presented. Throughout,

the quarks are limited to one flavor, but several values of the number of colors, N , are included.

$SU(N)$ gauge theories restricted to $1 + 1$ dimensions possess certain special properties which should be mentioned for the sake of orientation. Because there are no transverse directions, the gluons are not dynamical, and (in $A^+ = 0$ gauge) their presence is felt only by the constraint equation they leave behind. Likewise the quarks carry no spin. The fermion field may be represented as a two-component spinor, and chirality for massless fermions identifies only the direction of motion. The coupling constant g carries the dimension of mass, so that the theory is superrenormalizable. Also, for one quark flavor of mass m , the relevant measure of coupling strength is g/m . Finally, the restriction to one spatial dimension produces confinement automatically, even for QED_{1+1} . The electric field is unable to spread out and the energy of a non-singlet state diverges as the length of the system.

In spite of these idiosyncrasies, these models possess certain qualities to commend their study, not the least being tractability. There are only so many opportunities to solve, albeit numerically, a confining field theory with arbitrary coupling from first principles. With solutions in hand, conceptual questions, points of principle, or approximation schemes for QCD which do not depend on the dimensionality of the model may be addressed. Also, these models provide a concrete example on which to test approximation schemes and numerical techniques which may prove useful for realistic problems, and a means to check those, such as the large- N expansion, already in use. Ultimately, though, the motivation for this study is negative. If these models cannot be solved, there is no hope for applying this method to QCD in $3 + 1$ dimensions.

1. QUANTIZATION

1.1. LIGHT-CONE QUANTIZATION

Quantization on the light-cone is formally similar to standard canonical equal-time quantization, but with a few technical differences which nevertheless make life much easier.^[3] Given a (Lorentz-invariant) Lagrangian $\mathcal{L}(x^\mu)$, a new variable $x^+ \equiv x^0 + x^3$ is defined to play the role of time, along with new spatial variables (in four dimensions), $x^- \equiv x^0 - x^3$ and $x_\perp \equiv (x^1, x^2)$.

In these coordinates, the non-zero elements of the metric tensor are

$$\begin{aligned}g^{+-} &= g^{-+} = 2 \\g_{+-} &= g_{-+} = \frac{1}{2} \\g^{ij} &= g_{ij} = -\delta^{ij},\end{aligned}\tag{1.1}$$

with i and j representing the (transverse) directions 1 and 2. Under longitudinal Lorentz boosts (that is, in the x^3 direction) x^+ and x^- transform as $\exp(\pm\alpha)x^\pm$. The quantization surface $x^+ = 0$ is preserved, accounting for some of the simplified Lorentz properties of this scheme. This is especially true in two dimensions, where only this boost is possible. Because the Hamiltonian P^- changes by only an overall scale, its eigenstates are Lorentz-invariant. Under parity transformations, however, x^+ and x^- are interchanged, and while parity will be conserved, its realization will not be as simple.

Independent degrees of freedom are identified by the equations of motion. These are initialized to satisfy canonical commutation relations at $x^+ = 0$, and

the creation and annihilation operators from their momentum space expansion define the Fock space. The momenta conjugate to x^- and x_\perp , P^+ and P_\perp respectively, are diagonal in this space and conserved by interactions. P^- acts as a Hamiltonian; in general it is complicated, dependent on the coupling constant, and it generates evolution in x^+ . Diagonalizing it is equivalent to solving the equations of motion.

The mass shell condition, $p^2 = m^2$, for individual quanta implies that $p^- = (m^2 + p_\perp^2)/p^+$, so that positive (light-cone) energy quanta must also carry positive p^+ . This seemingly innocent detail is actually a very good thing; the positivity of p^+ combined with its conservation is responsible in large part for the simplicity of this approach. First, x^+ -ordered perturbation theory becomes calculationaly viable because a large class of diagrams which appear in the time-ordered analogue vanish.^[4] These include any diagram containing a vertex in which quanta are created out of the vacuum; since all p^+ are positive, at such a vertex the total momentum cannot be conserved.

More importantly for the work described here, but by essentially the same reasoning, the perturbative vacuum is an eigenstate of the full, interacting Hamiltonian, with eigenvalue zero. Pairs of quanta cannot be produced which conserve p^+ .^[5] One very desirable feature of this remarkable fact is that not only is the ground state trivial, but also that all the quanta occurring in higher states are associated with meson and baryon wavefunctions rather than disconnected pieces of the vacuum.

Finally, it greatly simplifies the numerical work, especially in 1+1 dimensions.^[6] The system is quantized in a box of length L in the x^- direction with appropriate

boundary conditions so that momenta are discrete and Fock space states denumerable. For the fixed total momentum P^+ , the relevant dimensionless momentum will be $K = \frac{L}{2\pi}P^+$. To see how K restricts the space of states, consider $K = 3$, which must be partitioned among the quanta in each state. The only three possibilities are (3), (2, 1), and (1, 1, 1). Contrast this with equal-time Fock states of definite P^1 . For equivalent numerical momentum, partitions will include not only those enumerated above, but also (4, -1), (104, -101), (5, 5, 3, 1, -1, -10), and so on. To keep the number of states finite, an additional cutoff in momentum must be introduced, whereas this is not necessary in the light-cone case.

Not only does a fixed K act implicitly as a momentum cutoff, it also severely limits both the total number of states of definite momentum and the number of quanta in each individual state, as the example above demonstrates. K serves one more role. The continuum limit $L \rightarrow \infty$ is equivalent to $K \rightarrow \infty$ as the physical momentum P^+ remains fixed. The size of K determines the physical size of the system, or equivalently, the fineness of the momentum space grid.

1.2. LONG RANGE FIELDS AND CONSERVED CHARGES

It is common in field theories in one spatial dimension for fields to persist at large distances because of the lack of dimensions in which to spread. Among other consequences, it leads almost trivially to confinement for both QED and QCD , and to severe infrared divergences associated with massless scalars which prohibit Goldstone bosons.^[7] Even in four dimensions, because they single out one direction, axial gauges such as $A^3 = 0$ or $A^+ = 0$ also lead to persistent fields.^[8] As a result,

boundary terms may not be discarded arbitrarily, and must be taken into account during quantization, particularly in two dimensions.^[9,10]

Light-cone quantization introduces this problem even for free fermions; when massless, physical degrees of freedom live on the boundaries in x^- . This simple case in two dimensions will be discussed first in some detail, because it is simple and the necessary outcome is known, and because it leads to a framework for handling related problems in less trivial systems. The approach here will follow that of McCartor,^[11] who has applied it to quantize the massless Schwinger Model on the light-cone.

To cope with fields which may not diminish sufficiently at large distances to discard, the system may be studied in a box of length $2L$ in both x^- and x^+ directions. In this way, boundary terms may be explicitly incorporated.

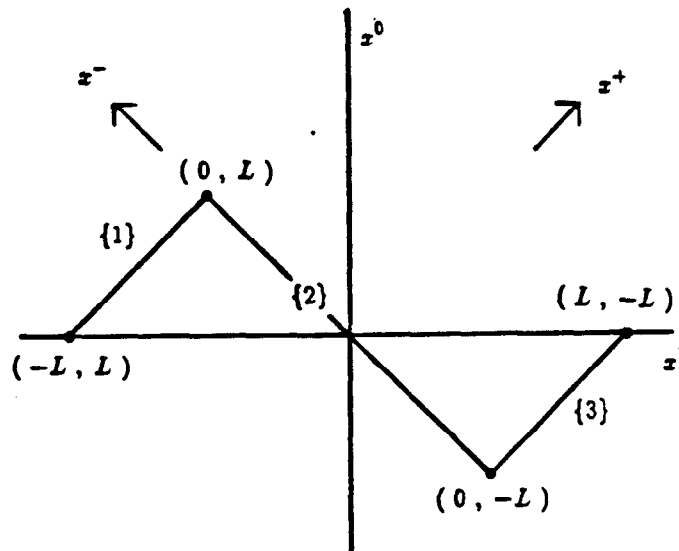


Figure 1. Surfaces Used to Define Charges.

The objective in quantizing a theory on the light cone is to cast it in terms of

convenient degrees of freedom while leaving intact its physical content. With this in mind, a time-independent charge Q derived from a conserved current j^μ which is conventionally defined on an initial surface $x^0 = 0$,

$$Q = \int_{-\sqrt{2}L}^{\sqrt{2}L} dx^1 j^0(0, x^1) \quad (1.2)$$

may be rewritten in terms of j^μ at $x^+ = 0$ provided that the flow through the boundaries {1} and {3} in Fig. 1 is accounted for:

$$Q = \frac{1}{2} \int_{-L}^L dy^- j^+(0, y^-) + \frac{1}{2} \int_{-L}^0 dy^+ j^-(y^+, L) + \frac{1}{2} \int_0^L dy^+ j^-(y^+, -L). \quad (1.3)$$

If the currents drop off sufficiently in x^- , this reduces to the more usual light-cone definition; this will not always be the case. The charge $Q(x^+)$ at an arbitrary x^+ , provided that it is defined by integrating on a surface extended to the $x^0 = 0$ axis, will be independent of x^μ and equivalent to Q defined as in Eq. (1.2). Specifically,

$$Q(x^+) = \frac{1}{2} \int_{-L}^L dy^- j^+(x^+, y^-) + \frac{1}{2} \int_{-L}^{x^+} dy^+ j^-(y^+, L) + \frac{1}{2} \int_{x^+}^L dy^+ j^-(y^+, -L). \quad (1.4)$$

satisfies $\partial_+ Q(x^+) = 0$ identically by $\partial_\mu j^\mu = 0$; the x^+ derivatives of the last two terms explicitly cancel the surface terms from the first.

With this prescription, the conserved momenta P^μ in terms of the energy-momentum tensor $\Theta^{\mu\nu}$ defined at $x^+ = 0$ are then

$$P^\mu = \frac{1}{2} \int_{-L}^L dy^- \Theta^{+\mu}(0, y^-) + \frac{1}{2} \int_{-L}^0 dy^+ \Theta^{-\mu}(y^+, L) + \frac{1}{2} \int_0^L dy^+ \Theta^{-\mu}(y^+, -L). \quad (1.5)$$

1.3. QUANTIZATION OF FREE FERMIONS

The Lagrangian density for free fermions,

$$\mathcal{L} = \bar{\psi}(\frac{1}{2}i\overleftrightarrow{\not{\partial}} - m)\psi, \quad (1.6)$$

in two dimensions and light-cone coordinates and explicitly in terms of left and right spinor components is

$$\mathcal{L} = \psi_L^\dagger i\overleftrightarrow{\partial}_- \psi_L + \psi_R^\dagger i\overleftrightarrow{\partial}_+ \psi_R - m(\psi_L^\dagger \psi_R + \psi_R^\dagger \psi_L). \quad (1.7)$$

The corresponding equations of motion are

$$i\partial_+ \psi_R = \frac{m}{2} \psi_L \quad (1.8)$$

$$i\partial_- \psi_L = \frac{m}{2} \psi_R \quad (1.9)$$

and both components satisfy

$$(\partial^2 + m^2)\psi_{L,R} = 0. \quad (1.10)$$

In standard light-cone quantization, independent fields are specified at $x^+ = 0$. However, $x^+ = 0$ (as well as $x^- = 0$) is a characteristic surface of the wave equation; as such, it is not in general possible to specify adequate initial conditions (or commutation relations to quantize them) on $x^+ = 0$ alone. See, for example, Refs. [12] to [14]. For the specific case when $m = 0$, ψ_L becomes a function of x^+ alone, and initial conditions must be given on a surface (that is, a line in two dimensions) at no point tangent to lines of constant x^+ , such as the surface $x^- = 0$.

To quantize this system in a way which incorporates the $m = 0$ case naturally and also takes advantage of the surfaces in Fig. 1 on which charges are defined, the system is confined to a box of length $2L$ in x^+ and x^- . By using Eqs. (1.8) and (1.9), it is simple to identify which fields are independent; that is, which initial conditions are appropriate. Suppose that ψ_R is specified along surface {2} at $x^+ = 0$. On this surface, Eq. (1.9) is a constraint. By fixing ψ_L at one point on this surface, at $(0, -L)$ for example, ψ_L may be determined along it by integration. Now that both ψ_R and ψ_L are known on {2}, Eq. (1.8) may be used to evolve ψ_R to the surface $x^+ = 0 + \Delta x^+$. Again, fixing ψ_L at an intersecting point on surface {3} allows ψ_L to be integrated out along $x^+ = \Delta x^+$ by Eq. (1.9), and so on. It is sufficient by construction then to specify ψ_R on $x^+ = 0$ and ψ_L on surfaces {1} and {3} (or alternatively on $x^- = 0$) to fully determine the solutions throughout the box. To quantize, the conjugate momenta which generate evolution off of these surfaces,

$$\pi_R = \frac{\delta \mathcal{L}}{\delta(\partial_+ \psi_R)} = i\psi_R^\dagger \quad (1.11)$$

on surface {2}, and

$$\pi_L = \frac{\delta \mathcal{L}}{\delta(\partial_- \psi_L)} = i\psi_L^\dagger \quad (1.12)$$

on {1} and {3} are assigned commutation relations

$$\{\pi_R(x^-), \psi_R(y^-)\} = -i\delta(x^- - y^-) \quad (1.13)$$

and

$$\{\pi_L(x^+), \psi_L(y^+)\} = -i\delta(x^+ - y^+). \quad (1.14)$$

To realize Eq. (1.13) on $x^+ = 0$, ψ_R may be expanded in normal modes after

imposing appropriate boundary conditions. Periodic boundary conditions require a state of momentum $k^+ = 0$, where k^+ is conjugate to x^- , for completeness, but such a state cannot be a solution of the free equation of motion $k^+k^- = m^2$ unless $m^2 = 0$. However, antisymmetric boundary conditions allow ψ_R to be expanded in a set of such solutions which is also complete.^[15] Then

$$\psi_R(0, x^-) = \frac{1}{\sqrt{2L}} \sum_{n=\frac{1}{2}, \frac{3}{2}, \dots}^{\infty} \left(b_n e^{-i\frac{n\pi}{L}x^-} + d_n^\dagger e^{i\frac{n\pi}{L}x^-} \right). \quad (1.15)$$

with anticommutation relations

$$\{b_n, b_m^\dagger\} = \{d_n, d_m^\dagger\} = \delta_{n,m}; \quad (1.16)$$

the remaining anticommutators are zero.

To treat ψ_L and ψ_R symmetrically, ψ_L is expanded on {1} and {3} such that

$$\psi_L(x^+, \pm L) = \frac{1}{\sqrt{2L}} \sum_{n=\frac{1}{2}, \frac{3}{2}, \dots}^{\infty} \left(\tilde{b}_n e^{-i\frac{n\pi}{L}x^+} + \tilde{d}_n^\dagger e^{i\frac{n\pi}{L}x^+} \right), \quad (1.17)$$

for which the argument x^- is $+L$ for $x^+ < 0$, $-L$ for $x^+ > 0$. The operators \tilde{b} and \tilde{d} and their adjoints satisfy similar anticommutation relations, but commute with b and d because they represent independent degrees of freedom.

The energy-momentum tensor for free fermions,

$$\Theta^{\mu\nu} = \frac{1}{4} \bar{\psi} \left(i\overleftrightarrow{\partial}^\mu \gamma^\nu + i\overleftrightarrow{\partial}^\nu \gamma^\mu \right) \psi - g^{\mu\nu} \mathcal{L} \quad (1.18)$$

has components

$$\begin{aligned}
\Theta^{++} &= 2\psi_R^\dagger i\overleftrightarrow{\partial}_- \psi_R \\
\Theta^{--} &= 2\psi_L^\dagger i\overleftrightarrow{\partial}_+ \psi_L \\
\Theta^{-+} &= \Theta^{+-} = m \left(\psi_L^\dagger \psi_R + \psi_R^\dagger \psi_L \right).
\end{aligned} \tag{1.19}$$

The evolution operators are then, by Eq. (1.5)

$$\begin{aligned}
P^+ &= \int_{\{2\}} dx^- \psi_R^\dagger i\overleftrightarrow{\partial}_- \psi_R + \frac{1}{2} m \int_{\{1\}+\{3\}} dx^+ \left(\psi_L^\dagger \psi_R + \psi_R^\dagger \psi_L \right) \\
P^- &= \frac{1}{2} m \int_{\{2\}} dx^- \left(\psi_L^\dagger \psi_R + \psi_R^\dagger \psi_L \right) + \int_{\{1\}+\{3\}} dx^+ \psi_L^\dagger i\overleftrightarrow{\partial}_+ \psi_L.
\end{aligned} \tag{1.20}$$

For the special case where $m = 0$, substitution of Eq. (1.15) into

$$P^+ = \int_{-L}^L dx^- \psi_R^\dagger i\overleftrightarrow{\partial}_- \psi_R \Big|_{(x^+=0)} \tag{1.21}$$

gives

$$P^+ = \sum_{n=\frac{1}{2}, \frac{3}{2}, \dots}^{\infty} \left(\frac{2\pi n}{L} \right) \left(b_n^\dagger b_n + d_n^\dagger d_n - 1 \right); \tag{1.22}$$

the divergent vacuum momentum may be discarded. Because ψ_L is expanded in Eq. (1.17) in deliberate analogy to ψ_R ,

$$P^- = \int_{-L}^0 dx^+ \psi_L^\dagger i\overleftrightarrow{\partial}_+ \psi_L(x^+, L) + \int_0^L dx^+ \psi_L^\dagger i\overleftrightarrow{\partial}_+ \psi_L(x^+, -L) \tag{1.23}$$

produces

$$P^- = \sum_{n=\frac{1}{2}, \frac{3}{2}, \dots}^{\infty} \left(\frac{2\pi n}{L} \right) (\tilde{b}_n^\dagger \tilde{b}_n + \tilde{d}_n^\dagger \tilde{d}_n - 1). \quad (1.24)$$

Because the untilded and tilded operators anticommute, states composed of the former have $P^- = 0$, while the latter satisfy $P^+ = 0$. Clearly then the b_n^\dagger and d_n^\dagger create massless, right-moving particles of equal-time momentum

$$P^1 = \frac{1}{2} (P^+ - P^-) = \frac{1}{2} P^+ = \frac{\pi n}{L} \quad (1.25)$$

and energy

$$P^0 = \frac{1}{2} (P^+ + P^-) = \frac{1}{2} P^+ = \frac{\pi n}{L}, \quad (1.26)$$

while the \tilde{b}_n^\dagger and \tilde{d}_n^\dagger have

$$P^1 = -\frac{1}{2} P^- = -\frac{\pi n}{L} \quad (1.27)$$

and

$$P^0 = \frac{1}{2} P^- = \frac{\pi n}{L} \quad (1.28)$$

and are left-moving. Also, the vacuum values subtracted correspond to

$$\begin{aligned} \langle P^0 \rangle &= \frac{1}{2} \langle P^+ \rangle + \frac{1}{2} \langle P^- \rangle = - \sum \left(\frac{2\pi n}{L} \right) \\ \langle P^1 \rangle &= \frac{1}{2} \langle P^+ \rangle - \frac{1}{2} \langle P^- \rangle = 0; \end{aligned} \quad (1.29)$$

as usual, only the energy P^0 requires a subtraction. The degrees of freedom and physical interpretation of the usual equal-time quantization have been preserved;

specifically, both left- and right-moving massless fermions have been retained. This is particularly important when defining the vector and axial vector currents

$$j^\mu = : \bar{\psi} \gamma^\mu \psi : \quad \text{and} \quad j_5^\mu = : \bar{\psi} \gamma^5 \gamma^\mu \psi : \quad (1.30)$$

with components

$$j_{(5)}^+ = 2 : \psi_R^\dagger \psi_R : \quad \text{and} \quad j_{(5)}^- = (-)2 : \psi_R^\dagger \psi_R : \quad (1.31)$$

Their corresponding charges are

$$Q_{(5)} = \frac{1}{2} \int_{-L}^L dx^- j_{(5)}^+(0, x^-) + \frac{1}{2} \int_{-L}^0 dx^+ j_{(5)}^-(x^+, L) + \frac{1}{2} \int_0^L dx^+ j_{(5)}^-(x^+, -L). \quad (1.32)$$

Note that if the ψ_L degrees of freedom were not retained, j^μ and j_5^μ would be indistinguishable. In momentum space,

$$Q_{(5)} = \sum_{n=\frac{1}{2}, \frac{3}{2}, \dots}^{\infty} \left(b_n^\dagger b_n - d_n^\dagger d_n \right) \binom{+}{-} \left(b_{-n}^\dagger b_{-n} - d_{-n}^\dagger d_{-n} \right) \quad (1.33)$$

where the left-moving \tilde{b}_n and \tilde{d}_n have been re-written as b_{-n} and d_{-n} .

When the fermion mass is not identically zero, then in P^- , for example, from Eq. (1.20), there is an additional term proportional to m which requires both ψ_R and ψ_L along the contour. On the surface $x^+ = 0$, where ψ_R is specified, ψ_L may be determined by Eq. (1.9). The most general solution is

$$\psi_L(0, x^-) = -\frac{im}{4} \int_{-L}^L dy^- \epsilon(x^- - y^-) \psi_R(0, y^-) + \frac{1}{2} [\psi_L(0, L) + \psi_L(0, -L)]. \quad (1.34)$$

The last boundary term depends on conditions chosen on the surfaces perpendicular to $x^+ = 0$ and is independent of ψ_R . Eq. (1.34) is true independent of discretization,

and the boundary term is essential so that $\psi_L(x^-)$ transforms correctly under symmetry transformations such as Lorentz boosts.

Substitution into the mass term in Eq. (1.20) for P^- gives, from the term with ψ_R in Eq. (1.34), the usual light-cone energy

$$\sum_{n=\frac{1}{2}, \frac{3}{2}, \dots}^{\infty} \left(\frac{m^2}{p_n^+} \right) (b_n^\dagger b_n + d_n^\dagger d_n) + \text{const.} \quad (1.35)$$

with $p_n^+ \equiv 2\pi n/L$. The boundary term contributes

$$\frac{m}{2} \left[\int_{-L}^L dx^- \psi_R^\dagger(0, x^-) \right] \frac{1}{2} [\psi_L(0, L) + \psi_L(0, -L)] + \text{conj.} \quad (1.36)$$

or in momentum space,

$$\frac{m}{2\pi} \sum_n \frac{(-1)^n}{n} (b_n^\dagger + d_n) \sum_\ell (\tilde{b}_\ell^\dagger + \tilde{d}_\ell) + \text{conj.} \quad (1.37)$$

For finite L , this represents a well-defined interaction between the formerly massless left- and right-moving quanta. However, in the continuum limit the integral over ψ_R (or the sum over n) reduces to a term proportional to $b_0^\dagger + d_0$, which contributes infinity from the factor m^2/p^+ in Eq. (1.35). Therefore, from this term, all of the \tilde{b} and \tilde{d} couple to states which contain b_0 or d_0 , with $P^+ = 0$ and $P^- = \infty$.

An analogous result is obtained for the operator P^+ , but with plus and minus, and tilded and untilded operators reversed. In the continuum limit for massive fermions, then, the Poincare algebra must be built either on the tilded or untilded operators. The two are related by parity, but separated by an infinite energy barrier, and the choice determines whether $x^+ = \text{constant}$ or $x^- = \text{constant}$ is

treated as the usual light-cone quantization surface. It is at this point, then, that the well-known phenomenon occurs in which light-cone quantization removes half of the fermionic degrees of freedom. Apparently, this is only appropriate for massive fermions.

The final result is physically sensible. In the continuum limit, the surface $x^+ = 0$ is inadequate for specifying initial conditions for massless particles because left-moving particles can run parallel to it; conditions on a surface such as $x^- = 0$ must also be specified. When massive, however, any particle with finite momentum will intercept this surface at some point. For extremely energetic particles, however, this point may be very far away in x^- , so this statement is only true if the length $2L$ of x^- included is infinite. In fact, it may be shown explicitly that the surface $x^+ = 0$ is sufficient to specify solutions to the massive wave equation by mapping these solutions onto those completely specified on a space-like surface, such as $x^0 = 0$.

Because the goal of this numerical work is to obtain continuum limit solutions, the fermion masses will be kept finite, terms such as that in Eq. (1.37) will be explicitly excluded, and massless fermions will be considered as a limit.

1.4. QUANTIZATION OF $SU(N)_{1+1}$

An $SU(N)$ gauge theory is defined by the Lagrangian

$$\mathcal{L} = -\frac{1}{4} F^{\mu\nu a} F_{\mu\nu}^a + \bar{\psi}(i\not{D} - m)\psi. \quad (1.38)$$

$F_{\mu\nu}^a$ is the field strength tensor

$$F_{\mu\nu}^a = \partial_\mu A_\nu^a - \partial_\nu A_\mu^a - gf^{abc} A_\mu^b A_\nu^c \quad (1.39)$$

and the covariant derivative is defined as

$$iD_\mu = i\partial_\mu - gA_\mu^a T^a. \quad (1.40)$$

Operator ordering is potentially important; for example, the fields A_μ^a will not commute after quantization, and in expressions such as Eq. (1.39) should be considered as appropriately symmetrized.

The gauge group generators satisfy

$$[T^a, T^b] = if^{abc} T^c \quad (1.41)$$

and are normalized such that

$$\text{Tr } T^a T^b = \frac{1}{2} \delta^{ab}; \quad (1.42)$$

the structure constants f^{abc} are fully antisymmetric. The completeness relation

$$[T^a]_j^i [T^a]_\ell^k = \frac{1}{2N} \left(N\delta_j^k \delta_\ell^i - \delta_j^i \delta_\ell^k \right) \quad (1.43)$$

will be useful when constructing the Hamiltonian. The second term on the right is a result of the tracelessness of the generators, and is not present for the gauge group $U(N)$.

In two dimensions, the fermion field (in a representation in which γ^5 is diagonal)

$$\psi = \begin{pmatrix} \psi_L(x)_c \\ \psi_R(x)_c \end{pmatrix} \quad (1.44)$$

is a two-component spinor in the fundamental representation. L and R indicate chirality, which, for massless fermions specifies only direction. In that case, ψ_L

is a function of only x^+ , ψ_R of x^- . The chiral γ matrix representation is used throughout. Explicitly,

$$\begin{aligned} \gamma^0 &= \begin{pmatrix} 0 & 1 \\ 1 & 0 \end{pmatrix} & \gamma^1 &= \begin{pmatrix} 0 & 1 \\ -1 & 0 \end{pmatrix} & \gamma^5 &= \begin{pmatrix} -1 & 0 \\ 0 & 1 \end{pmatrix} \\ \gamma^+ &= \begin{pmatrix} 0 & 2 \\ 0 & 0 \end{pmatrix} & \gamma^- &= \begin{pmatrix} 0 & 0 \\ 2 & 0 \end{pmatrix} \end{aligned} \tag{1.45}$$

with the chiral projection operators

$$\begin{aligned} \frac{1}{2}(1 - \gamma^5) &= \frac{1}{4}\gamma^+\gamma^- = \begin{pmatrix} 1 & 0 \\ 0 & 0 \end{pmatrix} \\ \frac{1}{2}(1 + \gamma^5) &= \frac{1}{4}\gamma^-\gamma^+ = \begin{pmatrix} 0 & 0 \\ 0 & 1 \end{pmatrix}. \end{aligned} \tag{1.46}$$

As usual,

$$\{\gamma^\mu, \gamma^\nu\} = 2g^{\mu\nu}. \tag{1.47}$$

A useful gauge choice is $A^{+a} = 0$. As is generally the case for axial gauges, there are neither ghosts nor negatively normed gauge bosons, so the Fock space quanta, and therefore the wavefunction constituents are physical and positively normed. In particular, these gauges allow constraint equations to be solved for explicitly at the Lagrangian level, so that only physical degrees of freedom are quantized and appear in the Hamiltonian and space of states. Also, in 1 + 1 dimensions, this gauge choice is Lorentz (but not parity) invariant.

The equations of motion are then

$$i\partial_- \psi_L = \frac{1}{2} m \psi_R \quad (1.48)$$

$$-\partial_-^2 A^{-a} = g \psi_R^\dagger T^a \psi_R \quad (1.49)$$

$$i\partial_+ \psi_R = \frac{1}{2} g A^{-a} T^a \psi_R + \frac{1}{2} m \psi_L \quad (1.50)$$

$$\partial_+ \partial_- A^{-a} = g \psi_L^\dagger T^a \psi_L - \frac{1}{2} g f^{abc} \partial_- A^{-b} A^{-c}. \quad (1.51)$$

Here and throughout, when not shown, color indices on the fermion fields are implied. As was the case with free fermions, it is important that all real degrees of freedom are identified, and in particular, that those associated with boundary terms are not discarded. This is necessary in axial gauges even for equal-time quantization and in four dimensions.^[9,10,16,17,8]

To quantize $SU(N)_{1+1}$, charges will again be defined to account for boundary terms and will be explicitly conserved. As discussed in Refs. [10] and [8], boundary terms for the gauge field appear which cannot be made to vanish at infinity, and which are related to the residual gauge symmetry under x^- -independent transformation.

In this gauge, the Lagrangian reduces to

$$\begin{aligned} \mathcal{L} = & \frac{1}{2} (\partial_- A^{-a})^2 - g \psi_R^\dagger A^{-a} T^a \psi_R \\ & + \psi_L^\dagger \overleftrightarrow{\partial}_- \psi_L + \psi_R^\dagger \overleftrightarrow{\partial}_+ \psi_R - m (\psi_R^\dagger \psi_L + \psi_L^\dagger \psi_R), \end{aligned} \quad (1.52)$$

while the elements of the energy-momentum tensor become

$$\begin{aligned}
\Theta^{++} &= 2\psi_R^\dagger i \overleftrightarrow{\partial}_- \psi_R \\
\Theta^{--} &= 2\psi_L^\dagger i \overleftrightarrow{\partial}_+ \psi_L - 2g\psi_L^\dagger A^{-a} T^a \psi_L \\
\Theta^{-+} &= \Theta^{+-} = (\partial_- A^{-a})^2 - m \left(\psi_R^\dagger \psi_L + \psi_L^\dagger \psi_R \right).
\end{aligned} \tag{1.53}$$

Also,

$$\begin{aligned}
j^{+a} &= 2g\psi_R^\dagger T^a \psi_R \\
j^{-a} &= 2g\psi_L^\dagger T^a \psi_L - gf^{abc} \partial_- A^{-b} A^{-c}
\end{aligned} \tag{1.54}$$

are the conserved currents associated with global gauge transformations.

The generators P^+ and P^- will be constructed in the same way as for free fermions, using Eq. (1.5). Because they are explicitly independent of x^+ , they may be defined at $x^+ = 0$, along the contours in Fig. 1. Including gauge fields,

$$\begin{aligned}
P^+ &= \int_{-L}^L dy^- \psi_R^\dagger i \overleftrightarrow{\partial}_- \psi_R \\
&+ \int_{-L}^L dy^+ \left[\frac{1}{2} (\partial_- A^{-a})^2 + \frac{m}{2} \left(\psi_R^\dagger \psi_L + \psi_L^\dagger \psi_R \right) \right]
\end{aligned} \tag{1.55}$$

and

$$\begin{aligned}
P^- &= \int_{-L}^L dy^- \left[\frac{1}{2} (\partial_- A^{-a})^2 + \frac{m}{2} \left(\psi_R^\dagger \psi_L + \psi_L^\dagger \psi_R \right) \right] \\
&+ \int_{-L}^L dy^+ \left[\psi_L^\dagger i \overleftrightarrow{\partial}_+ \psi_L - g\psi_L^\dagger A^{-a} T^a \psi_L \right].
\end{aligned} \tag{1.56}$$

The integrals over y^+ are to be understood as over contours {1} and {3} in Fig. 1

throughout this discussion. In order to quantize, the degrees of freedom may be determined from the equations of motion, Eqs. (1.48) to (1.51).

Again, consider the system in a box of length $2L$ in x^+ and x^- . Specifying ψ_R along $x^+ = 0$ allows ψ_L , A^{-a} and $\partial_- A^{-a}$ to be determined from Eqs. (1.48) and (1.49), which are constraint equations on this surface, provided that they are specified at one point; for example, at $(x^+ = 0, x^- = -L)$. Knowing these along $x^+ = 0$, Eq. (1.50) gives the evolution of ψ_R to the next $x^+ + \Delta x^+$ surface.

Within this box, then, it is sufficient to specify ψ_R at $x^+ = 0$ (that is, surface {2} of Fig. 1), and A^{-a} , $\partial_- A^{-a}$ and ψ_L on surfaces {1} and {3}; these are then the independent degrees of freedom.

Two comments are warranted. First, differentiating Eq. (1.51) with respect to x^- shows it to be consistent with Eqs. (1.48) to (1.50), but only up to a boundary term independent of x^- . Second, setting $A^{+a} = 0$ does not completely fix the gauge, as any x^- -independent gauge transformations preserve $A^{+a} = 0$. This residual freedom may be used to fix A^{-a} on one boundary.^[18,10,6] On the other boundary, A^{-a} would then be given in terms of other physical quantities. It will prove advantageous, however, to expand the phase space to include A^{-a} as a physical degree of freedom, and to eliminate it at later stage.

On surfaces of constant x^+ , Eqs. (1.48) and (1.49) are constraint equations and may be solved explicitly:

$$\begin{aligned} \psi_L(x) = & -\frac{im}{4} \int_{-L}^L dy^- \epsilon(x^- - y^-) \psi_R(x^+, y^-) \\ & + \frac{1}{2} [\psi_L(x^+, L) + \psi_L(x^+, -L)] \end{aligned} \quad (1.57)$$

$$\begin{aligned} \partial_- A^{-a}(x) = & -\frac{g}{2} \int_{-L}^L dy^- \epsilon(x^- - y^-) \psi_R^\dagger T^a \psi_R(x^+, y^-) \\ & + \frac{1}{2} [\partial_- A^{-a}(x^+, L) + \partial_- A^{-a}(x^+, -L)] \end{aligned} \quad (1.58)$$

and

$$\begin{aligned} A^{-a}(x) = & -\frac{g}{2} \int_{-L}^L dy^- |x^- - y^-| \psi_R^\dagger T^a \psi_R(x^+, y^-) \\ & + \frac{1}{2} x^- [\partial_- A^{-a}(x^+, L) + \partial_- A^{-a}(x^+, -L)] \\ & + \frac{1}{2} L Q_R^{a(0)}(x^+) + \frac{1}{2} [A^{-a}(x^+, L) + A^{-a}(x^+, -L)] \end{aligned} \quad (1.59)$$

where the moments $Q_R^{a(n)}$ are defined as

$$Q_R^{a(n)} \equiv \int_{-L}^L dy^- (y^-)^n \psi_R^\dagger T^a \psi_R(x^+, y^-). \quad (1.60)$$

In spite of the appearance of L , these solutions are completely general, as no boundary conditions have been imposed. Provided that the fields at $\pm L$, as well as L itself, transform as usual, these are fully invariant under Lorentz and residual-gauge transformations. Also, from Eqs. (1.57) to (1.59), these fields at $x^- = \pm L$ are related by

$$\psi_L(x^+, L) - \psi_L(x^+, -L) = -i\frac{m}{2} \int_{-L}^L dy^- \psi_R(x^+, y^-), \quad (1.61)$$

$$\partial_- A^{-a}(x^+, L) - \partial_- A^{-a}(x^+, -L) = g Q_R^{a(0)} \quad (1.62)$$

and

$$\begin{aligned}
A^{-a}(x^+, L) - A^{-a}(x^+, -L) &= gQ_R^a(1) \\
&+ L [A^{-a}(x^+, L) + A^{-a}(x^+, -L)].
\end{aligned}
\tag{1.63}$$

Eq. (1.62) in particular gives the integral form of Gauss' Law. Therefore, ψ_L , A^{-a} , and $\partial_- A^{-a}$ are independent variables at only one boundary. To completely solve the equations of motion they must be specified at either L or $-L$, but not both independently, and in particular, none of these be set to zero at both ends. As a convention, when $x^+ = 0$, the average of the two boundary terms, such as $(1/2)[A^{-a}(0, L) + A^{-a}(0, -L)]$, will be treated as the independent variable; see Fig. 1.

On surfaces {1} and {3}, ψ_L , A^{-a} , and $\partial_- A^{-a}$ are the independent degrees of freedom, and Eq. (1.50) becomes a constraint equation. In principle, ψ_R may be solved for by inverting $i\partial_+ - (g/2)A^{-a}T^a$. This may be expressed iteratively, but the explicit solution will not be needed.

The independent degrees of freedom may now be quantized by postulating canonical commutation relations for the momenta which generate translations perpendicular to the surfaces on which they are defined. Then, at $x^+ = 0$ (surface {2}),

$$\pi_R = \frac{\delta\mathcal{L}}{\delta(\partial_+\psi_R)} = i\psi_R^\dagger
\tag{1.64}$$

while on {1} and {3},

$$\begin{aligned}
\pi_L &= \frac{\delta\mathcal{L}}{\delta(\partial_-\psi_R)} = i\psi_L^\dagger \\
\pi_A^a &= \frac{\delta\mathcal{L}}{\delta(\partial_- A^{-a})} = \partial_- A^{-a}.
\end{aligned}
\tag{1.65}$$

The anticommutators for ψ_R and ψ_L are given in Eq. (1.13) and (1.14). In addition,

$$[\pi_A^a(x^+), A^{-b}(y^+)]_{\{1\}+\{3\}} = -i\delta^{ab}\delta(x^+ - y^+). \quad (1.66)$$

As usual, fields which are independent commute. The independent fields may be expanded in creation and annihilation operators such that the (anti)commutation relations are realized, and from these the Fock space may be constructed.

The final result of solving for dependent degrees of freedom where appropriate and substituting in Eqs. (1.55) and (1.56) at $x^+ = 0$ is that

$$\begin{aligned} P^- = & -\frac{im^2}{4} \int dx^- dy^- \epsilon(x^- - y^-) \psi_R^\dagger(x^-) \psi_R(y^-) \\ & - \frac{g^2}{4} \int dx^- dy^- \psi_R^\dagger T^a \psi_R(x^-) |x^- - y^-| \psi_R^\dagger T^a \psi_R(y^-) \\ & + \int dy^+ \left(\psi_L^\dagger i\overleftrightarrow{\partial}_+ \psi_L(y^+) - g\psi_L^\dagger A^{-a} T^a \psi_L(y^+) \right) \\ & + \frac{m^2}{2} \left[\int dx^- \psi_R^\dagger(x^-) \right] \psi_L(0) + \frac{m^2}{2} \psi_L^\dagger(0) \left[\int dx^- \psi_R(x^-) \right] \\ & + \frac{g^2}{4} L Q_R^{a(0)} Q_R^{a(0)} + L \pi_A^a \pi_A^a + g \pi_A^a Q_R^{a(1)} \end{aligned} \quad (1.67)$$

and

$$\begin{aligned} P^+ = & \int dx^- \psi_R^\dagger i\overleftrightarrow{\partial}_- \psi_R + \frac{1}{2} \int dx^+ (\pi_A^a)^2 \\ & + \frac{m^2}{4} \int dy^+ \left(\psi_L^\dagger [i\partial_+ - \frac{g}{2} A^{-a} T^a]^{-1} \psi_L + \left[[i\partial_+ - \frac{g}{2} A^{-a} T^a]^{-1} \psi_L \right]^\dagger \psi_L \right). \end{aligned} \quad (1.68)$$

Also, the total gauge charge defined at $x^+ = 0$ is

$$Q^a = Q_R^{a(0)} + \int dy^+ \left(\psi_L^\dagger T^a \psi_L - \frac{1}{2} f^{abc} \pi_A^b A^{-c} \right). \quad (1.69)$$

and the Lorentz boost generator is

$$\begin{aligned}
K_B &= -\frac{1}{2} M^{+-} \\
&= \frac{1}{4} \int_{\{2\}} dy^- (y^- \Theta^{++} - x^+ \Theta^{+-}) + \frac{1}{4} \int_{\{1\}+\{3\}} dy^+ (x^- \Theta^{-+} - y^+ \Theta^{--}) \\
&= \frac{1}{2} \int_{-L}^L dy^- y^- \psi_R^\dagger i \vec{\partial}_- \psi_R - \frac{1}{2} \int_{-L}^L dy^+ y^+ \left(\psi_L^\dagger i \vec{\partial}_+ \psi_L - g \psi_L^\dagger A^{-a} T^a \psi_L \right) \\
&\quad - \frac{1}{2} L \int_0^L dy^+ \left(\frac{1}{2} (\partial_- A^{-a})^2 + \frac{m}{2} \bar{\psi} \psi \right) + \frac{1}{2} L \int_{-L}^0 dy^+ \left(\frac{1}{2} (\partial_- A^{-a})^2 + \frac{m}{2} \bar{\psi} \psi \right)
\end{aligned} \tag{1.70}$$

with dependent fields replaced where appropriate.

The canonical momentum π_A^a is given by $\partial_- A^{-a} = (1/2) F^{+-a}$ on the boundary, and acts as an x^- -independent background chromoelectric field. As such, it contributes to P^- in Eq. (1.67) an energy proportional to the length of the system, and couples to the first moment of the charge density, $Q_R^{a(1)}$.

The momenta P^μ generate the equations of motion Eqs. (1.48) to (1.50), and the fourth equation, Eq. (1.51), up to a boundary term. However, the price paid for treating A^{-a} on surfaces $\{1\}$ and $\{3\}$ as a physical degree of freedom to allow the simple commutation relation Eq. (1.66) is that Eq. (1.51) on the x^- boundary,

$$G^a(x^+) \equiv \partial_+ \pi_A^a + \frac{g}{2} f^{abc} \pi_A^b A^{-c} - g \psi_L^\dagger T^a \psi_L \approx 0 \tag{1.71}$$

cannot be satisfied as an operator equation. $G^a(x^+)$ is, in fact, the generator of the residual x^- -independent gauge transformation, which acts by changing the

boundary conditions which would be necessary to fully fix the gauge.^[6] For example, on surface {3}, the commutator

$$\begin{aligned} & [-i \int dx^+ \Lambda^a(x^+) G^a(x^+) , A^{-b}(y^+, -L)] \\ & = \partial_+ \Lambda^b(y^+) + \frac{g}{2} f^{bac} \Lambda^a(y^+) A^{-c}(y^+, -L), \end{aligned} \quad (1.72)$$

with $\Lambda^a(x^+)$ parametrizing the residual transformation. Eq. (1.71) must then be imposed on the space of states. Because it generates residual gauge transformations, it commutes with the generators P^μ , so that these will not move the states off this surface. Replacing

$$\partial_+ \pi_A^a = -\frac{i}{2} [\pi_A^a , P^-] = \frac{g}{2} \psi_L^\dagger T^a \psi_L \quad (1.73)$$

this condition on matrix elements becomes

$$\langle \Phi'_{physical} | (f^{abc} \pi_A^b A^{-c}(x^+) - \psi_L^\dagger T^a \psi_L(x^+))_{\{1\}+\{3\}} | \Phi_{physical} \rangle = 0. \quad (1.74)$$

In this space,

$$\psi_L^\dagger A^{-a} T^a \psi_L(x^+) \approx f^{abc} A^{-a} \pi_A^b A^{-c}(x^+) = 0, \quad (1.75)$$

and $\psi_L^\dagger A^{-a} T^a \psi_L$ effectively vanishes from P^- and K_B , restoring some of the symmetry between ψ_R and ψ_L . Also, Eq. (1.69) for Q^a becomes, by Eq. (1.71),

$$\begin{aligned} Q^a & \approx Q_R^{a(0)} + [\pi_A^a(-L, L) - \pi_A^a(L, -L)] \\ & = Q_R^{a(0)} + [\pi_A^a(x^0 = 0, x^1 = -\sqrt{2}L) - \pi_A^a(x^0 = 0, x^1 = \sqrt{2}L)], \end{aligned} \quad (1.76)$$

and the generator of global gauge transformations may be given entirely in terms of ψ_R , and π_A^a at two points on the boundary.

This is reminiscent of equal-time quantization in the $A^0 = 0$ gauge. There the phase space is expanded to include (in four dimensions) the three spatial A^i with canonical conjugates E^i . Gauss' Law, $\partial_i E^i - \rho = 0$, which generates time-independent gauge transformations, is abandoned as an operator equation but imposed on the states.

Actually, this is more than reminiscent. The equations of motion in the gauge $A^{-a} = 0$ are

$$i\partial_+\psi_R = \frac{m}{2}\psi_L \quad (1.77)$$

$$i\partial_-\psi_L - \frac{g}{2}A^{+a}T^a\psi_L = \frac{m}{2}\psi_R \quad (1.78)$$

$$-\partial_+\pi_A^a = g\psi_L^\dagger T^a\psi_L \quad (1.79)$$

$$\partial_-\pi_A^a + \frac{g}{2}f^{abc}\pi_A^b A^{+c} = g\psi_R^\dagger T^a\psi_R \quad (1.80)$$

where the canonical momentum

$$\pi_A^a = \frac{\delta\mathcal{L}}{\delta(\partial_+A^{+a})} = \partial_+A^{+a}. \quad (1.81)$$

The fields initialized on the boundaries {1} and {3} in the $A^{+a} = 0$ gauge and appearing in P^+ and P^- evidently correspond to those which would have been obtained by usual light-cone quantization in the gauge $A^{-a} = 0$, with left and right, + and - interchanged; in particular, with x^- the time variable and $x^- = \text{constant}$ an initial surface. The condition on states, Eq. (1.74), after this interchange, corresponds to Eq. (1.80), which is Gauss' Law.

At this stage, an apparently consistent quantization scheme has been set up in which charges and spacetime generators are conserved by construction, and boundary terms have been explicitly included. No real use has been made of the box length $2L$, and once it is taken to infinity, the scheme is evidently also Lorentz invariant. This includes the constraint, Eq. (1.74), which was obtained from a Lorentz-invariant equation of motion.

In the continuum limit, ψ_L on the boundaries couples to ψ_R only through an infinite- P^- , zero- P^+ mode, as previously discussed for free fermions. With the introduction of gauge fields, new terms have appeared in P^- , Eq. (1.67), which also become infinite in this limit. To construct a state space in which this limit is sensible, that is, in which these terms vanish, consider first states only containing degrees of freedom associated with ψ_R . To couple these directly to ψ_L , an infinite energy ψ_R particle must first be produced. In addition, ψ_R couples to π_A^a by the term $\pi_A^a Q_R^{a(1)}$ in P^- , but $Q_R^{a(1)}$ is a non-singlet operator. States of ψ_R for which it does not vanish are infinite in energy due to the presence of the Casimir operator $LQ_R^{a(0)}Q_R^{a(0)}$ in P^- . This is in contrast to electrodynamics in two dimensions, where the moment $Q^{(1)}$ can still couple to a charge singlet, and for which π_A is related to the physically relevant θ parameter.^[19] These are the only couplings between ψ_R and the boundary degrees of freedom. Consequently, the sector of color-singlet states composed of only ψ_R is separated from that with ψ_L , A^{-a} and π_A^a by an infinite-energy barrier.

The result of this very long song and dance is that a representation of the color and Poincare algebra with finite matrix elements may be constructed in terms of singlet states of ψ_R alone. In particular, the condition on the states, Eq. (1.74), is

trivially satisfied. Another representation based on ψ_L and corresponding to the gauge $A^{-a} = 0$ could be constructed as an alternative; this will not be developed here.

Finally, in the ψ_R sector,

$$P^+ = \int_{-L}^L dx^- \psi_R^\dagger i \overleftrightarrow{\partial}_- \psi_R, \quad (1.82)$$

while the Hamiltonian

$$\begin{aligned} P^- = & -\frac{im^2}{4} \int_{-L}^L dx^- dy^- \epsilon(x^- - y^-) \psi_R^\dagger(x^-) \psi_R(y^-) \\ & - \frac{g^2}{4} \int_{-L}^L dx^- dy^- \psi_R^\dagger T^a \psi_R(x^-) |x^- - y^-| \psi_R^\dagger T^a \psi_R(y^-). \end{aligned} \quad (1.83)$$

These will be evaluated in the sector for which the charge operator

$$Q^a = Q_R^{a(0)} = \int_{-L}^L dx^- \psi_R^\dagger T^a \psi_R$$

vanishes. When not otherwise indicated, the products of fields $\psi_R^\dagger T^a \psi_R$, which come from the normal-ordered current j^{+a} , are independently normal-ordered, as in P^- and Q^a above.

1.5. DISCRETE HAMILTONIAN, MOMENTUM AND BOOST OPERATORS

As is typically done, the anticommutation relation for $\psi_R(x)$ at $x^+ = 0$, Eq. (1.13), may be realized by expanding ψ_R in solutions of the free equations of motion,

$$\psi_R(0, x^-)_c = \frac{1}{\sqrt{2L}} \sum_{n=\frac{1}{2}, \frac{3}{2}, \dots}^{\infty} \left(b_{n,c} e^{-i\frac{n\pi}{L}x^-} + d_{n,c}^\dagger e^{i\frac{n\pi}{L}x^-} \right). \quad (1.84)$$

and assigning the relations

$$\{ b_{n,c_1}, b_m^{\dagger c_2} \} = \{ d_n^{c_1}, d_{m,c_2}^\dagger \} = \delta_{c_1}^{c_2} \delta_{n,m}$$

to the coefficients. It has proven useful to maintain the distinction between upper and lower color indices, as in these relations, particularly in the computer code. The adjoint representation, however, is real and in it no such distinction exists.

To treat this system numerically, it is quantized in a box in x^- of length $2L$. Because fermionic fields appear in measurable quantities as bilinears, either periodic or antiperiodic boundary conditions are appropriate. As previously discussed, the latter will be employed to allow for an expansion in solutions of the free wave equation which is also complete.

The Fock space of states is constructed by applying creation operators to the vacuum in all possible independent color-singlet combinations. The operators P^+ and P^- in this basis are obtained by substituting the expansion in Eq. (1.84) into Eqs. (1.82) and (1.83).

The result is, for P^+ ,

$$P^+ = \left(\frac{2\pi}{L}\right) \sum_{n=\frac{1}{2}, \frac{3}{2}, \dots}^{\infty} n \left(b_n^{\dagger c} b_{n,c} + d_{n,c}^{\dagger} d_n^c \right) \quad (1.85)$$

after discarding an infinite vacuum momentum. P^+ is diagonal in this basis, and independent of both quark mass m and coupling g . Quarks carry a momentum $2\pi n/L$ in physical units. That P^+ generates translations in x^- may be explicitly verified:

$$[P^+, \psi_R(0, x^-)] = -i\partial^+ \psi_R = -i2\partial_- \psi_R. \quad (1.86)$$

The charge operator Q^a defined in terms of the normal-ordered current,

$$Q^a = \int_{-L}^L dx^- : \psi_R^{\dagger} T^a \psi_R : = \sum_{n=\frac{1}{2}, \frac{3}{2}, \dots}^{\infty} \left(b_n^{\dagger} T^a b_n - d_n^{\dagger} T^a d_n \right)$$

is also diagonal. It generates global color transformations,

$$[Q^a, \psi_{R,L}] = -T^a \psi_{R,L} \quad (1.87)$$

and

$$[Q^a, A^{-b}] = i f^{abc} A^{-c}, \quad (1.88)$$

with ψ_L and A^{-a} defined as functions of ψ_R .

Finally, P^- is relatively complicated, is dependent on the coupling constant, and acts as the Hamiltonian, evolving the system in x^+ . In two dimensions, g carries the dimension of mass. The quark mass m is the only other dimensional

parameter, and apart from an overall and arbitrary mass scale, solutions depend on the ratio g/m . It is convenient to introduce the dimensionless coupling constant

$$\lambda \equiv \left(\frac{1}{1 + \pi m^2/g^2} \right)^{\frac{1}{2}}, \quad \text{or} \quad \frac{g}{m} = \left(\frac{\pi \lambda^2}{1 - \lambda^2} \right)^{\frac{1}{2}}. \quad (1.89)$$

as in Ref. [20], where λ varies from zero when g/m is zero, to one when g/m is infinite.

Defining the dimensionless momentum

$$K \equiv \left(\frac{L}{2\pi} \right) P^+$$

and Hamiltonian

$$H \equiv \left(\frac{2\pi}{L} \right) \frac{\pi^2 \lambda^2}{g^2} P^- = \left(\frac{2\pi}{L} \right) \frac{(1 - \lambda^2)}{m^2} P^-, \quad (1.90)$$

the dependence on the box length drops out of the mass-squared operator, and

$$M^2 = P^+ P^- = \frac{g^2}{\pi \lambda^2} K H = \frac{m^2}{(1 - \lambda^2)} K H. \quad (1.91)$$

The dimensionless Hamiltonian H separates into the free and interacting terms, H_0 and H_I , with

$$H = (1 - \lambda^2) H_0 + \lambda^2 H_I. \quad (1.92)$$

The free Hamiltonian H_0 sums the energy m^2/k^+ of free quarks,

$$H_0 = \sum_{n=\frac{1}{2}, \frac{3}{2}, \dots}^{\infty} \frac{1}{n} \left(b_n^{\dagger c} b_{n,c} + d_{n,c}^{\dagger} d_n^c \right), \quad (1.93)$$

while the terms in H_I are displayed in Tables [1] and [2].

Table [1]

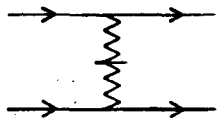
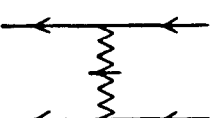
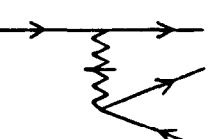
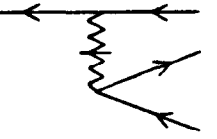


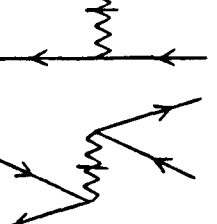
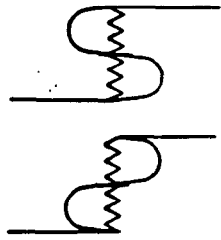
(1) 	$-\frac{1}{2} C_{c_4 c_3}^{c_1 c_2} [n_4 - n_2 n_3 - n_1] b_{n_4}^{\dagger c_4} b_{n_3}^{\dagger c_3} b_{n_2, c_2} b_{n_1, c_1}$
(2) 	$-\frac{1}{2} C_{c_2 c_1}^{c_3 c_4} [n_2 - n_4 n_1 - n_3] d_{n_4, c_4}^{\dagger} d_{n_3, c_3}^{\dagger} d_{n_2}^{c_2} d_{n_1}^{c_1}$
(3) 	$C_{c_4 c_3}^{c_2 c_1} [n_4 + n_1 n_3 - n_2] b_{n_4}^{\dagger c_4} b_{n_3}^{\dagger c_3} b_{n_2, c_2} d_{n_1, c_1}^{\dagger}$
(4) 	$C_{c_1 c_4}^{c_2 c_3} [n_3 - n_1 n_4 + n_2] b_{n_4}^{\dagger c_4} d_{n_3, c_3}^{\dagger} d_{n_2, c_2}^{\dagger} d_{n_1}^{c_1}$
(5) 	$C_{c_1 c_4}^{c_2 c_3} [n_1 + n_3 n_2 - n_4] b_{n_4}^{\dagger c_4} b_{n_3, c_3} b_{n_2, c_2} d_{n_1}^{c_1}$
(6) 	$C_{c_2 c_1}^{c_4 c_3} [n_2 - n_3 n_1 + n_4] b_{n_4, c_4} d_{n_3, c_3}^{\dagger} d_{n_2}^{c_2} d_{n_1}^{c_1}$
(7) 	$\left\{ -C_{c_4 c_1}^{c_2 c_3} [n_4 - n_3 n_2 - n_1] \right. \\ \left. + C_{c_4 c_1}^{c_3 c_2} [n_4 + n_2 -n_1 - n_3] \right\} b_{n_4}^{\dagger c_4} b_{n_3, c_3} d_{n_2, c_2}^{\dagger} d_{n_1}^{c_1}$

Table [2]

<p>(8)</p> 	$\frac{1}{2} \left(\frac{N^2-1}{2N} \right) \sum_{\ell} \{ [n-\ell \ell-n]$ $- [n+\ell -n-\ell] \} \{ b_n^{\dagger c} b_{n,c} + d_{n,c}^{\dagger} d_n^c \}$
--	--

These are summed over the half-integers n_i such that momentum is conserved.

The color matrix is defined by

$$C_{c_2 c_4}^{c_1 c_3} \equiv [T^a]_{c_4}^{c_1} [T^a]_{c_2}^{c_3} = \frac{1}{2N} (N \delta_{c_2}^{c_1} \delta_{c_4}^{c_3} - \delta_{c_2}^{c_3} \delta_{c_4}^{c_1}), \quad (1.94)$$

while the bracket

$$[n | m] \equiv \frac{1}{n^2} \delta_{n+m, 0} \quad (1.95)$$

represents the instantaneous gluon propagator corresponding to the linear potential in x^- .

The interaction Hamiltonian H_I is composed of a product of currents j^{+a} which are individually normal-ordered. Rearranging terms to put H_I in normal order, as in Table [1], produces the quark self-energy terms of Table [2]. These interactions include a finite renormalization of the quark mass, and, in color singlets, cancel infrared divergences from the four-quark interactions.

The possibility of infrared divergences due to the divergence of the gluon propagator, Eq. (1.95) at zero momentum transfer, is related to the long range confining behavior of the linear potential. Eq. (1.95) is only strictly correct for non-zero n

and m . The finite box length naturally regulates this behavior, and the contribution to the interacting part of P^- when either n or m or both are zero may be computed directly from Eq. (1.83). It gives

$$-\frac{g^2}{8} \left[\frac{1}{L} \left(Q^a Q^{a(2)} + Q^{a(2)} Q^a \right) + L Q^a Q^a \right]. \quad (1.96)$$

This vanishes between color singlets, and there are therefore no infrared divergences in this sector. It is consistent, then, to simply discard interactions with zero momentum transferred.

In the continuum, several prescriptions have been employed to regulate the gluon propagator, including a sharp cutoff in the momentum transfer p^+ near zero^[21,22] and pole prescriptions for $1/p^2$ such as^[23]

$$\frac{1}{2} \left(\frac{1}{(p^+)^2 + i\epsilon} + \frac{1}{(p^+)^2 - i\epsilon} \right) \quad (1.97)$$

and

$$\frac{1}{2} \left(\frac{1}{(p^+ + i\epsilon)^2} + \frac{1}{(p^+ - i\epsilon)^2} \right). \quad (1.98)$$

The differences are simplest to understand in terms of the spatial potentials that their Fourier transforms produce. The third is simply $|x^-|$, while the first two effectively shift the potential by an infinite and negative constant. As is clear from Eq. (1.83), such a shift adds a term to P^- proportional to $(g^2/\epsilon)Q^a Q^a$, which for the system in a box, is equivalent to including the term $(g^2/4)LQ^a Q^a$, which appears in P^- directly in the potential. This makes confinement manifest in both the potential and in quark propagators, and in Refs. [21] and [22] was used

to calculational advantage. In the space of color singlets, however, the various prescriptions are consistent.

As a final comment on the Hamiltonian, no terms appear in which quarks either disappear or emerge from the vacuum. This is a consequence of the combination of the positive-definiteness of the light-cone momenta and the requirement of its conservation at vertices. In contrast to equal-time quantization, the vacuum cannot be coupled to any other state, and so is an exact eigenstate.

The Lorentz boost generator in terms of only ψ_R fields,

$$K_B = \frac{1}{2} \int_{-L}^L dx^- x^- \psi_R^\dagger i \overleftrightarrow{\partial}_- \psi_R, \quad (1.99)$$

after discretization becomes

$$K_B = \frac{-i}{2} \sum_{m,n=\frac{1}{2},\frac{3}{2},\dots} \left[(-1)^{2(m-n)} \frac{(n+m+1)}{m-n} (b_m^\dagger b_n - d_n^\dagger d_m) + (-1)^{2(m+n+1)} \frac{(m-n)}{m+n+1} (b_m^\dagger d_n^\dagger + d_m b_n) \right]. \quad (1.100)$$

where the divergent term is discarded when $m = n$. As may be verified, at $x^+ = 0$, ψ_R obeys the boost relation appropriate for a right-handed, spin one-half field,

$$i[K_B, \psi_R(x^-)] = \left(\frac{1}{2} + x^- \partial_-\right) \psi_R(x^-) \quad (1.101)$$

even at finite L . Fields which depend upon ψ_R , such as ψ_L , will also transform correctly, apart from boundary terms, which would require the retention of boundary fields in Eq. (1.99).

Lorentz invariance is broken by choosing boundary conditions at a fixed L ; while not evident in Eq. (1.101), it can be seen in that K_B is not diagonal, and so does not annihilate the vacuum. In the continuum limit, however, the non-diagonal term oscillates to zero, and the Lorentz invariance of the vacuum is restored.

1.6. LORENTZ AND PARITY PROPERTIES OF WAVEFUNCTIONS

The effect of Lorentz boosts and parity transformations on wavefunctions is simplest to study in the continuum, where it is convenient to normalize the creation and annihilation operators relativistically.^[24] For example,

$$\{b_{p^+,c_1}, b_{k^+}^{\dagger c_2}\} = 4\pi k^+ \delta_{c_1}^{c_2} \delta(k^+ - p^+), \quad (1.102)$$

and so forth. With this normalization,

$$\psi_R(z^-)_c = \int_0^\infty \frac{dp^+}{4\pi p^{+\frac{1}{2}}} \left[b_{p^+,c} e^{-\frac{i}{2} p^+ z^-} + d_{p^+,c}^\dagger e^{\frac{i}{2} p^+ z^-} \right] \quad (1.103)$$

so that ψ_R satisfies

$$\{\psi_R(z)_{c_1}, \psi_L^\dagger(y)^{c_2}\}_{z^+=y^+} = \delta_{c_1}^{c_2} \delta(z^- - y^-). \quad (1.104)$$

Here, z is employed as a spacetime variable to avoid confusion with the momentum fraction, or Bjorken variable, x . Also,

$$\psi_L(z^-)_c = \int_0^\infty \frac{dp^+}{4\pi p^{+\frac{1}{2}}} \left(\frac{m}{p^+} \right) \left[b_{p^+,c} e^{-\frac{i}{2} p^+ z^-} - d_{p^+,c}^\dagger e^{\frac{i}{2} p^+ z^-} \right]. \quad (1.105)$$

Eigenstates may be normalized analogously,

$$\langle \phi(p^+) | \phi(k^+) \rangle = 4\pi k^+ \delta(k^+ - p^+). \quad (1.106)$$

Then, for example, if the valence meson is defined such that

$$|\phi(p^+)\rangle = \int_0^1 \frac{dx \phi(x)}{[4\pi N x(1-x)]^{\frac{1}{2}}} b_{(1-x)p^+}^{\dagger c} d_{xp^+,c}^\dagger |0\rangle, \quad (1.107)$$

the wavefunction $\phi(x)$ is normalized to one:

$$\int_0^1 dx \phi^2(x) = 1. \quad (1.108)$$

This normalization is convenient, as it matches that of the wavefunctions from the program.

The generator of Lorentz boosts at $z^+ = 0$,

$$K_B = \frac{1}{4} \int_{-\infty}^{\infty} dz^- z^- \Theta^{++} = \frac{1}{2} \int_{-\infty}^{\infty} dz^- z^- \psi_R^\dagger i \vec{\partial}_- \psi_R \quad (1.109)$$

is then

$$\frac{i}{8\pi} \int_0^\infty dp^+ \left[(\partial_{p^+} b_{p^+}^{\dagger c}) b_{p^+,c} - b_{p^+}^{\dagger c} \partial_{p^+} b_{p^+,c} + (\partial_{p^+} d_{p^+,c}^\dagger) d_{p^+}^c - d_{p^+,c}^\dagger \partial_{p^+} d_{p^+}^c \right]. \quad (1.110)$$

As a result,

$$[K_B, b_{p^+}^{\dagger c}] = ip^+ \partial_{p^+} b_{p^+}^{\dagger c}, \quad (1.111)$$

and after some algebra,

$$K_B |\phi(p^+)\rangle = ip^+ \partial_{p^+} |\phi(p^+)\rangle. \quad (1.112)$$

The corresponding finite transformation is then

$$e^{i\alpha K_B} |\phi(p^+)\rangle = |\phi(e^{-\alpha} p^+)\rangle; \quad (1.113)$$

boosting $|\phi(p^+)\rangle$ only scales the total momentum p^+ . The fraction x_n of p^+ carried by each constituent remains unchanged, so that the wavefunction $\phi(x)$ is boost-invariant.

While Lorentz invariance is greatly simplified by quantizing on the light cone, parity becomes less transparent. In two dimensions, there are only longitudinal boosts, and since these leave the quantization surface intact, it is possible to construct a Hamiltonian, P^+P^- , and therefore wavefunctions, which are boost invariant. On the other hand, parity ($x^1 \leftrightarrow -x^1$) interchanges x^+ and x^- , and P^+ and P^- , so the formalism treats left and right unevenly. Nevertheless, while parity interchanges P^+ and P^- , it clearly leaves the operator $M^2 = P^+P^-$ unchanged. It is therefore possible, and when non-degenerate necessary, for states to have definite parity.

To see how the parity operation affects wavefunction coordinates, consider a state of n particles of equal mass m , each carrying momentum fraction $x_i = k_i^+/P^+ = (k_i^0 + k_i^1)/P^+$ and $P^+ = \sum_i k_i^+$. Define \tilde{x}_i to be the corresponding momentum fractions of the parity transformed state. To solve for these, exploit the fact that the x_i are boost invariant to work in the center of mass frame so that

$\sum k_i^1 = 0$. This will also be true in the transformed state where $k_i^1 \rightarrow -k_i^1$. As a result,

$$P^+ = \sum_i (k_i^0 + k_i^1) = \sum_i k_i^0 \quad (1.114)$$

in both systems. Then

$$x_i = \frac{k_i^0 + k_i^1}{P^+}, \quad \tilde{x}_i = \frac{k_i^0 - k_i^1}{P^+} \quad (1.115)$$

and

$$x_1 \tilde{x}_1 = x_2 \tilde{x}_2 = \dots = x_n \tilde{x}_n = \frac{m^2}{P^+} . \quad (1.116)$$

Combined with

$$\sum_i x_i = \sum_i \tilde{x}_i = 1, \quad (1.117)$$

this yields

$$\tilde{x}_i = \frac{1}{x_i} \left(\frac{1}{\sum_j \frac{1}{x_j}} \right). \quad (1.118)$$

For the particular case of two equal mass particles, the momentum fractions x and $1 - x$ are simply interchanged. This inverse relation can be understood by noting that by $x = (k^0 + k^1)/P^+$, fast left-movers have x near zero as $-k^1$

approaches k^0 , fast right-movers have x near one, and parity interchanges left and right.

Finally note that discretization by setting boundary conditions at $\pm L$ on the z^- axis alone explicitly breaks parity. The x_i are restricted to a particular set of integers divided by the total integral momentum. Eqn. (1.118) then makes parity breaking evident, as the \tilde{x}_i will not in general be contained in this set. Obviously, this is remedied in the continuum limit. For the special case of two particles, however, it is soluble for any box size, since the x and $1 - x$ which are interchanged are already defined. Consequently, to determine the parity for a meson wavefunction, for example, it is only necessary to examine the minimum Fock ($q\bar{q}$) wavefunction, at any K , for symmetry under momentum interchange. For example, the lowest mass eigenstates for any N or coupling are of the form

$$\int_0^1 \frac{dx \phi(x)}{(4\pi N x(1-x))^{\frac{1}{2}}} b_{(1-x)p^+}^{\dagger c} d_{xp^+,c}^{\dagger} |0\rangle \quad (1.119)$$

with ϕ symmetric under interchange of x and $1 - x$. Interchanging these in the creation operators and accounting for the opposing signs for particles and antiparticles under parity produces an over-all minus sign and shows this to be a pseudoscalar. An odd $\phi(x)$ represents a scalar.

Alternatively, parity may be determined by computing the vacuum to one meson matrix elements of the scalar and pseudoscalar color singlet operators $\bar{\psi}\psi$ and $\bar{\psi}\gamma^5\psi$.^[22] These may be evaluated directly in terms of fields and the $q\bar{q}$ component of the meson wavefunction:

$$\langle 0 | : \bar{\psi} \psi(z) : | \phi(k^+) \rangle = -m N^{\frac{1}{2}} e^{-ikz} \int_0^1 \frac{dx \phi(x)}{(4\pi)^{\frac{1}{2}}} \left(\frac{1}{x} - \frac{1}{1-x} \right) \quad (1.120)$$

and

$$\langle 0 | : \bar{\psi} \gamma^5 \psi(z) : | \phi(k^+) \rangle = -m N^{\frac{1}{2}} e^{-ikz} \int_0^1 \frac{dx \phi(x)}{(4\pi)^{\frac{1}{2}}} \left(\frac{1}{x} + \frac{1}{1-x} \right). \quad (1.121)$$

As expected, a $\phi(x)$ odd under $x \leftrightarrow 1-x$ is a scalar and couples only to $\bar{\psi}\psi$, while an even $\phi(x)$ is a pseudoscalar.

Finally, charge conjugation on these $q\bar{q}$ components interchanges quark and antiquark. Permuting operators and redefining momentum variables gives the same sign as parity, and all meson states are charge-parity even.

1.7. CHIRAL ANOMALY

The interacting part of the Hamiltonian P^- is expressed entirely as a function of the current

$$j^{+a} = 2 : \psi_R^\dagger T^a \psi_R : . \quad (1.122)$$

The commutator of j^{+a} with itself is relatively easy to compute, and the evolution of j^{+a} due to the interaction follows immediately. This allows for a quick and dirty calculation of the non-Abelian axial anomaly, assuming only that the gauge current is conserved.

The axial current

$$j_5^{+a} = 2\psi_R^\dagger T^a \psi_R \quad (1.123)$$

$$j_5^{-a} = -2\psi_L^\dagger T^a \psi_L,$$

differs from the vector current

$$j^{+a} = 2\psi_R^\dagger T^a \psi_R \quad (1.124)$$

$$j^{-a} = 2\psi_L^\dagger T^a \psi_L - f^{abc} \partial_- A^{-b} A^{-c},$$

in the j^{-a} term,

$$j_5^{-a} = -j^{-a} - f^{abc} \partial_- A^{-b} A^{-c}. \quad (1.125)$$

The gauge fields should be considered as appropriately symmetrized, and the currents as normal-ordered. If the vector current is conserved, then

$$\partial_- j^{-a} = -\partial_+ j^{+a} \quad (1.126)$$

and therefore

$$\partial_\mu j_5^{\mu a} = 2\partial_+ j^{+a} - f^{abc} \partial_-^2 A^{-b} A^{-c}. \quad (1.127)$$

By the constraint equation

$$-\partial_-^2 A^{-b} = \frac{g}{2} j^{+b} \quad (1.128)$$

for A^{-b} ,

$$\partial_\mu j_5^{\mu a} = 2\partial_+ j^{+a} - f^{abc} A^{-b} j^{+c}. \quad (1.129)$$

Because the anomalous term depends only on the interaction, only that part of P^- is needed to compute $\partial_+ j^{+a}$, and the term in P^- proportional to m will be neglected.

The commutators involving j^{+a} are defined by first point splitting the two ψ_R factors in j^{+a} a distance ϵ along x^- . The exponential in A^{+a} needed to preserve gauge invariance is absent due to the choice of gauge. Then, using the expansion in Eq. (1.84), at $x^+ = 0$

$$[j^{+a}(x^-), j^{+b}(y^-)] = 2if^{abc}j^{+c}(x^-)\delta(x^- - y^-) - \frac{i\delta^{ab}}{2L \sin(\pi\epsilon/L)} \left[\delta(x^- - y^- - \epsilon) - \delta(x^- - y^- + \epsilon) \right]. \quad (1.130)$$

As ϵ vanishes, the second (Schwinger) term on the right may be represented in the more conventional form

$$\frac{i}{\pi} \delta^{ab} \partial_{x^-} \delta(x^- - y^-). \quad (1.131)$$

After some algebra and to leading order in ϵ ,

$$2\partial_+ j^{+a}(x^-) = i[P^-, j^{+a}(x^-)] = -\frac{g^2}{8\pi} \int_{-L}^L dy^- \epsilon(x^- - y^-) j^{+a}(y^-) - \frac{g^2}{4} \int_{-L}^L dy^- |x^- - y^-| j^{+b}(y^-) j^{+c}(x^-). \quad (1.132)$$

The constraint equations for A^{-a} and $\partial_- A^{-a}$, neglecting boundary terms and using

$$\partial_- A^{-a} = \frac{1}{2} \epsilon_{\mu\nu} F^{\mu\nu a}, \quad (1.133)$$

produces

$$2\partial_+ j^{+a}(x^+) = \frac{g}{4\pi} \epsilon_{\mu\nu} F^{\mu\nu a} + g f^{abc} A^{-b} j^{+c}. \quad (1.134)$$

This may be rewritten as

$$D_+ j^{+a} = \frac{g}{4\pi} \epsilon_{\mu\nu} F^{\mu\nu}, \quad (1.135)$$

using

$$D_+^{ac} = \partial_+ \delta^{ac} - \frac{1}{2} f^{abc} A^{-b}; \quad (1.136)$$

also, in this gauge,

$$D_-^{ac} = \partial_- \delta^{ac}. \quad (1.137)$$

Finally, combining Eqs. (1.127) and (1.135),

$$D_\mu j_5^\mu = \frac{g}{4\pi} \epsilon_{\mu\nu} F^{\mu\nu a}. \quad (1.138)$$

This result is referred to as the covariant anomaly, and is discussed in Ref. [25].

The discussion in this work will be conducted predominantly in momentum space, and it is convenient to have a version of the algebra of Eq. (1.130) in terms of the transformed operators

$$V_k^a = \frac{1}{2} \int_{-L}^L dx^- e^{-i\frac{k\pi}{L}x^-} j^{+a}(x^-). \quad (1.139)$$

The fermion fields satisfy antiperiodic boundary conditions, but the current, which is a product of these, satisfies periodic conditions, and the momentum k in this expansion is then an integer. By Eq. (1.130), these operators satisfy the Kac-Moody algebra^[26]

$$[V_k^a, V_\ell^b] = i f^{abc} V_{k+\ell}^c + \frac{1}{2} \ell \delta^{ab} \delta_{k+\ell,0}. \quad (1.140)$$

Because states are restricted to color singlets, the transform of the $U(1)$ current will be particularly important, as will be discussed in Chapter (3).

2. NUMERICAL RESULTS

2.1. OVERVIEW OF PROGRAM

The momentum, charge and Hamiltonian operators have been expressed as the dimensionless functions K , Q and H of a discrete and denumerable Fock basis. K is already diagonal, so that it only remains to diagonalize H in a space in which Q vanishes to determine the masses and wavefunctions of this system. This is best done by computer, and this section gives a brief outline the program used to accomplish this. This was run on an IBM 3081, with CPU time for the cases to be presented typically in the range of a few minutes.

Once N , B and $2K$ are specified, all possible color-singlet combinations of N -colored quarks consistent with the conserved quantities B and $2K$ are generated. (The momentum K is the sum of half-integer quark momenta, so that it is convenient to use $2K$, which is always an integer, in this discussion.) In particular, to satisfy baryon number, all states begin with B N -tuplets of quarks. (B is restricted to be zero or positive, which is sufficiently general by charge conjugation invariance.) These quarks are understood to be contracted into $SU(N)$ singlets by antisymmetrizing in color, although in practice it is not necessary to explicitly introduce color indices in order to compute color factors. To these baryons are appended quark- antiquark ($q\bar{q}$) pairs, from zero to the maximum permitted by the momentum $2K$ which is divided into the positive-definite momenta carried by individual quarks. Again, these mesons are contracted into singlets. As for the baryons, color is fully contracted, and it is enough to know only which quarks are grouped into which singlet.

In addition to mesons, baryon-antibaryon pairs could be added; however, these are redundant to states formed by adding mesons. Finally, for $U(N)$, B is required to be zero, as baryon number is essentially an electric charge for the extra $U(1)$ and is also confined.

The program to construct the Fock space is built around two subroutines. The first generates all possible combinations of n integers such that they sum to a fixed number, but with a particular integer limited to at most i appearances in each permutation. This is used to subdivide a fixed momentum among various particles. The index i accounts for Fermi statistics; for example, $i = N$ for quarks (with one flavor) because the color degree of freedom allows the same momentum to be carried by at most N quarks. These permutations are stored and their locations recorded. The second routine is similar, except that rather than permuting momenta, it generates permutations of the locations of the entire momentum distributions previously stored. The result has something of a tree structure. For example, for a subset of states with three mesons and two baryons, the possible ways of splitting momentum between mesons and baryons are run through. Within this, the total momentum of the mesons is split among the three mesons with bosonic statistics; the rest is split between the baryons with fermionic or bosonic statistics depending on N being odd or even. Once assigned, the possible momenta within the individual mesons or baryons are iterated through. The final momentum assignment to individual quarks is checked to ensure that no more than N are the same before the state is stored.

The resulting Fock space is in general not orthonormal and frequently over-complete. To remove redundant states, the inner-product matrix is computed

and diagonalized, in the same way as the Hamiltonian is later computed. Over-completeness is indicated by zero eigenvalues. Appropriate states are dropped, the new matrix is again diagonalized, and so on, until no zero eigenvalues remain. The resulting matrix of eigenvectors with the eigenvalues divided out orthonormalizes the final set of states. Finally, options to further restrict the states by limiting the total number particles in each state by hand, or by discarding those whose invariant mass exceeds a cutoff, are included.

The operators in the individual terms in the Hamiltonian are represented in the same form as the Fock states. The Hamiltonian matrix is evaluated by sandwiching these between the complete but not orthonormal states, and then iterating through the momenta which these operators could carry. The original states are used in this stage because they are in general simpler to represent. As elaborated in the Appendix A, these matrix elements are then contracted and the gluon propagators and color factors are computed. Finally, the resulting Hamiltonian matrix is converted to the corresponding matrix in the orthonormal basis.

Finally, the Hamiltonian is diagonalized by standard, packaged routines, using LU decomposition; see, for example, Ref. [27]. This produces both the full spectrum of states and the corresponding normalized wavefunctions, from which any computable quantity can be extracted up to the resolution K . Typical values for K used here were between 5 and 10, and in these cases, the time required to diagonalize the Hamiltonian was insignificant relative to that needed to evaluate it.

Because the Hamiltonian $m^2 H_0 + g^2 H_I$ breaks up into a free and interacting part such that the parameters m^2 and g^2 appear as overall constants before each,

the matrices H_0 and H_I are stored separately. Computing the spectrum for different g or m then only involves computing H_0 and H_I once, and then recombining and re-diagonalizing at each g and m , with effectively no extra cost in time.

2.2. SPECTRA

One of the advantages of directly diagonalizing the Hamiltonian is that it produces information about the entire spectrum of the theory in the form of eigenvalues (masses) and eigenfunctions (wavefunctions), rather than of only the lightest states.

Figs. (2) and (3) display the development of the 1 + 1 dimensional spectra for three colors, with baryon number of zero and one at relatively weak ($\lambda = .3325$ or $m/g = 1.6$) and relatively strong ($\lambda = .9847$ or $m/g = .1$) coupling.

As is evident, the number of states is limited by the total momentum K . As K increases and the continuum limit is approached, Figs. (2a) and (2b) show the development of both a discrete set of bound states at low mass and a continuum of states with a threshold at $4M^2$, with M the mass of the lightest meson or baryon. It is clear that these states are both filling in the continuum with increasing K , and also maintaining some structure.

At a particular K , the states in the spectrum are eigenstates of both P^+ and P^- ; in particular, individual states cannot decay. Information about resonances, for example, must be contained within this structure.

For the case with strong coupling, Figs. (3a) and (3b), a large number of states cluster near zero mass, above which sets a relatively large gap. In the

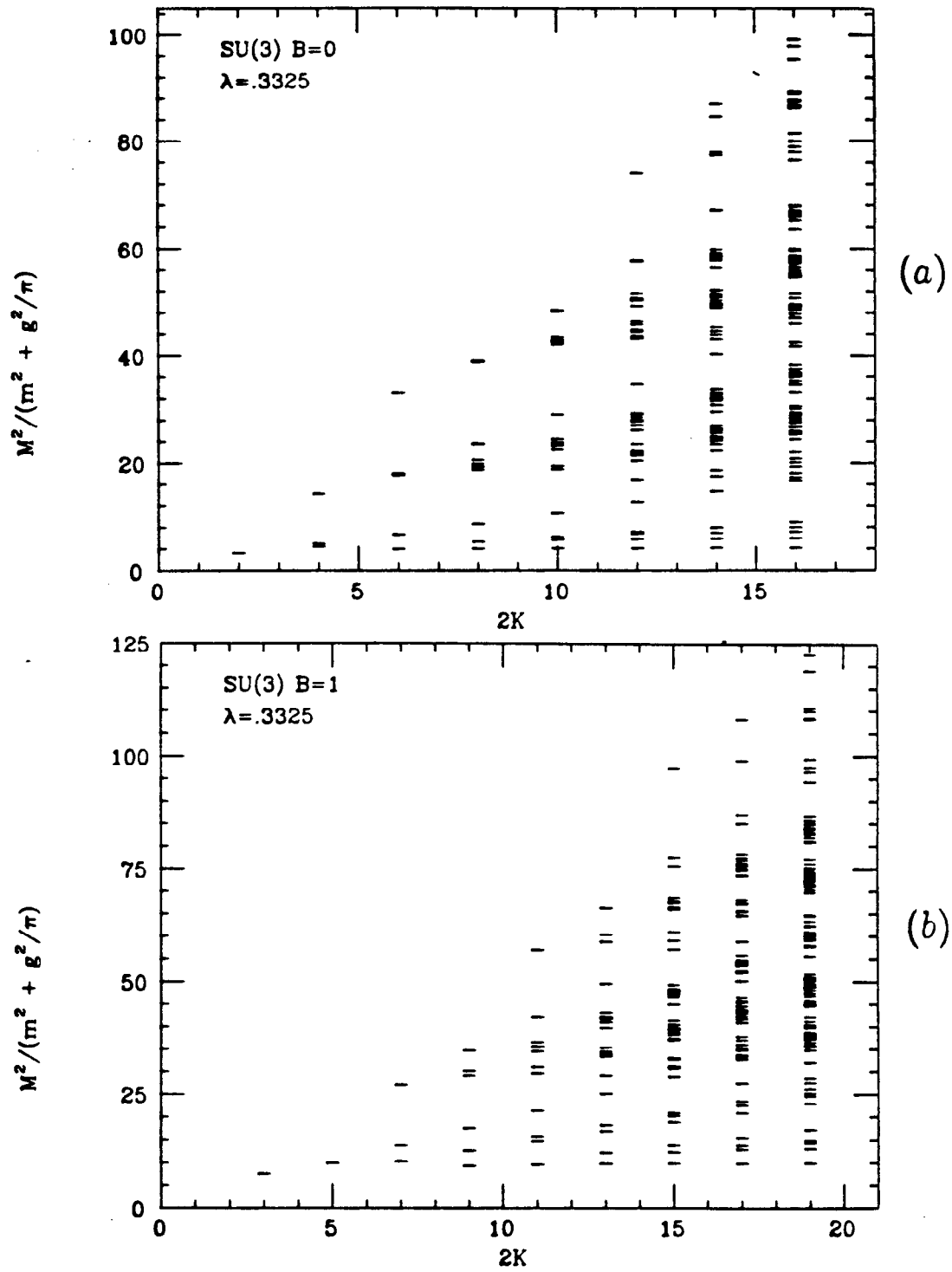


Figure 2. Development of $N = 3$ Spectrum with Increasing K ; Weak Coupling. (a) Meson Spectrum ($B = 0$). (b) Baryon Spectrum ($B = 1$).

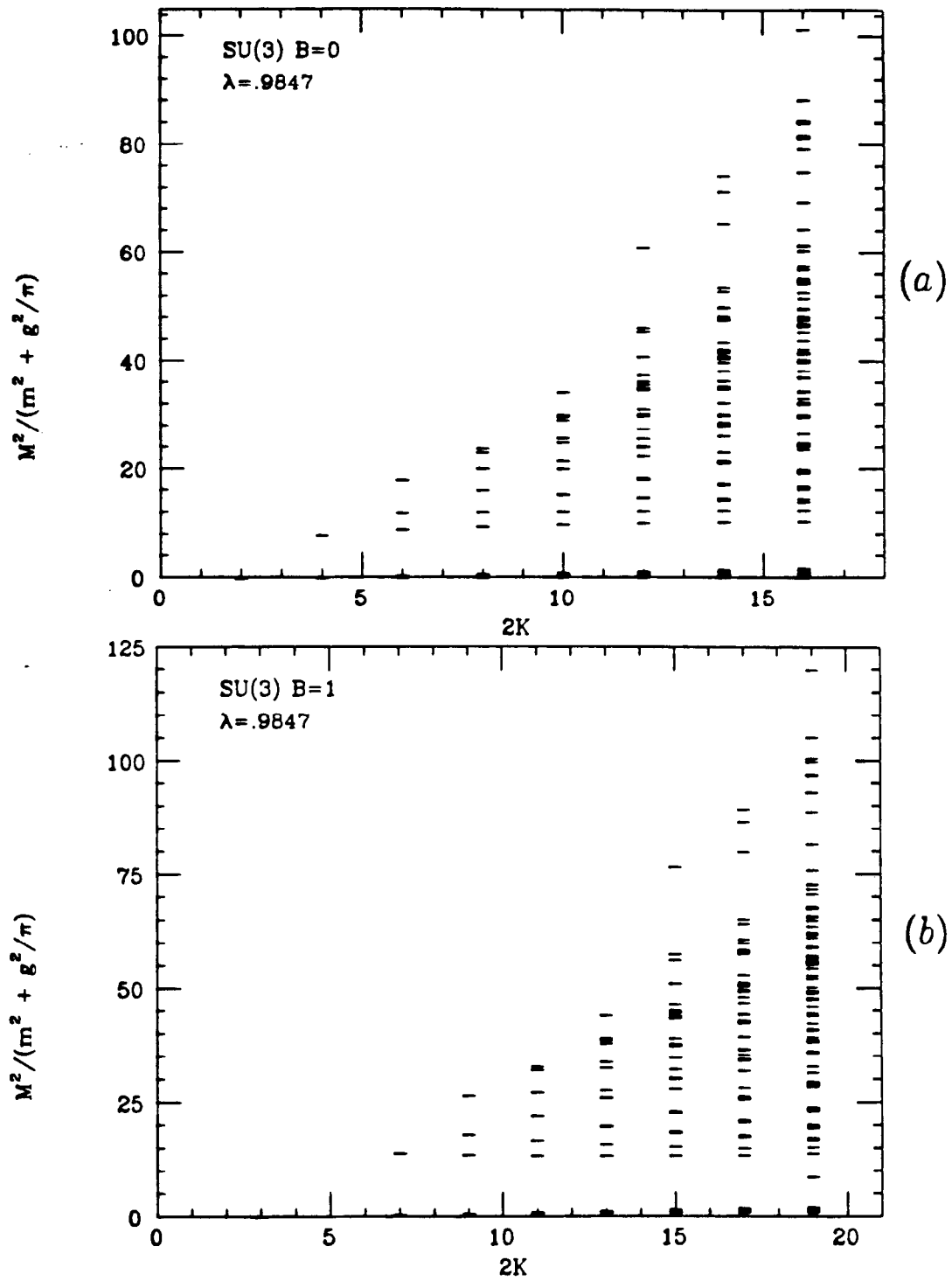


Figure 3. Development of Spectrum with Increasing K ; Strong Coupling. (a) Meson Spectrum ($B = 0$). (b) Baryon Spectrum ($B = 1$).

continuum limit, the number of states in this cluster will become infinite, generating a continuum of levels which begins near zero.

That this method produces an entire spectrum is a great advantage, but it can also have its drawbacks. In particular, for very large K the number of eigenstates can become enormous. The higher states will in general contain both new, excited states as well as states with multiple copies of lighter particles with some relative momentum. Developing methods to extract those of interest will become particularly important in four dimensions, due to the large number of degrees of freedom. In a sense, being able to control the number of states by keeping K finite becomes an advantage. Restricting states by means of a Lorentz-invariant cutoff, which will be introduced later, may be even more useful, as a continuum limit may be taken while a fixed cutoff is imposed. Finally, it will be essential in four dimensions to take advantage of all the residual spacetime and internal symmetries in the light-cone Hamiltonian to separate the Fock space into disjoint sectors, as was done with baryon number in these cases.

In Figs. (4a-c), the meson ($B = 0$), single baryon ($B = 1$), and double baryon ($B = 2$) spectra are traced from zero coupling (or infinite quark mass) at $\lambda = 0$ to infinite coupling (zero mass) at $\lambda = 1$ with K held fixed. The dimensionless coupling λ , as well as M^2 in units of $m^2 + g^2/\pi$ are quantities employed directly in the program. For each of these plots, the Hamiltonian matrices H_0 and H_I are computed once and stored. At each value of λ (or m/g), these are added to form the full Hamiltonian

$$H = m^2 H_0 + g^2 H_I, \tag{2.1}$$

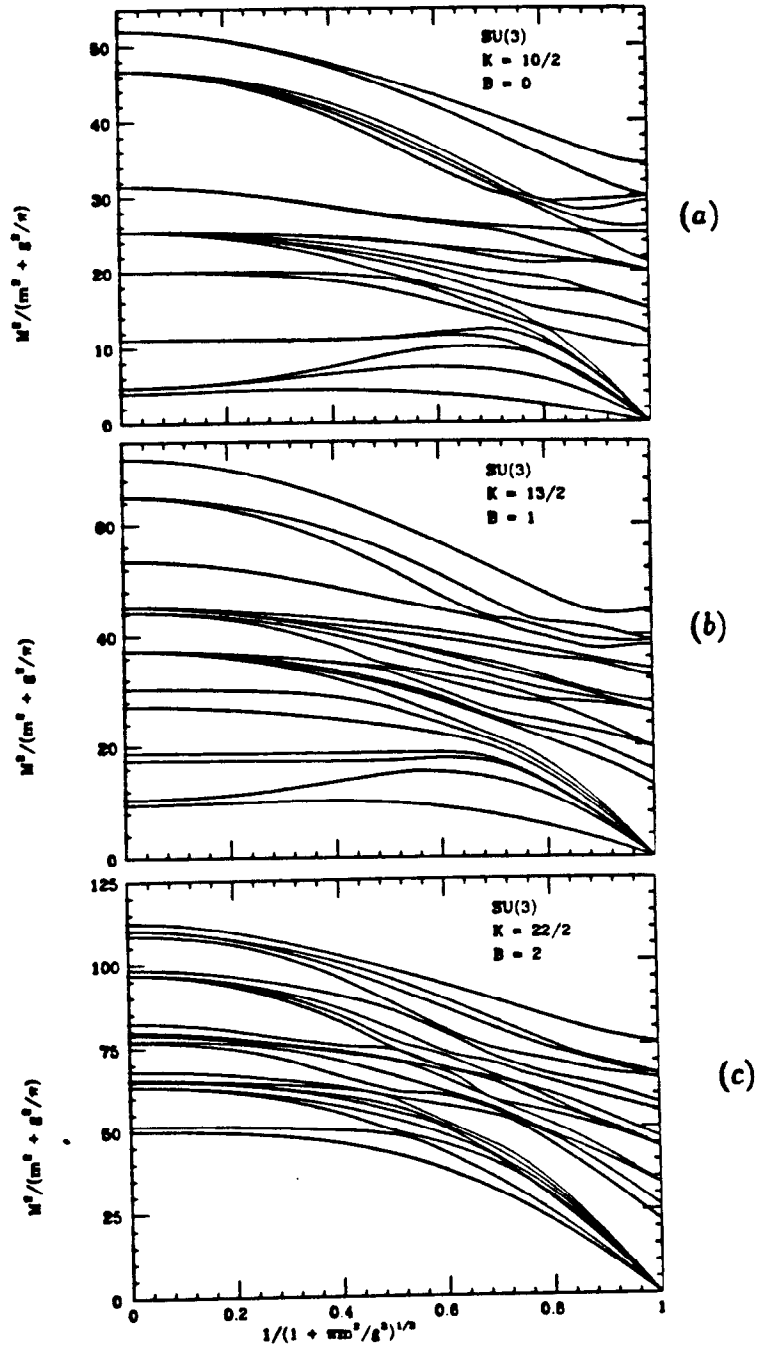


Figure 4. Development of $N = 3$ Spectrum with Coupling Constant λ . (a) Meson Spectrum ($B = 0$); (b) Baryon Spectrum ($B = 1$); (c) Two Baryon Spectrum ($B = 2$).

which is then diagonalized. The cost in processor time to diagonalize H is insignificant compared to that of computing it once; after computing these spectra at some λ , the rest come essentially for free.

At $\lambda = 0$, the spectrum consists of collections of free massive quarks grouped into color singlets, beginning at $M^2 = m^2$ and $9m^2$ for $B = 0$ and 1 , respectively. Higher states at this coupling have quarks with relative momentum and extra $q\bar{q}$ pairs. For $B = 2$, fermi statistics prohibit the quarks from having zero relative momenta; presumably in the continuum limit, as this restriction becomes less important, the lowest mass will drop to $36m^2$.

As the interaction is turned on and increased, the degeneracy of the non-interacting quarks is split, and a fair number of pseudo-crossings become apparent between the weak and strong coupling limits. At infinitely large g , a large number of states collapse to zero mass. As will be discussed later, these are composed of a single massless meson, baryon, or baryon pairs (for $B = 0, 1$, and 2) together with massless states created by adding extra massless mesons to these. In four dimensions, two massless particles can be combined to form a zero mass system when collinear; in two dimensions, all particles are collinear. Also, degeneracies in the higher states reappear, as might be expected. Combining a massless meson with some state can produce a degenerate state in the absence of interactions, as will be shown to be the case.

Spectra with $B = 0, 1$, and 2 are presented here, but systems with arbitrarily large numbers of baryons may be studied by selecting the appropriate baryon number to see if, among other things, there is interesting nuclear physics in two dimensions. In particular, because baryon number is conserved, the lightest $B = 2$

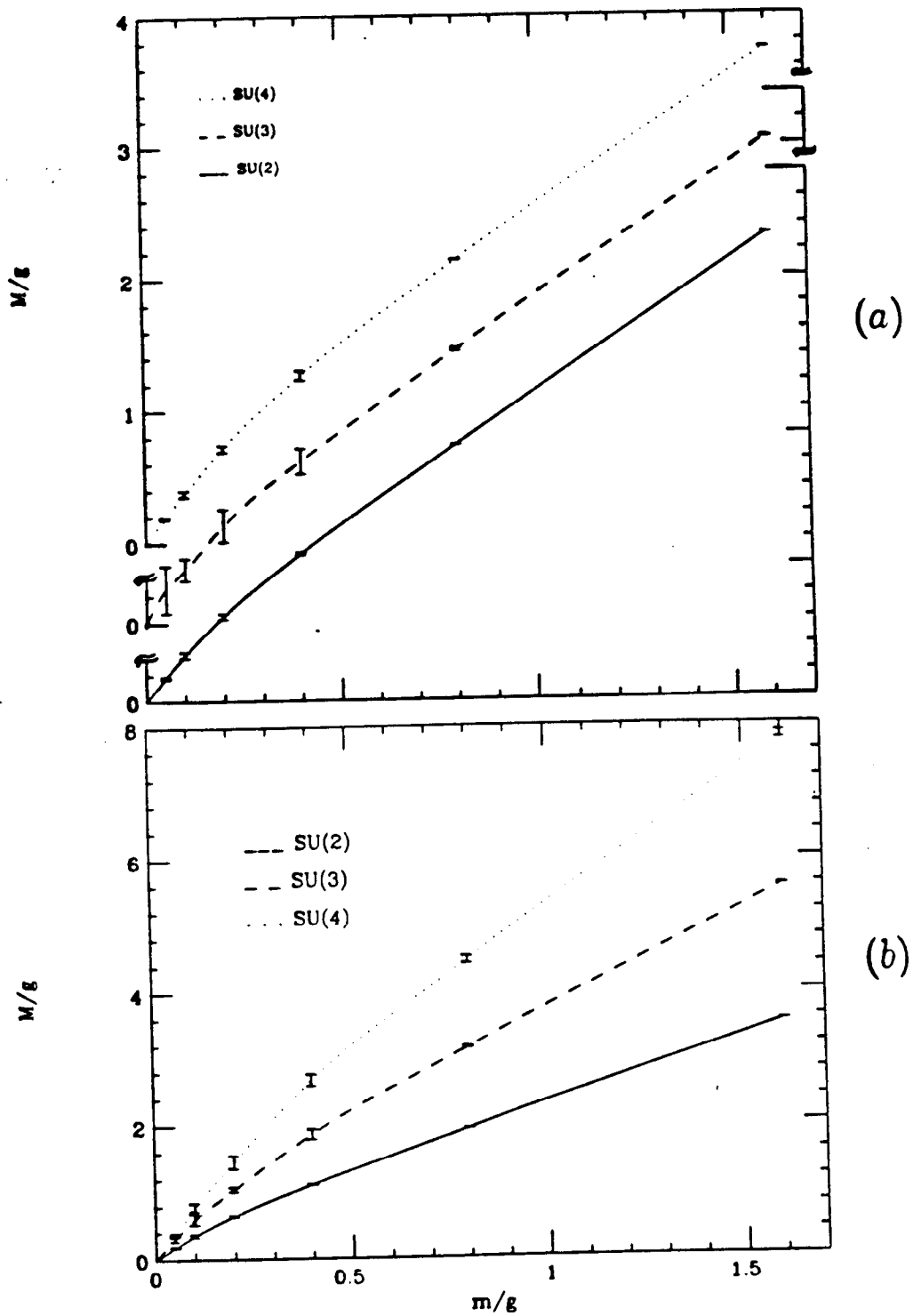


Figure 5. Lightest Meson and Baryon Mass versus Quark Mass for $N = 2, 3$ and 4. (a) Meson; (b) Baryon.

state mass (for example) state mass can be compared to twice that of $B = 1$ to see if quark interactions saturate within each baryon, and if not, to compute the nuclear binding energy.

The masses of the lowest-lying states are generally of the most interest and are the quantities most likely available for comparison from other methods, especially lattice calculations. The masses of the lowest-lying meson and baryon for N of 2, 3, and 4 at a selected set of couplings are listed in Table [3] and displayed in Figs. (5a) and (5b).

Table [3]

λ	m/g	M_{mes}/g			M_{bar}/g	
		$N = 2$	3	4	3	4
.3325	1.6	4.314(4)	4.618(6)	4.845(2)	10.71(2)	21.2(3)
.5763	.8	3.913(4)	4.40(5)	4.743(2)	10.4(1)	20.9(5)
.8158	.4	2.61(5)	3.1(5)	3.4(2)	7.3(6)	15(1)
.9425	.2	1.17(7)	1.5(5)	1.4(1)	3.1(2)	6.0(8)
.9847	.1	.38(5)	.5(2)	.43(5)	1.1(3)	1.9(3)
.9961	.05	.10(1)	.2(2)	.12(1)	.31(9)	.42(6)
1.0	0	0	0	0	0	0

In all cases, that is, at every λ and K , the lightest $N = 2$ meson and baryon have identical masses, and that $M_{mes}/M_{bar} = 1$ for $N = 2$ is an exact result. The results quoted in Table [3] are extrapolations to continuum results by matching to a series in $1/K$ for $2K$ in the range of roughly 16 to 24, as will be discussed in Chapter (3). The numbers in parenthesis give the magnitude of the last term in the series fit. For $\lambda \lesssim .9425$, these are reasonable estimates of the actual error. Beyond

this, the largest K employed is likely not large enough for these to be more than a rough guide, as will be discussed. However, when $m/g = 0$ ($\lambda = 1$) identically, the lightest state for any N or B is exactly zero, independent of K . The nature of solutions in this limit will be discussed below.

Although the lightest $N = 2$ meson and baryons have identical mass, the spectra are not equivalent. In particular the masses of the next lightest $N = 2$ meson and baryon are listed in Table [4], in units of the lightest mass. This ratio measured at various K is more stable than the absolute value, and is likely to give a more accurate extrapolation.

Table [4]

λ	m/g	$M_{(2^{nd}state)}/M_{(1^{st})}$	
		$B = 0$	1
.3325	1.6	1.33(1)	1.59(3)
.5763	.8	1.73(2)	2.41(2)
.8158	.4	2.4(1)	3.7(2)
.9425	.2	2.8(1)	3.7(4)
.9847	.1	2.8(1)	3.7(3)
.9961	.05	2.6(2)	3.6(3)

Results for λ beyond .9425 should be regarded only as estimates at the values of K used here. In particular, it is not certain that these ratios are actually reaching a fixed value.

It might be worth mentioning that at strong coupling but insufficiently large K , the numerical results for masses may be duplicated by using the exact infinite-

coupling wavefunctions to compute the Hamiltonian's expectation value. At infinite coupling (or zero mass) the wavefunctions do not vanish at small x ; for non-zero mass, the kinetic terms m^2/x_i will force them to zero. However, the smallest available numerical x is $1/2K$. When m/g is small, the kinetic term will not be felt until K is large enough to compensate. A great deal of information is contained in this small- x region, and until this K is reached the continuum limit is still far off for quantities sensitive to this region.

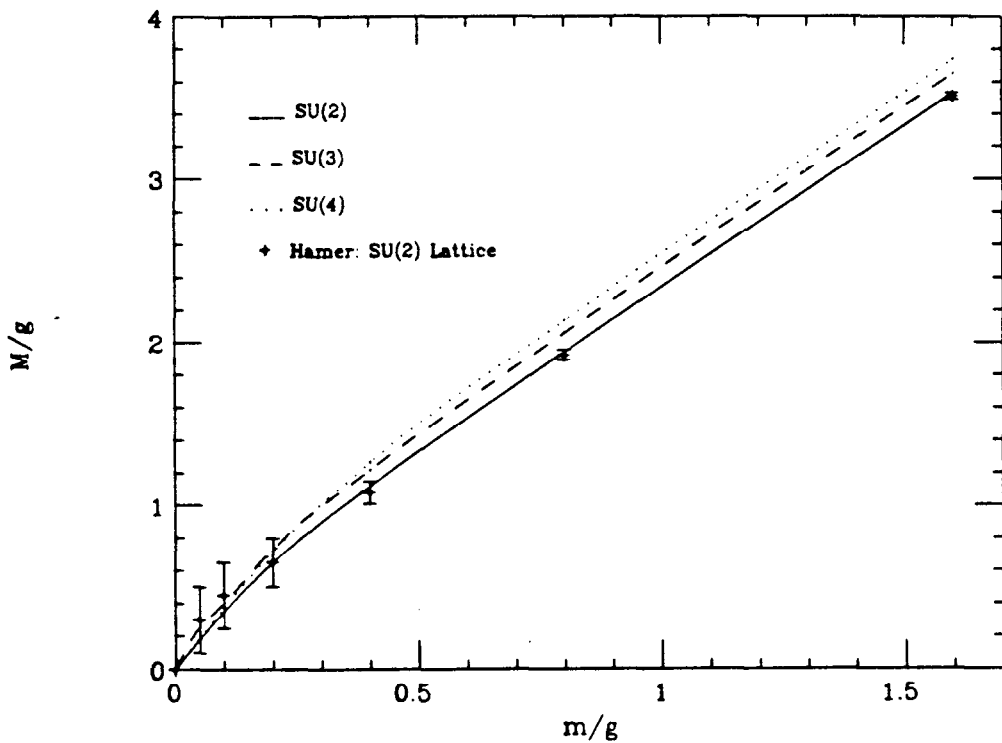


Figure 6. Comparison of Lightest Meson Mass for $N = 2, 3$ and 4 with Lattice Calculation for $N = 2$.

In certain cases, results from this work may be compared with those from other sources. In particular, Hamer has computed the mass of the lightest $N = 2$ meson and baryon using a Hamiltonian lattice with Wilson fermions.^[26] His results are

plotted in Fig. (6) along with the results from this calculation for N from 2 to 4, as in Fig. (5a). For ease of comparison, only his error bars are displayed here. Also, the actual data points from this work sit on the same m/g locations as his; the curves are fits intended only as guides.

Clearly the agreement is quite good. This is especially reassuring, as the methods employed are very different. In particular, Hamer works in a different gauge ($A^0 = 0$ versus $A^+ = 0$), a different space (position rather than momentum), a different quantization prescription (equal-time versus light-cone), uses a different infrared regulator (lattice size versus isolating by discretization and discarding zero momentum states) and takes a different continuum limit (lattice spacing versus box size in x^-). Both methods find accuracy in the chiral limit ($m/g \rightarrow 0$) increasingly difficult, but much less so at $m/g = 0$ identically. As is well known, implementing chiral symmetry in a lattice formulation requires some effort, and is related to the difficulty in adequately defining single derivatives for fermions. For light-cone quantization, the difficulty is from a seemingly unrelated source. In particular, as $m/g \rightarrow 0$, the kinetic term m^2/x which forces the wavefunction to zero in this limit becomes dominant at increasingly smaller values of x ; as a result, the wavefunction turn-over in x becomes more drastic, and ever larger values of K are necessary to adequately sample this region. However, as will be shown, this severe behavior is necessary to compensate for the very asymmetric treatment which ψ_L and ψ_R receive during quantization. Although the constraint equation for ψ_L appears to condemn it to decouple as $m \rightarrow 0$, this endpoint behavior for wavefunctions compensates so that matrix elements with ψ_L couple symmetrically with those for ψ_R . Because the system is quantized in momentum space, there is no difficulty with

fermion doubling. Perhaps the price to pay is that the fermion mass must be initially finite to ensure that ψ_L doesn't disappear, but that as $m \rightarrow 0$, wavefunctions become increasingly ill-behaved, making numerical accuracy difficult to obtain.

The study of $SU(N)$ in $1+1$ dimensions began with 't Hooft,^[21] who solved the meson spectrum in the large- N limit. By solving for these mesons at finite N here, it is possible to determine both how good the approximation is at a particular N of interest (three, for instance) as well as how quickly the large- N limit is approached.

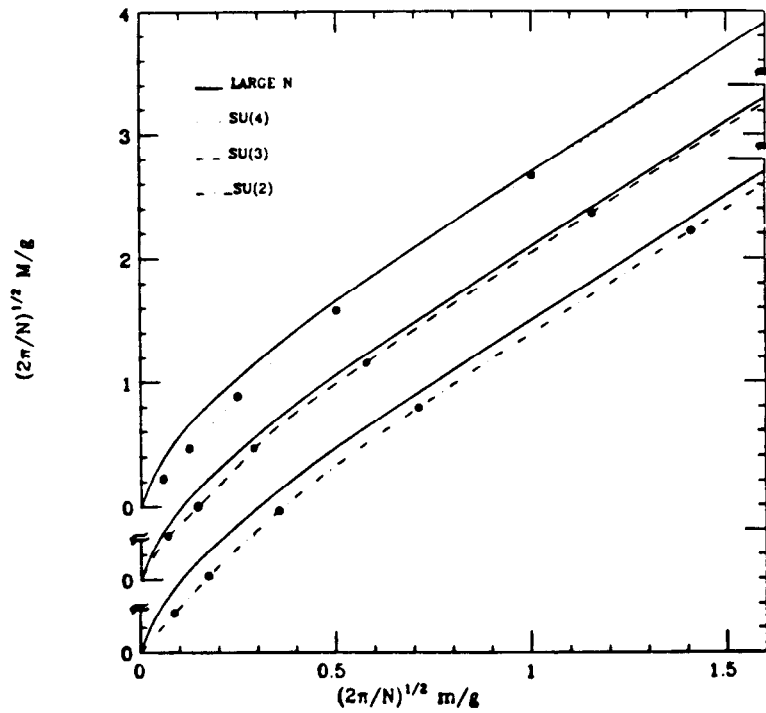


Figure 7. Comparison of Lightest Meson Mass for $N = 2, 3$ and 4 with Large- N Meson from Ref. [21].

In Fig. (7), the lightest meson masses for $N = 2, 3$, and 4 are compared with 't Hooft's lightest large- N meson. Masses in this plot are rescaled into units of $gN^{1/2}$, as this is the expansion parameter considered fixed as $N \rightarrow \infty$. Even for $N = 2$

there is surprisingly good agreement, except for small but finite m/g , where the light-cone numerical results are not sufficiently accurate for comparison. Increasing N from two to four brings results to almost within errors of the large- N limit for most m/g .

In assessing the large- N approximation, two different questions can be addressed. First, how good a description does the leading large- N term provide of solutions at a particular finite N ; that is, is it accurate? And second, do actual measured quantities scale with N as assumed in this scheme; that is, is it consistent? Evidently, for the lightest meson, it is accurate at all N and m/g . The latter is somewhat surprising; because the relevant coupling is really $g^2 N/m^2$, an expansion in this parameter is unreliable at small enough m .

Baryon masses are expected to scale proportionally with N , based mainly on nonrelativistic reasoning.^[29,30] Consequently, baryon masses are infinite in this limit and they decouple. From Fig. (5b), unlike Fig. (7), it is clear that two is not a large number. In fact, for $N = 2$, the lightest baryon has the same mass as the meson, and so it is not reasonable to neglect it. Nevertheless, for most values of m/g , the baryon mass does indeed scale with N . For any finite fixed m/g , the baryon will decouple at large enough N .

In the limit that $m/g \rightarrow 0$, N fixed, the baryon mass goes to zero; as m decreases, the N at which this approximation is sensible must increase; or, for fixed N , the approximation becomes progressively less accurate as m decreases. Also, it will be argued that in the valence quark approximation, the baryon mass is proportional to $mgN^{1/2}$ as $m \rightarrow 0$, and so at least in this approximation, the

baryon mass grows as $N^{1/2}$ rather than N . The inclusion of higher-Fock states will adjust this, but most likely not enough to restore the power to one.

The surprisingly good agreement for mesons even at $N = 2$ may be understood by noting that the large- N meson Bethe-Salpeter equation derived diagrammatically in Ref. [21] is identical to that derived for the light-cone Schrodinger equation restricted to the $q\bar{q}$ Fock space as in Chapter (3), after replacing the coupling $g^2(N^2 - 1)/2N$ by its large- N limit, $g^2N/2$. If the valence approximation for mesons is accurate, then, insofar as $(N^2 - 1)/2N$ is close to $N/2$, the large- N approximation must be accurate as well. For large quark mass m , this is guaranteed to be the case; for identically zero m , it will also be shown that a massless meson can be created from only a single $q\bar{q}$ pair. It is then not surprising that the valence approximation, which is exact at both extremes, is reasonable at all m/g . Because this is true regardless of N , the accuracy of the large- N approximation at these small N should probably be considered coincidental.

Finally, converting the program to solve for the gauge group $U(N)$ as opposed to $SU(N)$ involves only removing the term in the interaction which cancels the trace. This is equivalent to crossing $SU(N)$ with massive electrodynamics, or $U(1)$. In the large- N limit, $U(N)$ and $SU(N)$ are identical, and so their actual difference at finite N gives another indication of accuracy. The lightest meson masses for $U(2)$ and $SU(2)$ are plotted in Fig. (8). In particular, for most values of m/g , $U(2)$ is even closer to the large- N meson than $SU(2)$, because in the $q\bar{q}$ integral equation, to be presented in Chapter (3), the factor $g^2(N^2 - 1)/2N$ is replaced by its large- N limit, $g^2N/2$, for $U(2)$. However, there is another term which will appear in that equation for $U(N)$ proportional to $g^2/2\pi$, which is a reflection of

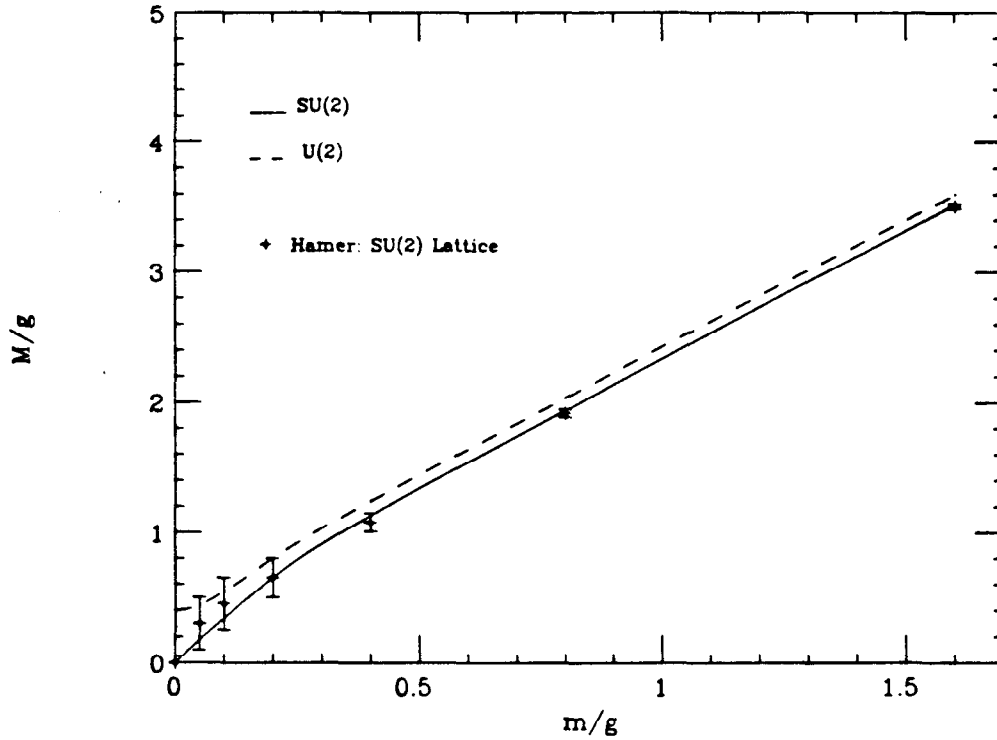


Figure 8. Lightest Meson Mass for $SU(2)$ and $U(2)$.

the axial anomaly that gives the Schwinger Model boson its mass. In fact, for all $U(N)$, the lightest meson at $m = 0$ will have a mass of $g/(2\pi)^{1/2}$. Because $g^2 N$ is considered fixed as $N \rightarrow \infty$, this mass is neglected to leading order in $1/N$.

As an aside, the particular case of $U(1)$, or the massive Schwinger model, was also studied. The program produces results consistent with those of Ref. [20]. These are themselves consistent with other calculations of this model and, in particular, give exact results for massless electrons.

2.3. QUARK-ANTIQUARK VALENCE WAVEFUNCTIONS

Because the wavefunction in the valence approximation involves only a $q\bar{q}$ pair, it is possible to plot the wavefunction directly. This is done in Figs. (9a-e) for the lowest-lying $N = 3$ meson and the first three excited states as m/g ranges from 1.6 to .1. In these, $2K = 90$, and the corresponding step size in x is $1/90$. As a consequence, the accessible values for x nearest the endpoints are $1/90$ and $89/90$.

For weak coupling, the wavefunctions are reminiscent of the quantum mechanical (momentum-space) wavefunctions for a particle in a linear potential, and as m/g becomes large, that is what they become. The kinetic term m^2/x forces the wavefunctions to zero at $x = 0$ and 1 , and as m becomes large relative to g , as in Fig. (9a), this endpoint suppression is evident for an increasing range in x .

For highly excited states with a large number of oscillations, the relative importance of the endpoints decreases. As discussed in Refs. [21] and [30] it is not a bad approximation to incorporate the effect of the kinetic term as simply the boundary condition $\phi(0) = \phi(1) = 0$. The n^{th} excited state ϕ_n is analogous to that of a free particle in a box in x ,

$$\phi_n \sim \sin n\pi x \tag{2.2}$$

with a mass

$$M_n^2 \sim g_N^2 \pi n. \tag{2.3}$$

When m/g is very large, n must be large before the actual form of the kinetic term is unimportant. For $m/g \sim 0$, this picture will be seen to break down altogether. From Fig. (9b), it seems that it is most likely to be accurate for $m/g \sim 1$.

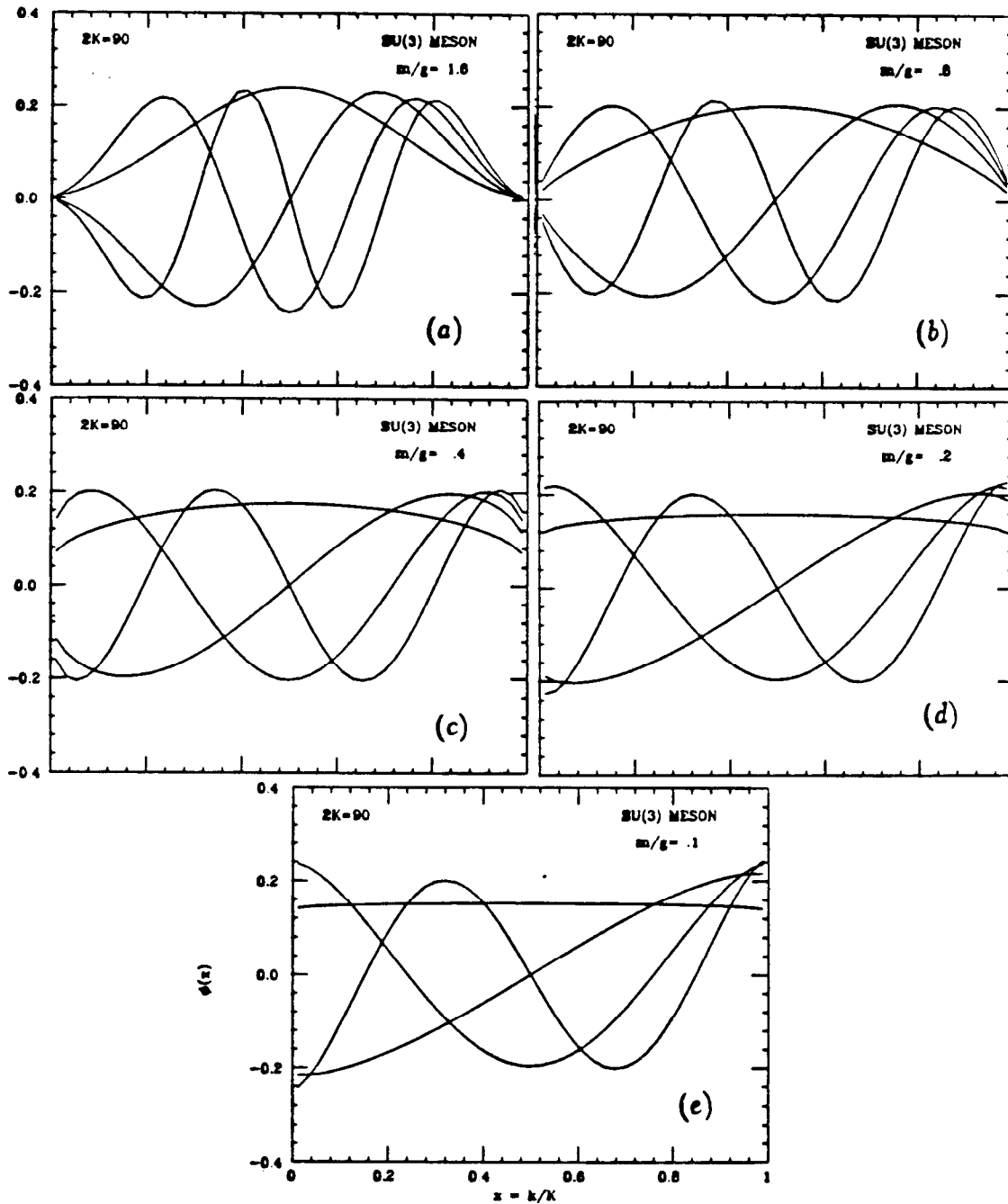


Figure 9. Wavefunctions for First Five $N = 3$ Mesons in $q\bar{q}$ (Valence) Approximation.
 (a) $m/g = 1.6$; (b) $m/g = .8$; (c) $m/g = .4$; (d) $m/g = .2$; (e) $m/g = .1$.

Finally, in the strong coupling limit, as in Fig. (9e) where $m/g = .1$, the interaction term dominates so much so that the turnover of the wavefunction to zero at the ends is not discernable at this resolution in x , that is $\Delta x = 1/90$. In fact, over most of x , the wavefunction is much more like an oscillating string with free rather than fixed ends.

2.4. STRUCTURE FUNCTIONS

Apart from valence mesons, which involve only two particles, it is not convenient to display wavefunctions directly, due to the large number of potential plotting variables and the inability to distinguish quarks with the same quantum numbers. The quark (and antiquark) structure functions are defined by

$$q_k = \langle \phi(K) | b_k^{\dagger c} b_{k,c} | \phi(K) \rangle ,$$

with $d_{k,c}^{\dagger} d_k^c$ replacing $b_k^{\dagger c} b_{k,c}$ for \bar{q}_k . They describe the manner in which the momentum K is distributed among the quarks, and have the advantage of being functions of a single variable. The q_k automatically satisfy a baryon number sum rule

$$\sum_k (q_k - \bar{q}_k) = \begin{cases} 0 & \text{for mesons} \\ N & \text{for baryons} \end{cases} , \quad (2.4)$$

the momentum sum rule

$$\sum_k (q_k + \bar{q}_k) = K, \quad (2.5)$$

and so on. In the continuum limit, k/K becomes the Bjorken variable x , and the

continuum structure function is $q(x) = Kq_k$. These are then normalized such that

$$\int_0^1 dx (q(x) - \bar{q}(x)) = 0 \text{ or } N \quad (2.6)$$

for mesons or baryons.

Besides being simple to plot, these functions are physically useful, and are measurable in deep inelastic scattering, at least in four dimensions. (Note that these are related to the commonly used parton model structure functions $f(x)$ by $xq(x) = f(x)$.) This provides one of the main motivations for attempting to solve *QCD* on the light cone. Apart from the apparent numerical advantages, the wavefunctions which result are directly related to experimentally measured quantities.

2.5. VALENCE STRUCTURE FUNCTIONS

The structure functions $q(x)$ for the lowest-lying *SU*(3) meson and baryon are displayed in Fig. (10), at relatively weak ($m/g = 1.6$) and strong ($m/g = .1$) coupling. These correspond to values of .3325 and .9847 for the dimensionless coupling λ . Specifically, these are the contributions to $q(x)$ from the valence wavefunctions. Higher-Fock wavefunctions contribute very little to these states, as will be discussed later.

When m/g is large, $k^+ = (k^2 + m^2)^{1/2} + k$ is dominated by the quark mass. The total P^+ is then approximately m times the number of quarks. Consequently, $q(x)$ peaks strongly about $1/2$ and $1/3$ (or $1/N$) for the meson and baryon, respectively. As m/g decreases, the effect of the quark mass diminishes, and the distribution

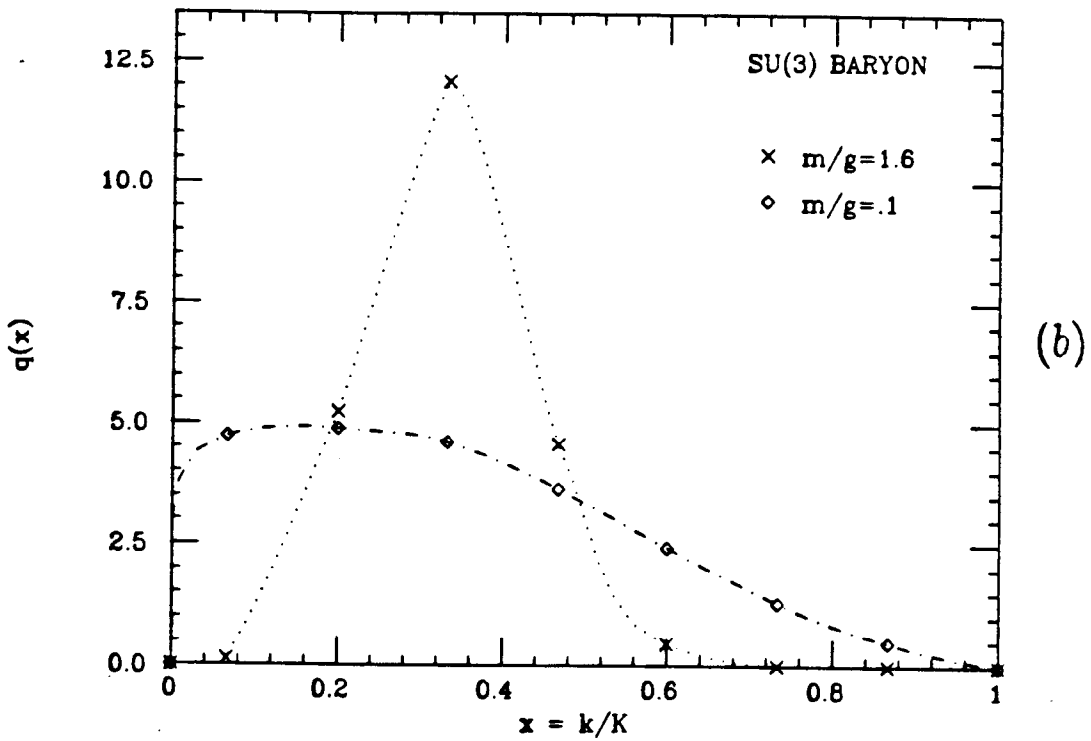
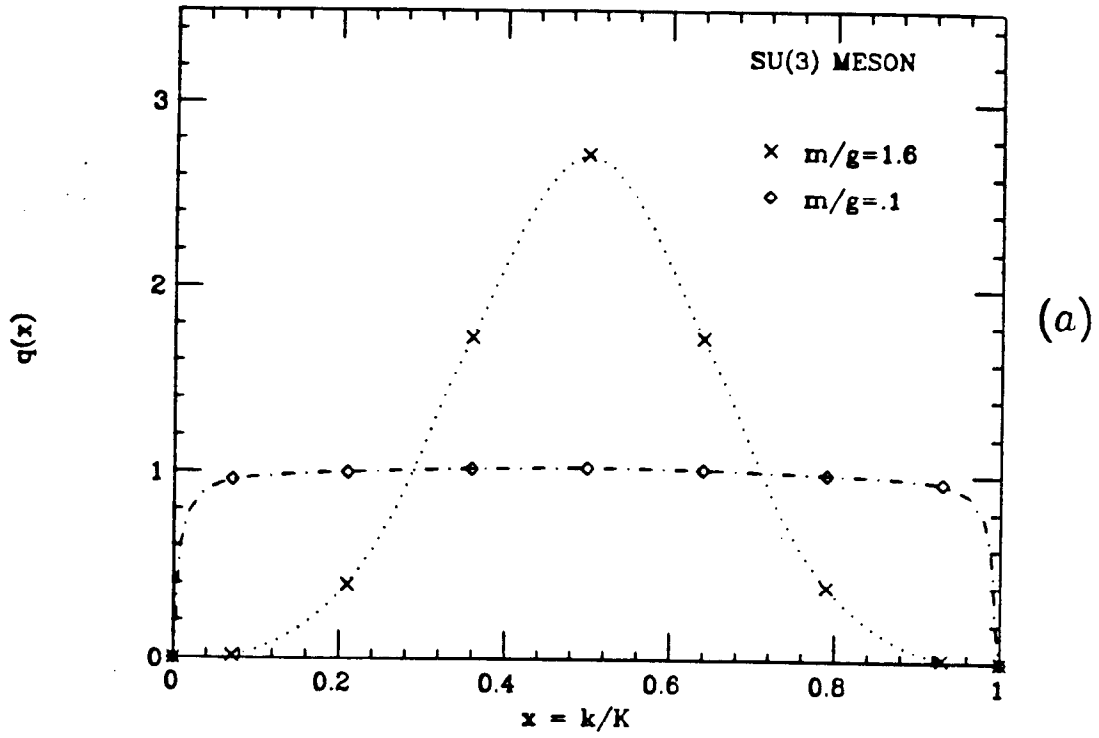


Figure 10. Structure Functions for the Lightest $N = 3$ Meson and Baryon. (a) Meson; (b) Baryon.

in x spreads. As will be shown, at strong coupling $q(x)$ is governed entirely by combinatorics; any momentum is as likely as another, subject only to momentum conservation, $\sum x_i = 1$. In all cases, wavefunctions, and therefore structure functions, are forced to zero when any quark carries zero momentum due to the kinetic term m^2/x . The relative strength of g/m , which multiplies the interaction term, determines the x at which this suppression sets in. It should be noted that the value of $q(x)$ at the data points $x = 0$ and 1 in these plots are inferred; the smallest x actually carried by a quark is $1/2K$.

2.6. GENERAL WAVEFUNCTION RESULTS

Because of the simplicity of the vacuum, all of the quanta appearing in eigenstates, or wavefunctions, are directly associated with hadrons. Consequently, the nature of a particular state is often relatively simple to deduce from the form of the wavefunction.

In Figs. (11a-c), the valence and four quark contributions to the quark structure function for the first three $N = 3$ meson ($B = 0$) states are plotted for relatively weak coupling and $2K$ of 24. These can be interpreted as the $q\bar{q}$ meson and its first two radial (in x^-) excitations. Their interpretation is particularly simple because the higher-Fock contribution is so strongly suppressed, due, at least in part, to the large quark mass. Fig. (11d), the eleventh state in the spectrum, is composed predominantly of two $q\bar{q}$ pairs, peaked at $x = 1/4$. This evidently corresponds to a pair of the lightest mesons, and its mass is twice that of the lightest meson.

Corresponding plots for the first three $SU(3)$ baryon ($B = 1$) states are shown in Figs. (12a-c). These also represent a predominantly valence (three-quark)

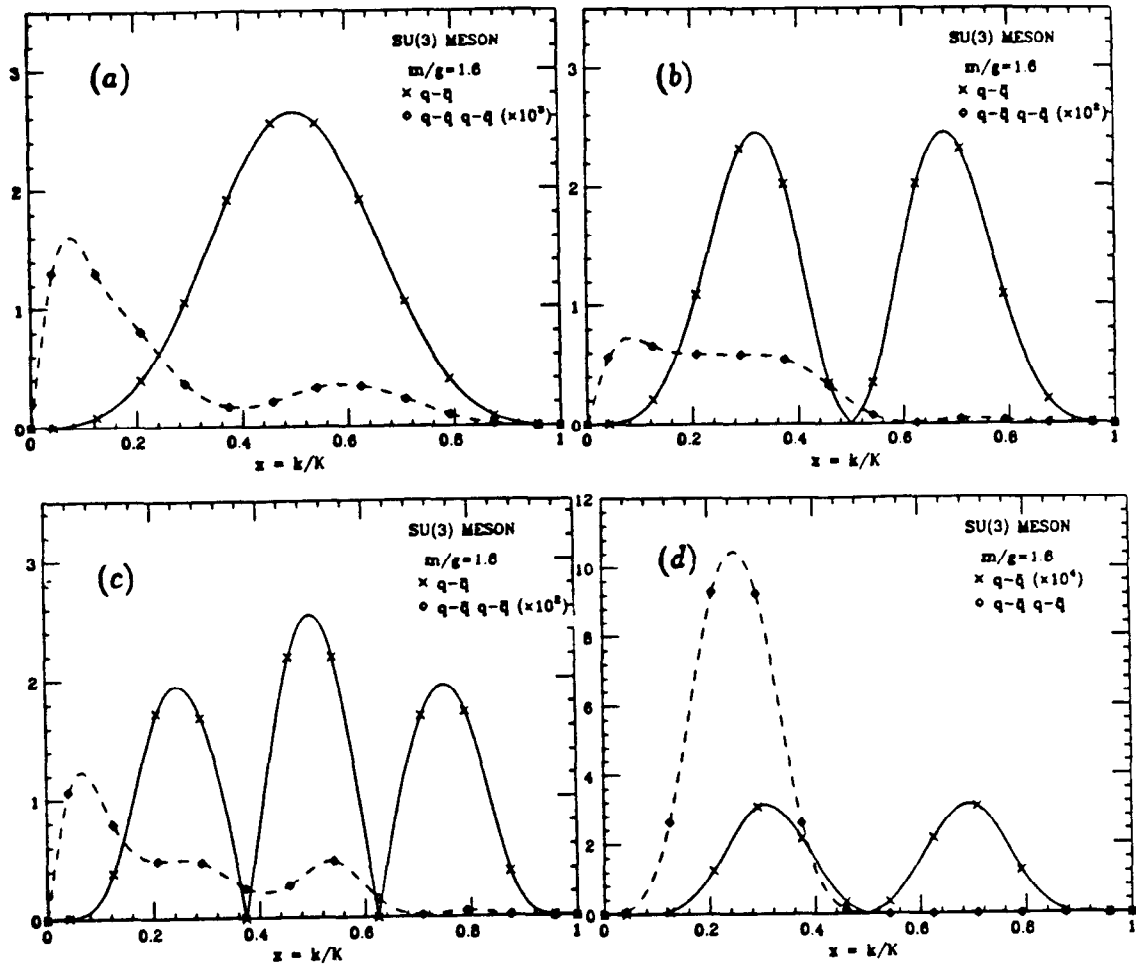


Figure 11. Structure Functions for the Valence and Four-Quark $N = 3$ Meson Wavefunctions at Weak Coupling. (a) Lowest State; (b) Second State; (c) Third State; (d) Eleventh State.

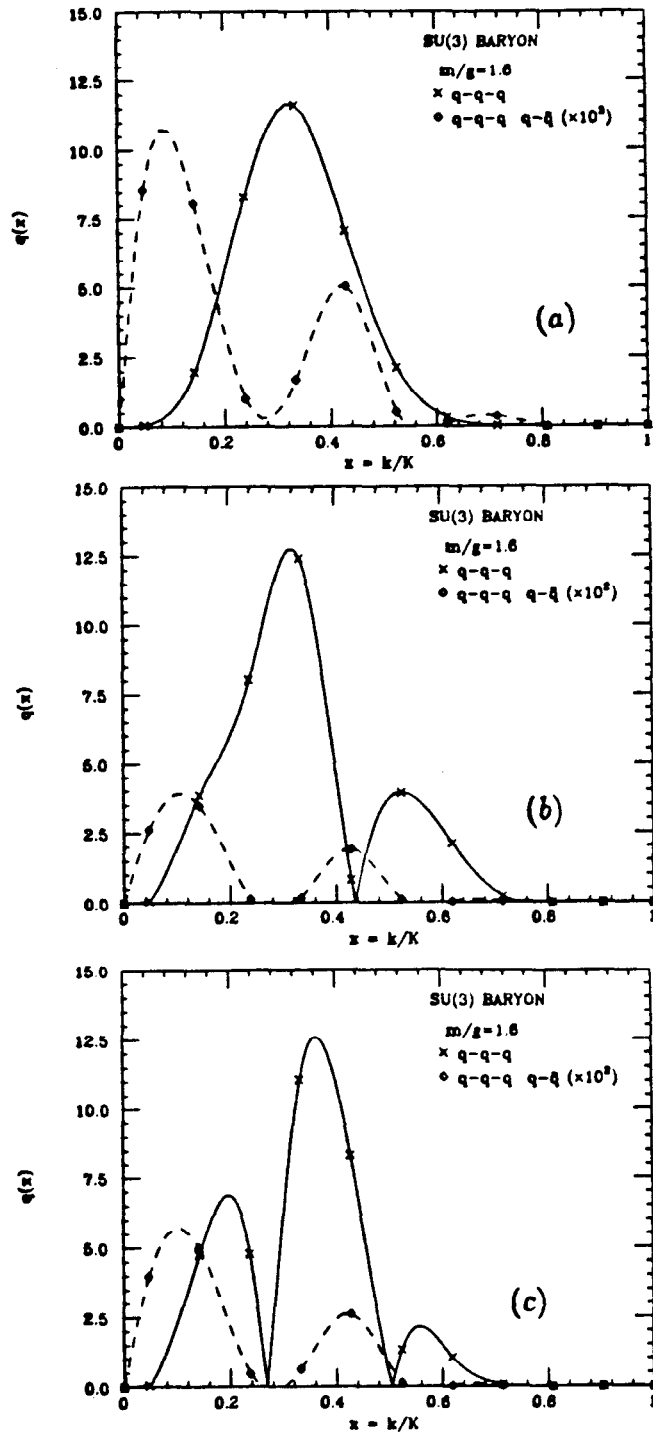


Figure 12. Structure Functions for the Valence and Five-Quark $N = 3$ Baryon Wavefunctions at Weak Coupling. (a) Lowest State; (b) Second State; (c) Third State.

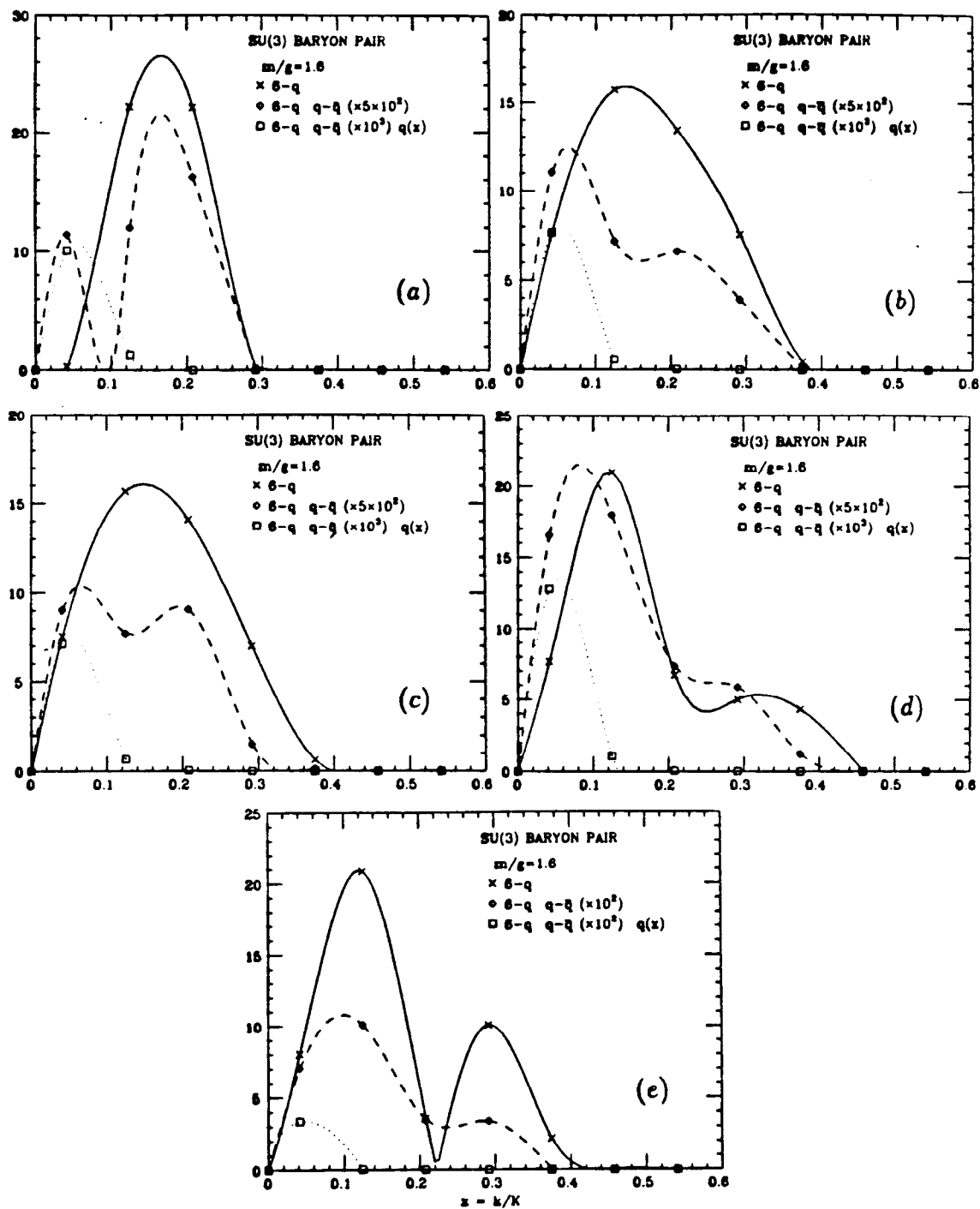


Figure 13. Structure Functions for the Valence and Eight-Quark $N = 3$ Two-Baryon Wavefunctions at Weak Coupling. (a) Lowest State; (b) Second State; (c) Third State; (d) Fourth State; (e) Fifth State. Note the change in Scale.

baryon and its radial excitations, with suppressed contributions from the component with an extra $q\bar{q}$. The state with a pair of the lightest baryons may be formed as the lightest state in the $B = 2$ spectrum, Fig. (13a). Included in this plot is the antiquark function $\bar{q}(x)$, which gives an indication of the magnitude and momentum distribution for the meson content of the $SU(3)$ baryon. For completeness, Figs. (13d-e) give the next four $B = 2$ states. These are easy to interpret as various combinations of the first few $B = 1$ states.

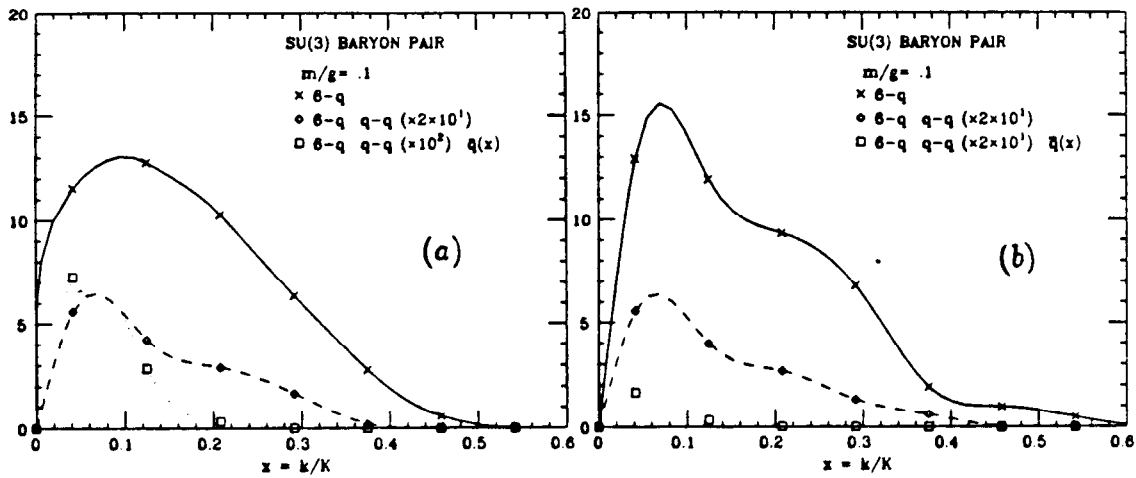


Figure 16. Structure Functions for the Valence and Eight-Quark $N = 3$ Two-Baryon Wavefunctions at Strong Coupling. (a) Lowest State; (b) Second State.

In Figs. (14) to (16), the corresponding first several states' structure functions are plotted at strong coupling, $m/g = .1$. The connecting curves are simply cubic spline fits; the resolution is in some cases not good enough for these to accurately depict the actual structure. It is apparent from these plots that an interpretation of the spectrum in this limit as constructed of various combinations of essentially valence mesons and baryons and their radial excitations is not as obvious. Such a

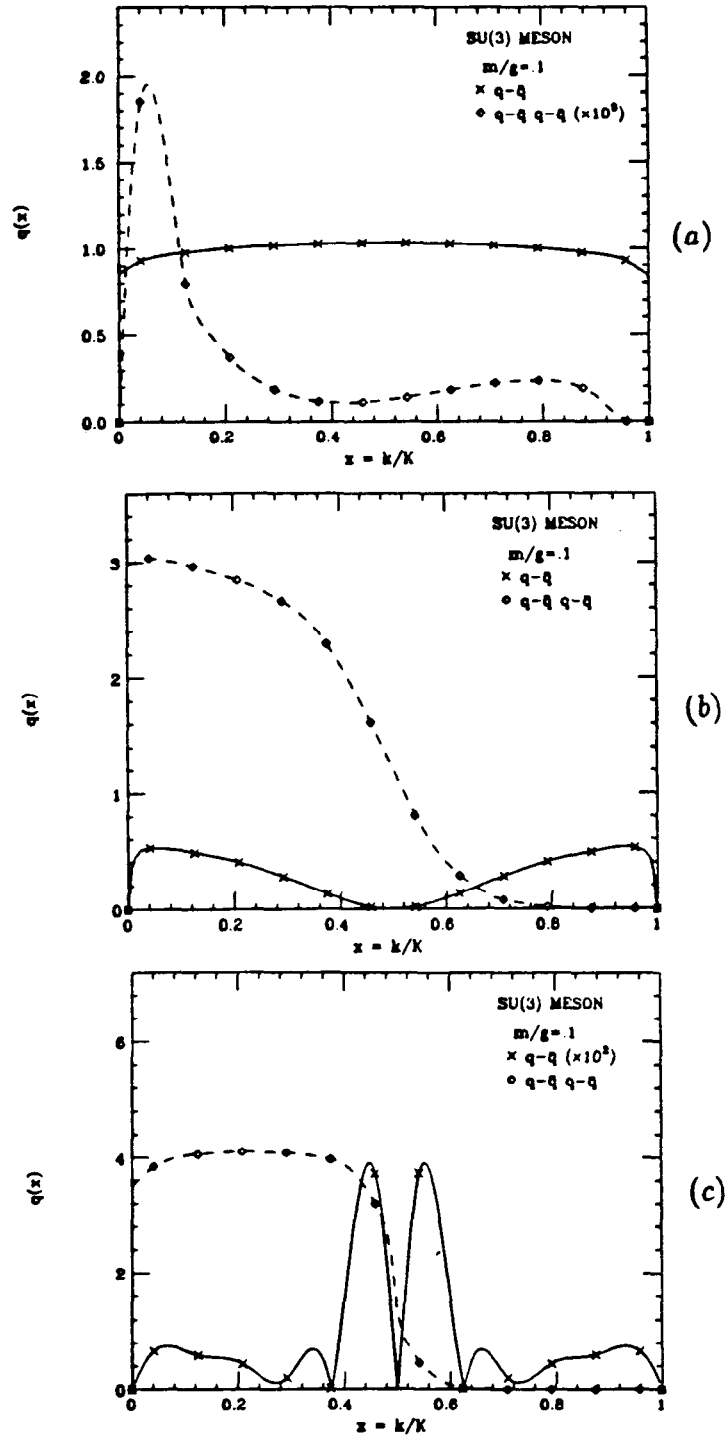


Figure 14. Structure Functions for the Valence and Four-Quark $N = 3$ Meson Wavefunctions at Strong Coupling. (a) Lowest State; (b) Second State; (c) Third State.

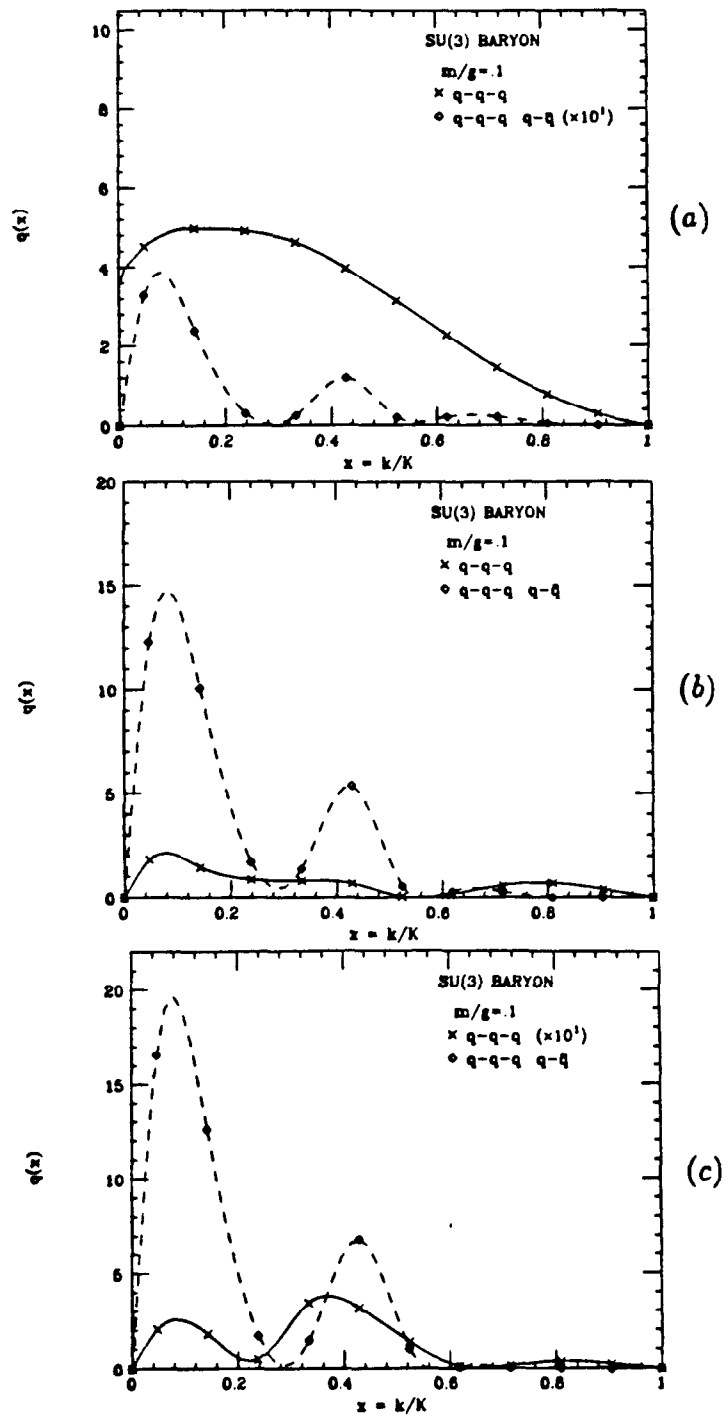


Figure 15. Structure Functions for the Valence and Five-Quark $N = 3$ Baryon Wavefunctions at Strong Coupling. (a) Lowest State; (b) Second State; (c) Third State.

characterization based on essentially valence hadrons is not even necessarily meaningful. As will be shown, in the continuum limit for vanishing quark mass, it will be possible to append extra massless, zero momentum $q\bar{q}$ pairs to existing states without altering their mass, producing large degeneracies which include states with arbitrarily large numbers of quarks.

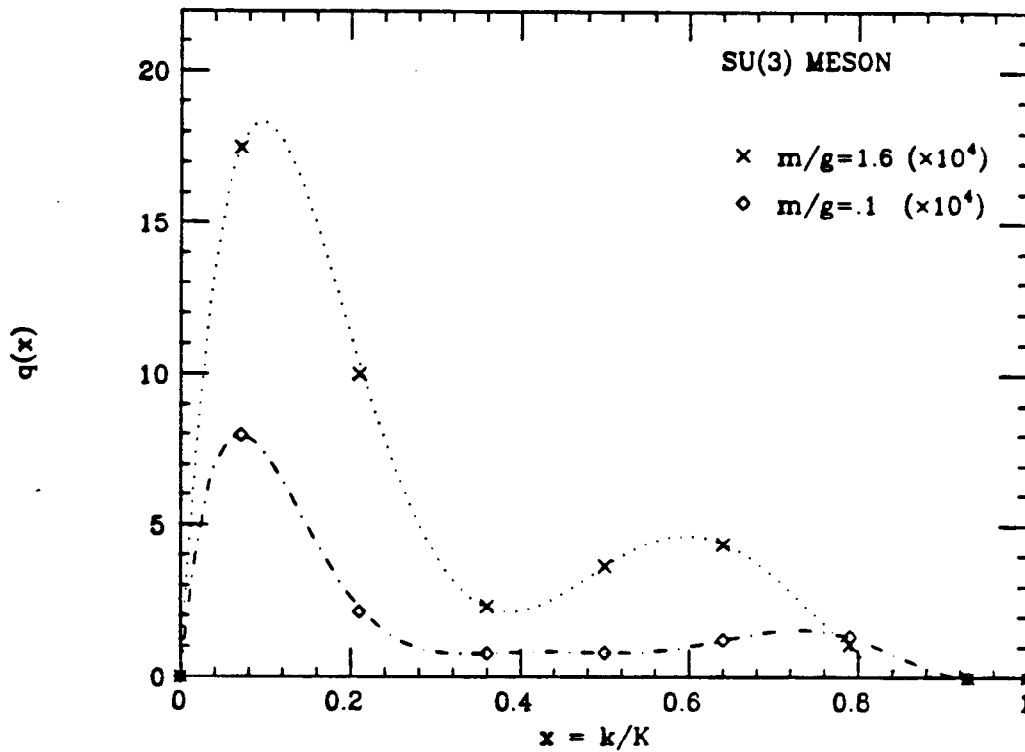


Figure 17. Contribution to Lightest $N = 3$ Meson Structure Function from Four-Quark Wavefunction.

One of the advantages of this numerical approach is that it is not necessary to make a priori simplifying assumptions regarding the Fock state structure of the eigenstates. In particular, the role which higher-Fock states play in the composition of hadronic light-cone wavefunctions can be studied for arbitrarily fine resolution in momentum, subject of course to available computing power. This is a potentially

rich field for future work, even in two dimensions, and particularly when flavor is included. In this section, only the general features of these states will be discussed.

First, for all couplings g/m , the content of the next higher Fock states is strongly suppressed, typically by several orders of magnitude, for the lowest-lying mesons and baryons. The $SU(3)$ hadrons in Figs. (17) and (18) are typical. Note that in Fig. (18b), the probability for the state with two extra $q\bar{q}$ pairs is comparably suppressed relative to one extra, and in most cases states with greater than one pair could be safely neglected. For very massive quarks this is expected for all low-lying states, as more quarks mean more mass. It is not clear why it is true when the quark mass is small, although this is only true for the very lightest states in this case. Other low-lying states have substantial, even dominant, higher-Fock components.

Second, typical behavior for the lightest meson Fock state with one extra quark pair as a function of N is displayed in Fig. (19) for $SU(N)$ and Fig. (20), for $U(N)$. For fixed, weak coupling, the content is strongly suppressed but relatively insensitive to N , while at strong coupling it diminishes rapidly as N increases. For $U(N)$ in this limit, the higher Fock content vanishes altogether in the strong coupling limit; the massive Schwinger meson is known to be composed entirely of a $q\bar{q}$ pair.^[23,20] Since in this limit these $q\bar{q}$ pairs carry a mass-squared of $g^2/2\pi$, extra pairs cannot mix with the lightest meson without significantly increasing its mass.

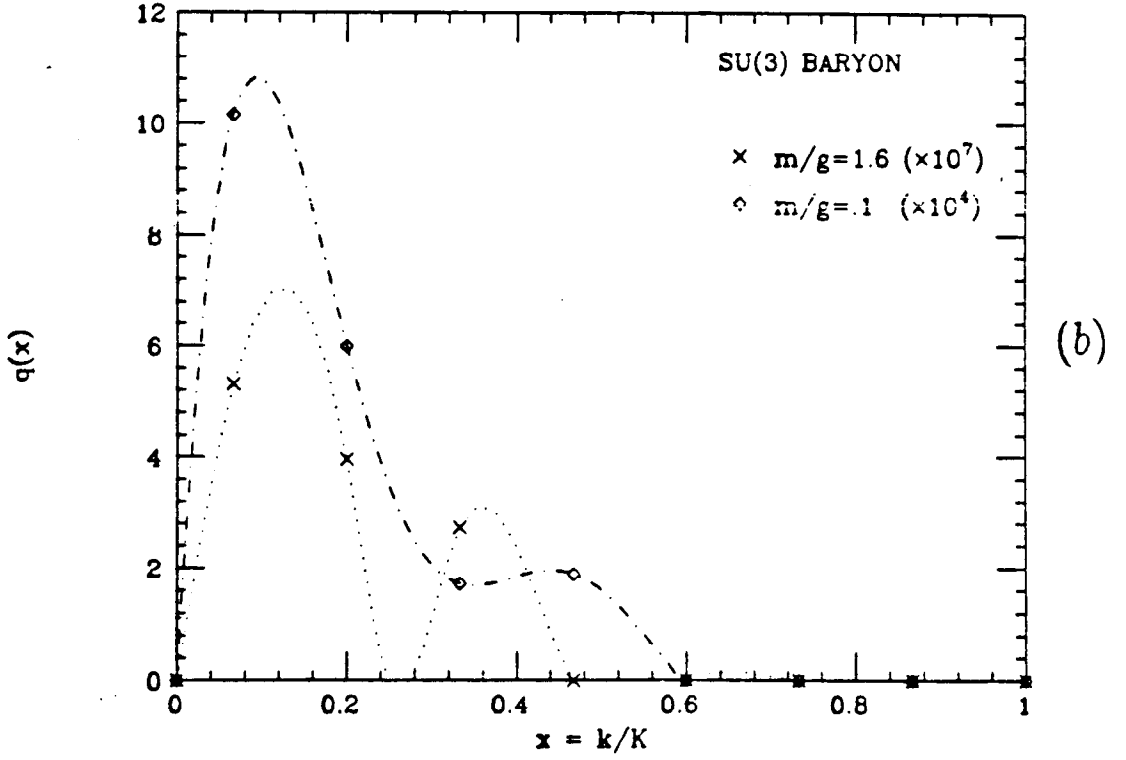
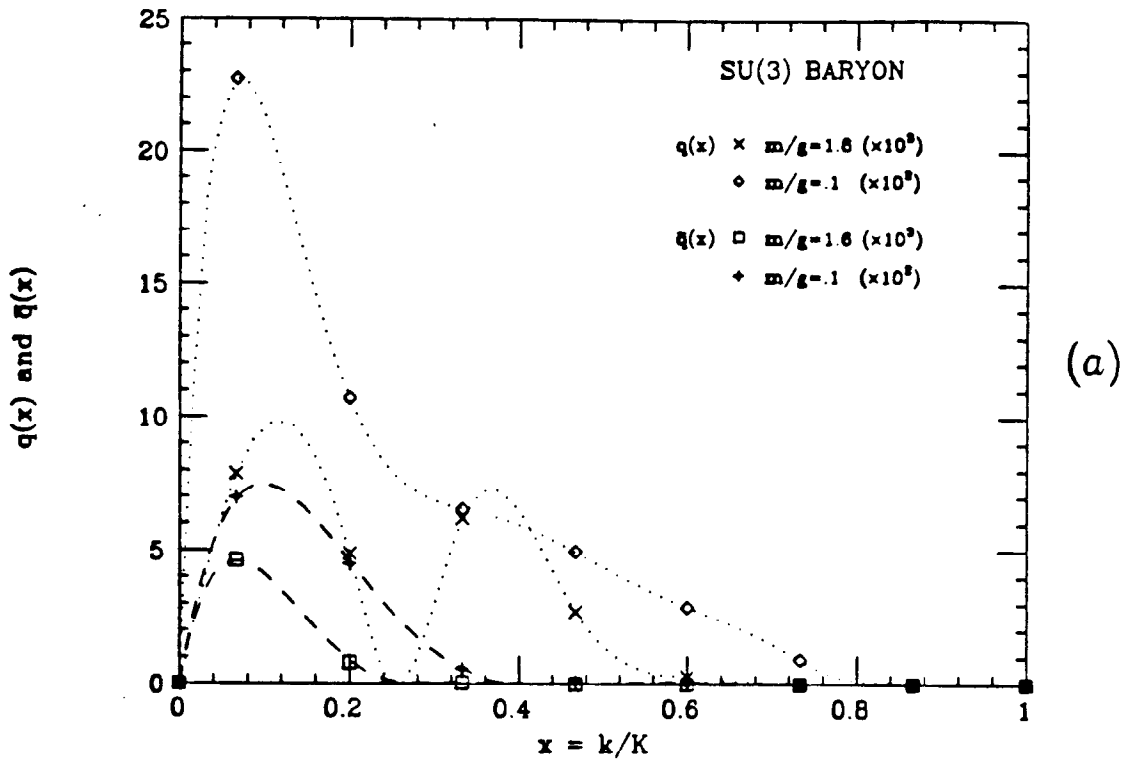


Figure 18. Contribution to Lightest $N = 3$ Baryon Structure Function. (a) From Five-Quark Wavefunction; (b) From Seven-Quark Wavefunction.

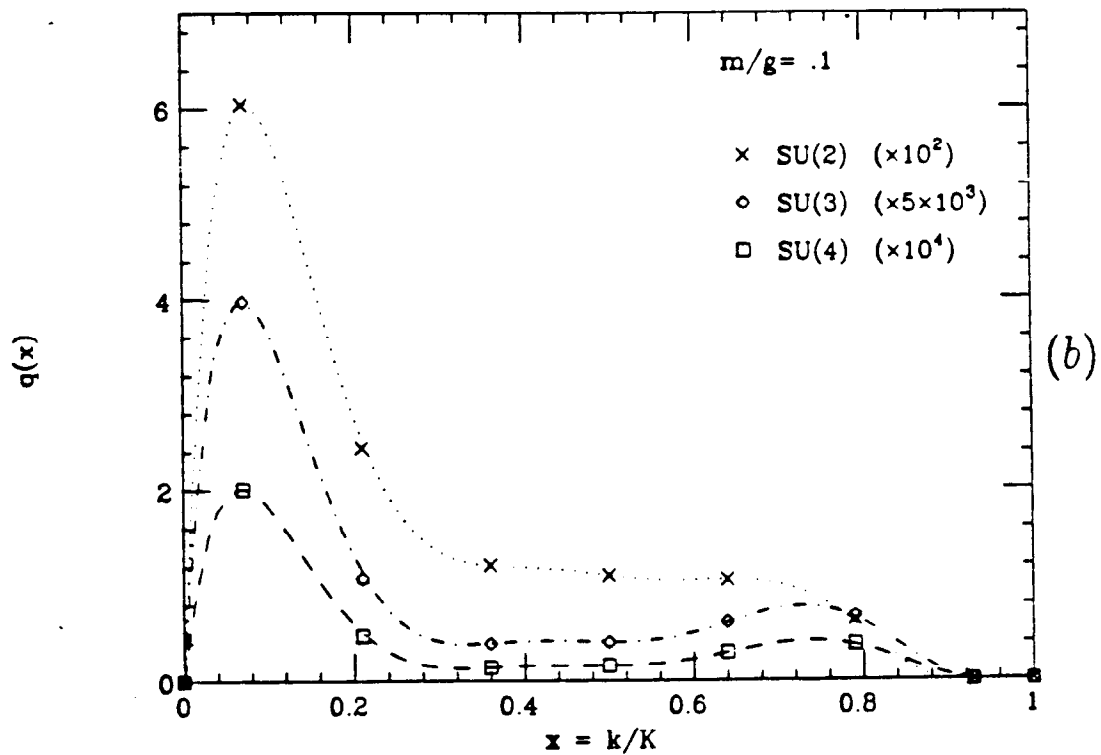
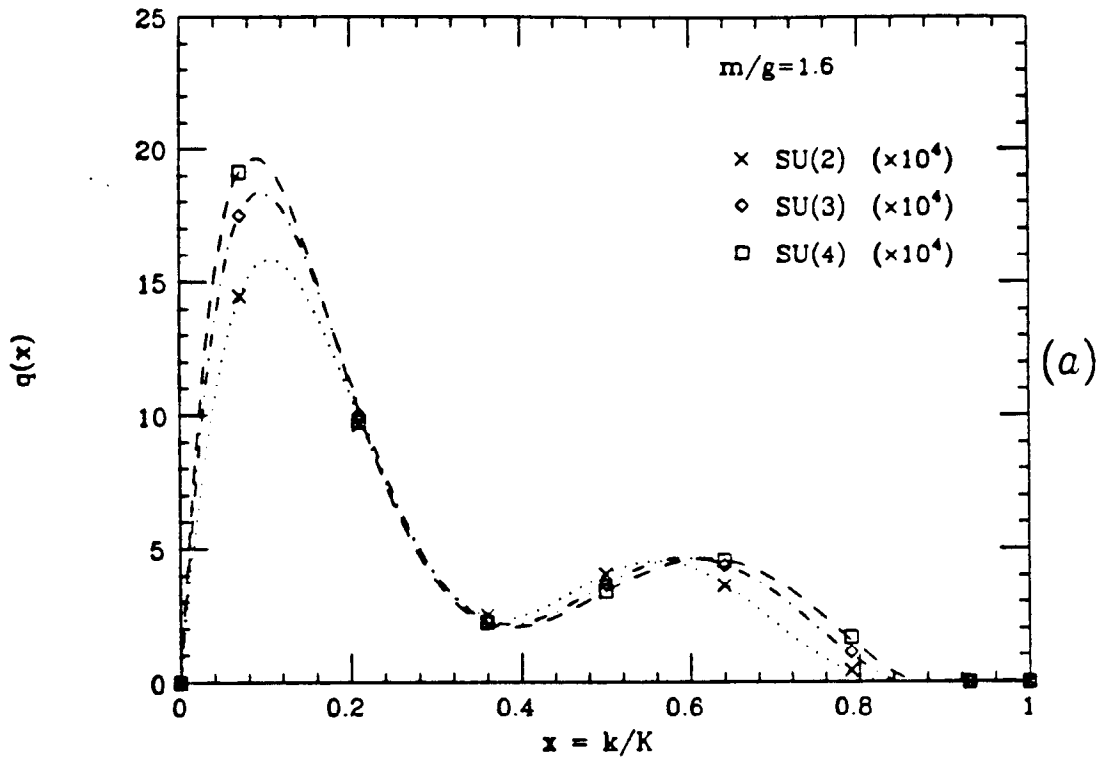


Figure 19. Contribution to Lightest Meson Structure Function from the Four-Quark Wavefunction as a Function of N_c . (a) Weak Coupling; (b) Strong Coupling.

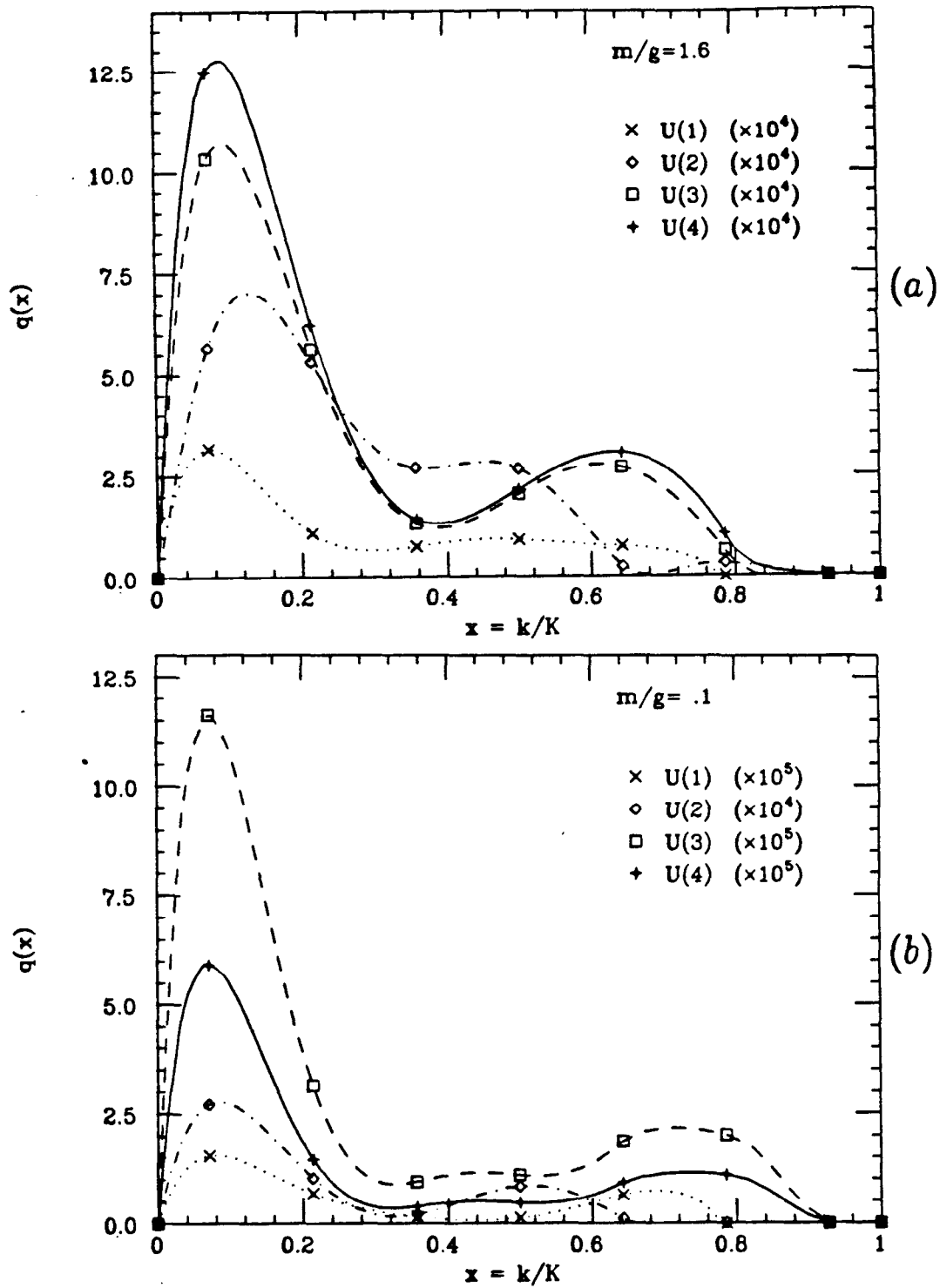


Figure 20. Contribution to Lightest $U(N)$ Meson Structure Function from the Four-Quark Wavefunction as a Function of N . (a) Weak Coupling; (b) Strong Coupling.

Table [5]

N	m/g	$1 - P(q\bar{q})$
2	1.600	$.2072 \times 10^{-3}$
3	1.960	$.1325 \times 10^{-3}$
4	2.263	$.9579 \times 10^{-4}$
2	.1000	$.9889 \times 10^{-2}$
3	.1225	$.2921 \times 10^{-3}$
4	.1414	$.1277 \times 10^{-3}$

In the large- N limit, the higher-Fock content would be expected to vanish, as the meson is composed entirely of valence quarks, and meson-meson couplings are suppressed by an extra power of N . In this expansion, $g^2 N$, rather than g , is held fixed. In order to determine the importance of higher-Fock states as a function of N with this limit in mind, g should be scaled by $N^{-1/2}$. In Table [5], the probability for finding the lowest-lying meson in other than its valence wavefunction is listed for $N = 2, 3$ and 4 for both weak and strong coupling. For these results, $2K$ is fixed at 20. Only states with at most two $q\bar{q}$ pairs are included, as higher-Fock states are negligible relative to these. For the weak and strong coupling cases, m/g is set to 1.6 and .1, respectively, for $N = 2$, and g is scaled to keep $g^2 N$ fixed for $N = 3$ and 4.

Clearly the importance of the higher-Fock states diminish with N . Holding $g^2 N$ fixed for increasing N is equivalent to decreasing g or to increasing m , so this result is not surprising. Larger N means heavier quarks, and it is kinematically more costly to have states with more of them. However, this does not explain why,

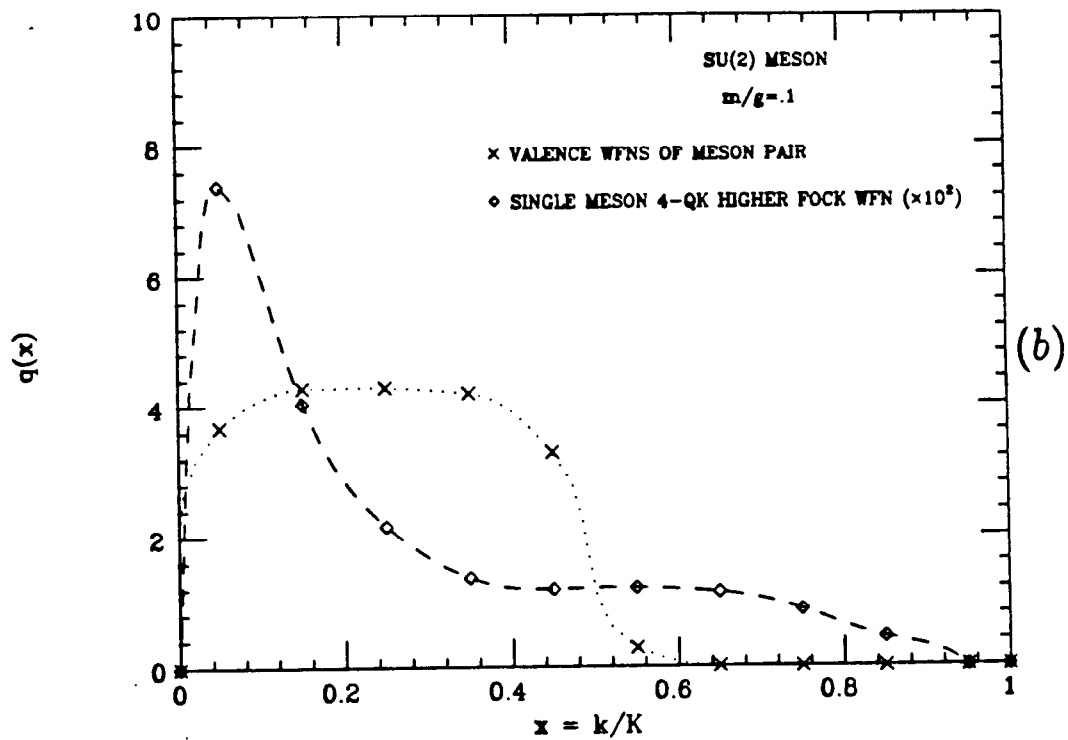
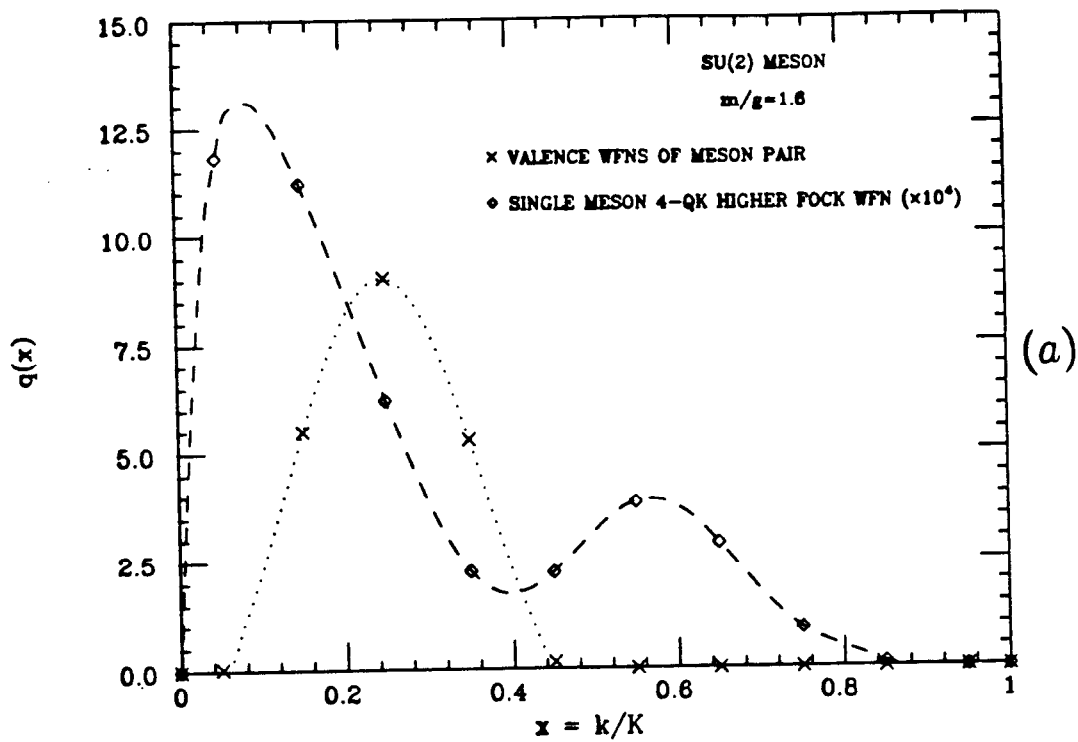


Figure 21. Comparison of Single Meson Four-Quark Higher-Fock Wavefunction with Wavefunction of a Pair of Valence Mesons. (a) Weak Coupling; (b) Strong Coupling.

even for the very small m/g near .1, this probability is so small to begin with.

Finally, most higher-Fock states share a characteristic, double-bump structure in x , regardless of g/m or N . It is likely that there are more peaks in these states, but at these values of K the resolution is not high enough to discern any finer structure. Because of this characteristic shape, it is not difficult to distinguish by shape as well as magnitude, for example, four-quark continuum states made from a pair of lighter $q\bar{q}$ mesons from the higher-Fock component for a single meson, as in Fig. (21).

2.7. HIGHER-FOCK WAVEFUNCTIONS

Many successful approximation schemes such as the $1/N$ expansion for mesons, and phenomenological models, such as the nonrelativistic quark model, begin by describing hadrons as predominantly composed of valence quarks. This is certainly a reasonable assumption for very massive quarks, but there is no good reason to believe the same for light quarks. In fact, the probability of finding a hadron composed of light quarks in its valence state could conceivably be negligible. Because no such approximation need be made in the approach here, it is possible to determine explicitly the importance of higher-Fock states in describing mesons and baryons, at least in two dimensions. As the quark mass or coupling constant are varied, the region where such a picture breaks down may also be determined.

A rough estimate of the higher-Fock component to expect in an eigenstate of mass M may be made by comparing the invariant mass of these higher states to M . Each Fock state of n particles may be assigned a mass-squared based on the

light-cone energies of free quarks,

$$\Lambda_n^2 \equiv \sum_{i=1}^n \frac{m^2}{x_i}, \quad (2.7)$$

which is minimum when all the x_i are approximately $1/n$; that is, when the light-cone momentum is equally distributed. In that case,

$$\Lambda_n^2 \gtrsim n \cdot \frac{m^2}{1/n} = n^2 m^2. \quad (2.8)$$

A Fock state for which $\Lambda_n^2 \gg M^2$ should not contribute significantly to a state of that mass. States with n quanta should appear prominently in such a state only when their minimum invariant masses satisfy

$$\Lambda_n^2 \text{ min} \sim M^2, \quad (2.9)$$

so that, by Eq. (2.8),

$$n \sim M/m. \quad (2.10)$$

This is clearly true when the quark mass m is large. In the opposite limit, as the quark mass vanishes,

$$M \sim (gm)^{\frac{1}{2}} \quad (2.11)$$

for all hadrons, and therefore

$$n \sim \left(\frac{g}{m}\right)^{\frac{1}{2}}. \quad (2.12)$$

The exponent $1/2$ is correct in the large- N limit, and it is likely that it provides a reasonable estimate at finite N , as will be discussed below. In this limit, Fock

states with any number of quanta can appear. How many actually do may be determined numerically.

Consider first the lightest meson in $SU(2)$. The contribution to the wavefunction from higher-Fock states may be measured by how much the probability of finding the meson in its valence state differs from one. This has been computed numerically for various coupling constants:

Table [6]

λ	m/g	$1 - P(q\bar{q})$
.3325	1.6	$.15(3) \times 10^{-3}$
.5763	.8	$.9(1) \times 10^{-3}$
.8158	.4	$.30(2) \times 10^{-2}$
.9425	.2	$.74(6) \times 10^{-2}$
.9847	.1	$.111(3) \times 10^{-1}$
.9961	.05	$.1296(5) \times 10^{-1}$

The values and errors were determined using Richardson extrapolation from values of $2K$ ranging from 10 to 24. The numbers in parentheses give an estimate of the uncertainty in the last digit given by the magnitude in the final term in the Richardson series. In practice it was possible to restrict the space to at most four-quark states. When computed, six-quark and higher states contributed less than .1% to these values at any value of K , and so fall below the errors.

As expected, the probability for higher numbers of quarks is negligible when very massive. Their presence increases steadily with decreasing mass (or increasing coupling) up to m/g around .2, where it appears to level off at about a per cent.

As will be discussed, results for couplings of λ beyond .9425 are probably not reliable enough to allow any firm conclusions about this region to be drawn. What is surprising is that even as the quarks become massless, the contribution from one extra quark pair remains extremely small, and that that from more quarks is essentially negligible. On the other hand, very light states, which become massless with the quark mass, do exist in the spectrum which are in fact dominated by higher-Fock states. So states with large numbers of extra quarks do dominate the low energy spectrum as the quark mass vanishes, but this cannot be detected in the very lightest meson.

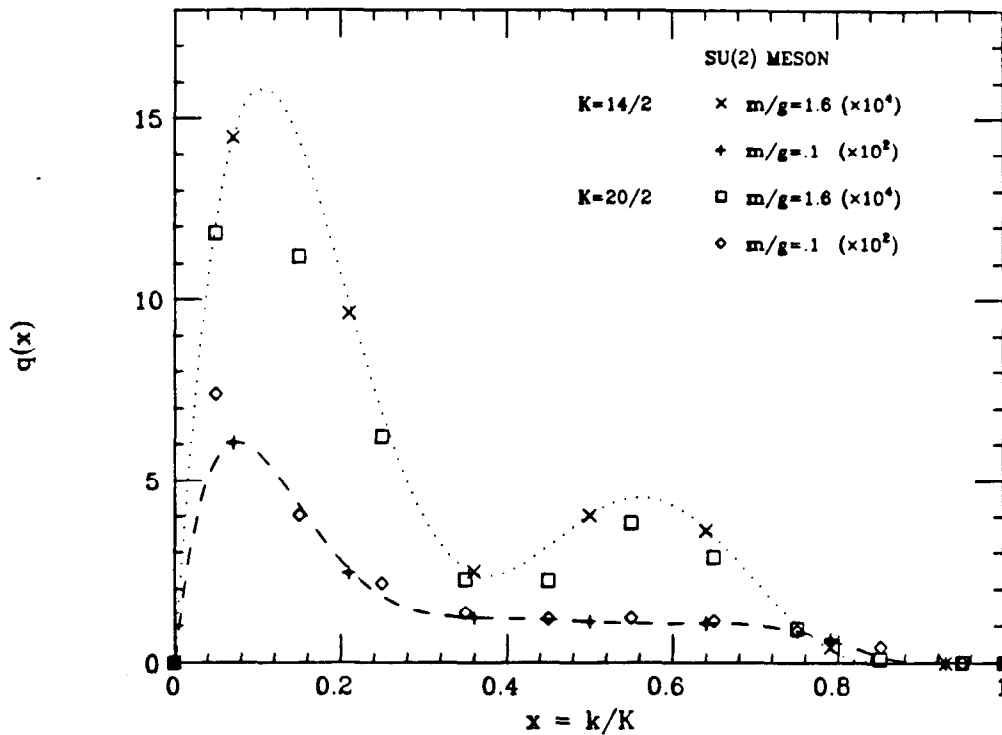


Figure 22. Dependence of $N = 2$ Meson Higher-Fock Wavefunction on Momentum K .

Valence wavefunctions, especially for the lowest-lying states, display only mi-

nor sensitivity to the numerical momentum, or resolution, K . To estimate the sensitivity of higher-Fock state wavefunctions, the four-quark contribution to the quark structure function is plotted in Fig. (22) at $2K$ equal to 14 and 20 for both the weakly and strongly coupled $SU(2)$ meson. The curves are cubic spline fits to the points from $2K = 14$ and are included for ease of comparison.

Note that in order to meaningfully compare these at different K , it is necessary to plot the structure function $q(x_k) \equiv K q_k = K \langle b_k^+ b_k \rangle$, which has a sensible continuum limit, rather than, for example, $\langle b_k^+ b_k \rangle$. Even at these relatively low values for K , the curve shapes and magnitudes are fairly stable, differing by, at most, slightly less than 30% in the region where x is less than .2. For larger x the agreement is much better. For strong coupling, in fact, the points differ by only a few percent. This suggests that the qualitative features of the higher-Fock wavefunctions, and in particular their magnitude, can be reliably produced at fairly small K .

2.8. HIGHER-FOCK WAVEFUNCTIONS AT WEAK COUPLING

The structure functions from the higher-Fock components of the lightest mesons and baryons have displayed a fairly universal, roughly double-bump form. For relatively weak coupling, lower-lying mesons and baryons are dominated by their valence wavefunctions, and higher-Fock states may be considered perturbations of these. The structure of the leading higher-Fock wavefunction, which contains an additional $q\bar{q}$ pair, may be understood by following the flow of momentum as valence quarks split off extra $q\bar{q}$ pairs.^[31]

The valence wavefunction for a meson at weak coupling is strongly peaked at $x = .5$. Assuming that upon splitting the momentum is evenly shared, the final

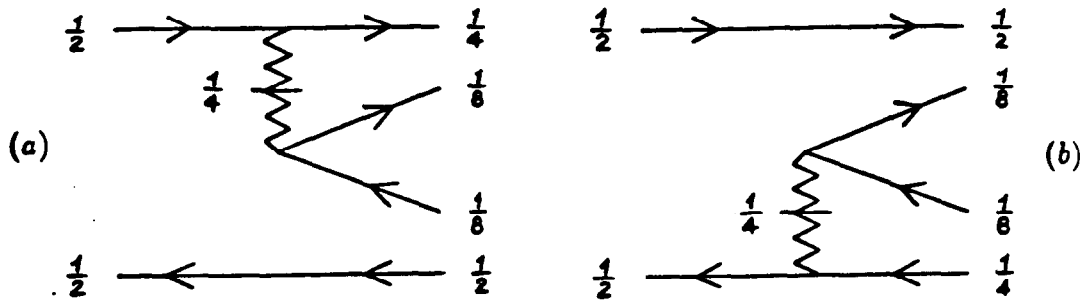


Figure 23. Momentum Splitting from $q\bar{q}$ to $q\bar{q}q\bar{q}$ Fock States in Meson. (a) Quark Splitting; (b) Antiquark Splitting.

four-quark wavefunction might be expected to have momenta distributed according to Fig. (23). For the quark structure function, the sum of equal-magnitude functions peaked at .25 and .125 (from Fig. (23a)) and .125 and .5 (from Fig. (23b)) would produce a total distribution with essentially two peaks, within the resolution of the numerical data. The first would be at roughly .17 (averaging .25, .125 and .125) with three times the magnitude of the second peak at .5. This structure is evident in Fig. (17) with $m/g = 1.6$. Apparently, as the coupling constant increases, the spreading of the valence distribution toward larger x is reflected in the spreading and increased x of the second peak of the higher-Fock state.

For an $SU(3)$ baryon, Fig. (24a) implies a quark distribution with roughly equal peaks at $x = .33$ and $x = .13$ (averaging .083 and .17). An antiquark peak should appear at $x = .083$ with about half the height of the quark peaks. Again, this provides a fairly accurate description of the weak coupling ($m/g = 1.6$) curves in Fig. (18a). For the strongly coupled baryon, there is not only a spreading toward larger x , but a factor of greater than ten increase in the total probability for finding an extra $q\bar{q}$ pair; note the change in scale. Because of the lack of resolution,

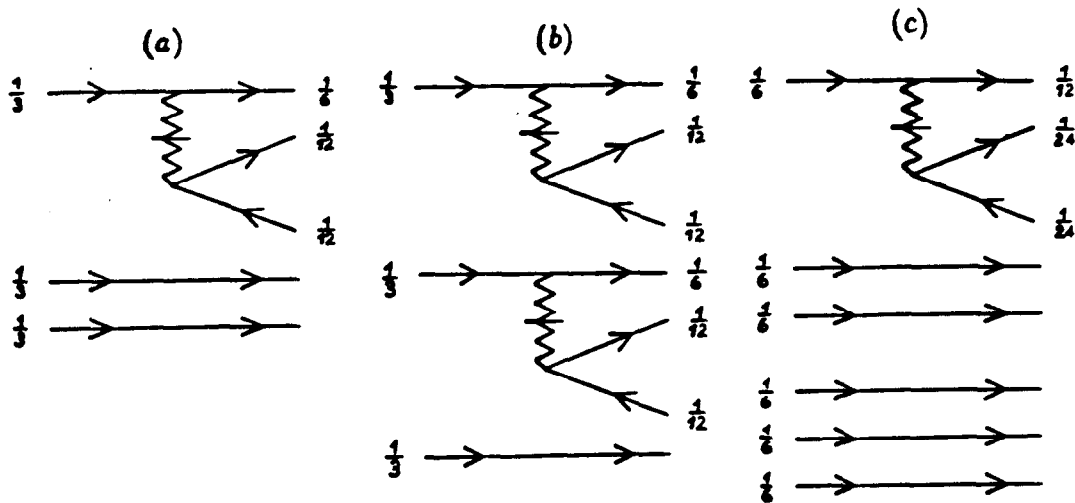


Figure 24. Momentum Splitting in $SU(3)$ Baryons. (a) Into Five-Particle State; (b) Into Seven-Particle State; (c) Baryon Pair into Eight-Particle State.

the pairs of peaks anticipated at small x merge into single peaks. These would presumably be resolved if K were sufficiently increased, providing an additional test of this general picture.

As a final exercise Figs. (24b) and (24c) may be used to understand the structure of the seven-quark Fock state for the $N = 3$ baryon with two additional $q\bar{q}$ pairs, and the two-baryon state with one extra pair. Following the previous analysis and assuming peaks closer than about .1 are unresolved, Fig. (24b) predicts peaks in the quark structure function at x of about .13 and .33 in a ratio of 4 to 1. Fig. (24c) for the two baryon case suggests peaks at .06 and .17 with a ratio of roughly 2 to 5, and also incidentally a single peak for the antiquark at .04 of relative height 1. Within their resolution, Figs. (18b) and (16a) are consistent with this picture. The curves in these plots are drawn to guide the imagination.

2.9. A PRELIMINARY LOOK AT RENORMALIZATION

QCD in $1 + 1$ dimensions requires no regularization beyond the subtraction of the vacuum energy. This is not the case in four dimensions, where an appropriate renormalization prescription is essential. In such a scheme, symmetries such as Lorentz and gauge invariance must either be preserved during discretization or recovered in the continuum limit.

Although superfluous, renormalizing QCD in two dimensions provides an initial example of how this might be approached. Following Ref. [24], an ultraviolet cutoff is imposed directly on the Fock space. States are restricted to those whose (free) invariant masses satisfy

$$\sum_i \left[\frac{m^2 + k_{\perp}^2}{x} \right]_i < \Lambda^2, \quad (2.13)$$

where the cutoff Λ is much larger than the scale of interest. In four dimensions, this regulates both large transverse momentum k_{\perp} and small x , while in two dimensions, k_{\perp} is absent. This prescription is Lorentz invariant and analogous to a Pauli-Villars cutoff in perturbation theory. It will be important in four dimensions to ensure that such a cutoff is applied in a way that is also gauge-invariant.

As Λ increases, so does the available resolution. In Table [7], the number of states in the Fock space with various numbers of particles are listed as a function of Λ for the case where $N = 2, B = 0$ and the momentum $2K = 14$.

Table [7]

$(\Lambda/m)^2$	$q\bar{q}$ states	$q\bar{q}q\bar{q}$	$q\bar{q}q\bar{q}q\bar{q}$	Total
5	3	—	—	3
10	5	—	—	5
20	7	2	—	9
30	7	14	—	21
50	7	28	1	36

As Λ increases, the number of states available to describe a $q\bar{q}$ system grows, until limited by the scale of discretization K . Also, contributions from states with increasing numbers of extra $q\bar{q}$ pairs can be resolved. In general, a particular system at a mass scale M should be well-described if $\Lambda \gg M$, and K is large enough so as not to cut off the states available at that Λ .

The running coupling constant $g(\Lambda)$ may be defined by requiring some physical quantity, such as a meson mass, to be fixed, presumably by an experiment. At each Λ , this mass is computed with K increasing until convergence. Finally, g is adjusted until the computed and physical quantities match, defining $g(\Lambda)$.

Fig. (25) illustrates this for the case where the physical quantity is an $N = 2$ meson of mass $(M/m)^2 = 6$. The momentum $2K$ is fixed at 26, which is reasonably close to convergence, but not quite large enough to produce a smooth curve. $g(\Lambda)$ behaves as might be expected for a finite theory. It has a threshold at $(\Lambda/m)^2 = 4$, where a $q\bar{q}$ pair can first be produced, and begins to turn over and flatten when the physical scale $(\Lambda/m)^2 = 6$ is reached. As Λ becomes much larger than this scale, it approaches a fixed value.

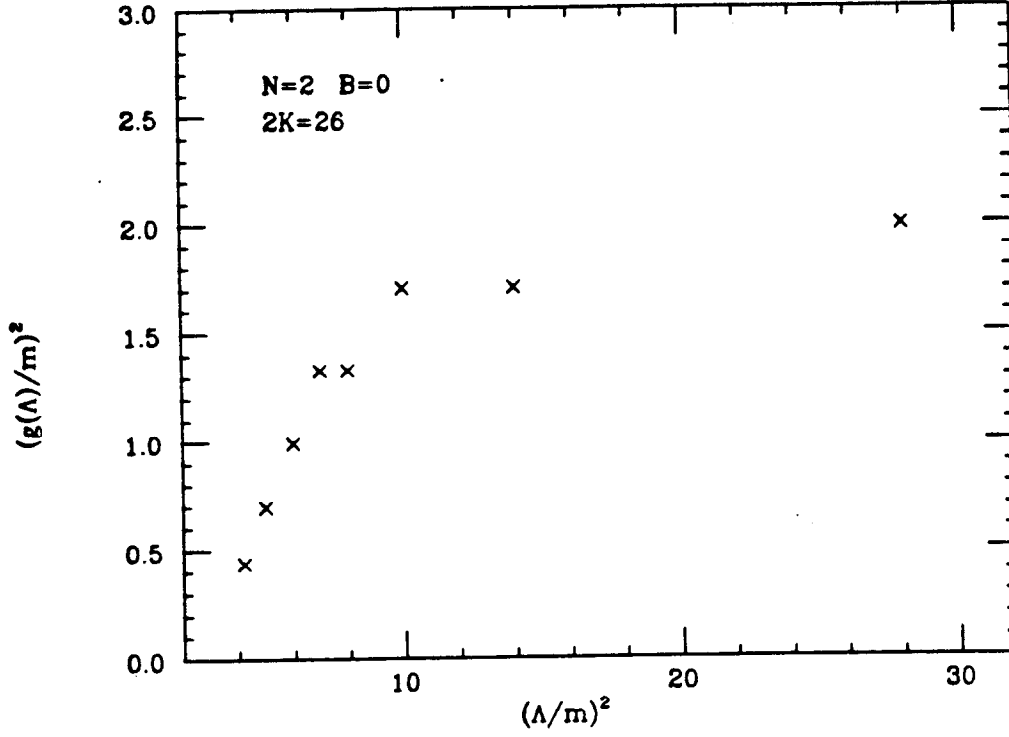


Figure 25. Running Coupling Constant Defined by Holding Fixed the $N = 2$, $B = 0$ Meson Mass to $M^2/m^2 = 6$.

3. ANALYTIC RESULTS

3.1. VALENCE MESON INTEGRAL EQUATIONS

The momentum-space Schrodinger equation

$$P^{\vec{z}} P^- |\phi(p^+)\rangle = M^2 |\phi(p^+)\rangle \quad (3.1)$$

may be expressed as an infinite set of coupled integral equations by expanding $|\phi(p^+)\rangle$ in a Fock state basis and projecting onto the singlet basis states

$$b_{(p^+ - q^+)}^{\dagger c} d_{q^+, c}^{\dagger} |0\rangle, \quad b_{(p^+ - q_1^+ - q_2^+ - q_3^+)}^{\dagger c_2} d_{q_3^+, c_2}^{\dagger} b_{q_2^+}^{\dagger c_1} d_{q_1^+, c_1}^{\dagger} |0\rangle, \quad (3.2)$$

and so on. Quantizing in a box to discretize the momenta and solving Eq. (3.1) by

diagonalizing the Hamiltonian is equivalent to evaluating these integral equations on a regularly spaced grid. A great deal of information about the continuum limit of this numerical approach to solving Eq. (3.1) may be extracted by studying these equations. Following Ref. [32], these continuum equations may be derived directly from the discretized Hamiltonian in the $K \rightarrow \infty$ limit. As a bonus, this derivation will demonstrate that the limit is sensible.

As a first step, consider the eigenvalue equation for the meson in the $q\bar{q}$ subspace. The only relevant interactions in the Hamiltonian

$$H = \left(\frac{2\pi}{L}\right) \left(\frac{\pi\lambda^2}{g^2}\right) P^- \quad (3.3)$$

are those which connect $q\bar{q}$ to $q\bar{q}$:

$$\sum_{n=\frac{1}{2}, \frac{3}{2}, \dots}^{\infty} \left[(1 - \lambda^2) \frac{1}{n} + \frac{\lambda^2}{2} S(n) \right] \left(b_n^{\dagger c} b_{n,c} + d_{n,c}^{\dagger} d_n^c \right), \quad (3.4)$$

and

$$\lambda^2 \sum_n \left[\mathcal{C}_{c_4 c_1}^{c_3 c_2} [n_2 + n_4 | - n_1 - n_3] \right. \\ \left. - \mathcal{C}_{c_4 c_1}^{c_2 c_3} [n_3 - n_4 | n_1 - n_2] \right] b_{n_4}^{\dagger c_4} b_{n_3, c_3} d_{n_2, c_2}^{\dagger} d_{n_1}^{c_1}. \quad (3.5)$$

The self-energy $S(n)$ here is defined as

$$S(k) \equiv \left(\frac{N^2 - (1 - \alpha)}{2N} \right) \sum_{n=\frac{1}{2}, \frac{3}{2}, \dots}^{\infty} \left[[k - n | n - k] - [k + n | -k - n] \right] \quad (3.6)$$

and appears in diagonal terms after putting the Hamiltonian into normal order. The instantaneous gluon propagator $[m|n]$ and the color tensor \mathcal{C} are discussed in Chapter (1). The parameter α allows $S(N)$ and $U(N)$ to be treated simultaneously; for $SU(N)$, $\alpha = 0$ and $\alpha = 1$ for $U(N)$.

The eigenstate $|\phi(K)\rangle$ may, in general, be expanded in this subspace

$$|\phi(K)\rangle = \sum_{n=\frac{1}{2}, \frac{3}{2}, \dots}^{K-\frac{1}{2}} \phi_n b_{K-n}^{\dagger c} d_{n,c}^{\dagger} |0\rangle. \quad (3.7)$$

Sandwiching the eigenvalue equation

$$H|\phi\rangle = \frac{M_0^2}{K} |\phi\rangle,$$

with $\langle 0|d_{\ell}^{\dagger} b_{K-\ell,c'}$ results in the discrete equation

$$\begin{aligned} & \left[N(1-\lambda^2) \left(\frac{1}{\ell} + \frac{1}{K-\ell} \right) + \frac{1}{2} \lambda^2 N [S(\ell) + S(K-\ell)] \right] \phi_{\ell} \\ & + \frac{1}{2} \lambda^2 \sum_{n=\frac{1}{2}, \frac{3}{2}, \dots}^{K-\frac{1}{2}} \left[-(N^2 - (1-\alpha)) \frac{1}{(\ell-n)^2} + \alpha N \frac{1}{K^2} \right] \phi_n \\ & = \frac{M_0^2 N}{K} \phi_{\ell} . \end{aligned} \quad (3.8)$$

M_0^2 is the numerical mass squared which appears in the program and is $M^2/(m^2 + g^2/\pi)$ in dimensional units. The singularity at $n = \ell$ is excluded by hand in the definition of H .

Using the identity^[32]

$$S(\ell) + S(K-\ell) = 2 \left(\frac{N^2 - (1-\alpha)}{2N} \right) \sum_{\substack{n=\frac{1}{2}, \frac{3}{2}, \dots \\ n \neq \ell}}^{K-\frac{1}{2}} \frac{1}{(\ell-n)^2}, \quad (3.9)$$

defining the momentum fractions $x = \ell/K$ and $y = n/K$, converting ϕ_{ℓ} into the continuum wavefunction $\phi(x)$, and reintroducing dimensional parameters produces

in the continuum limit $K \rightarrow \infty$

$$\begin{aligned}
m^2 \left(\frac{1}{x} + \frac{1}{1-x} \right) \phi(x) - \frac{g^2}{\pi} \left(\frac{N^2 - (1-\alpha)}{2N} \right) \int_0^1 dy \frac{\phi(y) - \phi(x)}{(y-x)^2} \\
+ \frac{g^2 \alpha}{2\pi} \int_0^1 dy \phi(y) = M^2 \phi(x).
\end{aligned} \tag{3.10}$$

The principal value prescription is fixed by the infrared regularization of the discrete Hamiltonian before the $K \rightarrow \infty$ limit is taken. Specifically,

$$\int_0^1 dy \equiv \lim_{\epsilon \rightarrow 0} \int_0^{x-\epsilon/2} + \int_{x+\epsilon/2}^1 dy, \tag{3.11}$$

where $\epsilon = 1/K$. With this prescription, Eq. (3.10) is well-defined, lending confidence that the regularization adopted for numerical calculations has a sensible continuum limit.

Although this equation is in a severely restricted space, a great deal of information about the continuum limit of the model may be extracted from it, beyond the observation that such a limit exists. For example, if the quark mass m is set to zero, $\phi(x) = 1$ is clearly an eigenfunction, with M^2 equal to zero for $SU(N)$ ($\alpha = 0$). For $U(N)$ ($\alpha = 1$), the presence of the extra term from $q\bar{q}$ annihilation, $(g^2/2\pi) \int_0^1 dy \phi(y)$, is related to the $U(1)$ anomaly and gives these mesons a mass-squared of $M^2 = g^2/2\pi$. Eq.(3.10) thus reproduces by inspection the masses and wavefunctions for $SU(N)$ and $U(N)$ mesons in the $m/g \rightarrow 0$ limit. In fact, for $U(1)$ (the Schwinger model), it yields the exact mass for the only particle in the theory.^[23,20] Because of the Fock space restriction, however, this equation cannot

describe states which contain pairs of these mesons, nor the higher Fock content of individual mesons.

The equation also makes apparent the possibly singular nature of the $m = 0$ limit. The free Hamiltonian, which is proportional to m^2 , diverges for quarks carrying zero momentum, forcing wavefunctions to vanish at $x_i = 0$. For m^2 identically zero, this restriction disappears; it is not necessarily true that the exact solutions at $m = 0$ are related to those for small, but finite, m .

Interestingly, this equation contains all of the information necessary to compute the spectrum of mesons in the opposite, nonrelativistic, limit where $g/m \rightarrow 0$. In this limit, the large mass of the quark dynamically restricts the states to quark-antiquark pairs. The equation and its solutions in this limit, as well as that for baryons, will be discussed later in this chapter.

Finally, in the large- N limit ($N \rightarrow \infty$, with $g^2 N$ fixed) retaining only terms of order $g^2 N$ in Eq. (3.10) reproduces the equation derived in Ref. [21] by summing the leading planar diagrams which contribute to the valence meson propagator. In this limit, the $U(N)$ and $SU(N)$ cases are equivalent. The extra term in the $U(N)$ equation which produces the massive Schwinger bosons as $m/g \rightarrow 0$ is proportional to g^2 and so is suppressed by one power of N . As a result, when $m/g \rightarrow 0$, the large- N limit neglects the leading contribution to the mass of these mesons, and they become massless as in $SU(N)$.

It should be noted that some references, beginning with Ref. [21], discuss a finite renormalization of the quark mass $m^2 \rightarrow m^2 - (g^2 N/2\pi)$, to order $g^2 N$ and in my conventions. In these references, a slightly different principal value prescription

is used. With that prescription, the second term in the integrand of

$$-\left(\frac{g^2 N}{2\pi}\right) \int_0^1 dy \frac{\phi(y) - \phi(x)}{(y-x)^2} \quad (3.12)$$

in Eq. (3.10) yields

$$-\left(\frac{g^2 N}{2\pi}\right) \left(\frac{1}{x} + \frac{1}{1-x}\right) \phi(x), \quad (3.13)$$

which finitely renormalizes m^2 . This is simply a rearrangement of terms and the equations are identical. Incidentally, in the space of color singlets, this renormalization is of no direct physical consequence. In perturbation theory, it alters only the gauge-dependent quark propagator.^[30]

3.2. VALENCE BARYON INTEGRAL EQUATIONS

The continuum limit integral equation for the baryon, restricted to the minimum N valence quarks, may be derived in the same manner as the meson equation. The relevant terms in the discretized Hamiltonian are

$$\sum_{n=\frac{1}{2}, \frac{3}{2}, \dots}^{\infty} \left((1 - \lambda^2) \frac{1}{n} + \frac{\lambda^2}{2} S(n) \right) b_n^{\dagger c} b_{n,c} \quad (3.14)$$

and

$$-\frac{\lambda^2}{2} \sum_n C_{c_4 c_3}^{c_1 c_2} [n_2 - n_4 | n_1 - n_3] b_{n_4}^{\dagger c_4} b_{n_3}^{\dagger c_3} b_{n_2, c_2} b_{n_1, c_1}. \quad (3.15)$$

Consider first the case where $N = 3$; the generalization to arbitrary N will follow.

A color singlet valence baryon state will have the form

$$|\phi_B(K)\rangle = \sum_n \delta_{K,\Sigma n} \phi_B(n_i) \epsilon_{c_1 c_2 c_3} b_{n_1}^{\dagger c_1} b_{n_2}^{\dagger c_2} b_{n_3}^{\dagger c_3} |0\rangle. \quad (3.16)$$

As was done for the meson, the Schrodinger equation

$$H |\phi_B\rangle = \frac{M_0^2}{K} |\phi_B\rangle \quad (3.17)$$

is projected onto the singlet state

$$\epsilon_{c'_1 c'_2 c'_3} b_{\ell_1}^{\dagger c'_1} b_{\ell_2}^{\dagger c'_2} b_{\ell_3}^{\dagger c'_3} |0\rangle, \quad (3.18)$$

where $\sum \ell_i = K$. Contracting color and momentum indices and taking the continuum limit $K \rightarrow \infty$ converts Eq. (3.17) into

$$\begin{aligned} & \sum_{i=1}^N \frac{m^2}{x_i} \phi_B(x) - \frac{g^2}{\pi} \left(\frac{N+1}{2N} \right) \left[\right. \\ & \int_{\epsilon/2}^{x_1} \frac{ds}{s^2} \left(\phi_B(x_1 - s, x_2 + s, x_3) + \phi_B(x_1 - s, x_2, x_3 + s) - (N-1)\phi_B(x) \right) \\ & + \int_{\epsilon/2}^{x_2} \frac{ds}{s^2} \left(\phi_B(x_1 + s, x_2 - s, x_3) + \phi_B(x_1, x_2 - s, x_3 + s) - (N-1)\phi_B(x) \right) \\ & \left. + \int_{\epsilon/2}^{x_3} \frac{ds}{s^2} \left(\phi_B(x_1 + s, x_2, x_3 - s) + \phi_B(x_1, x_2 + s, x_3 - s) - (N-1)\phi_B(x) \right) \right] \\ & = M^2 \phi_B(x). \end{aligned} \quad (3.19)$$

Here $\phi_B(x) \equiv \phi_B(x_1, x_2, x_3)$ and $\sum_i x_i = 1$. The $\epsilon/2$ cutoff for small x is the same principal value prescription employed in the meson equation.^{[33][34][35]} This equation

has been derived both by Feynman diagrams in Ref. [33] and by means of an equivalent string theory in Ref. [34], and has been studied numerically in Ref. [35].

In this form the equation is readily extended to arbitrary N . The wavefunction takes N arguments, there are N rather than 3 integrals, and in the i^{th} integral there are $(N - 1)$ terms in which momentum is transferred consecutively from the i^{th} quark to the remaining $N - 1$ quarks.

3.3. MESON WAVEFUNCTION ENDPOINT BEHAVIOR

The asymptotic behavior of the valence $SU(N)$ meson wavefunction when one quark carries momentum fraction $x \sim 0$ may be determined using the continuum integral equation Eq. (3.10).^[36] The behavior for valence baryons and higher-Fock states may also be computed from the relevant integral equations, as will be shown later. The wavefunctions in this limit will provide a great deal of information about continuum solutions, particularly when m/g is small, or for form factors, when Q^2 is large. In addition, it will be employed to determine the dependence of numerical results on K .

Assuming the form $\phi(x) \sim cx^a$ as $x \sim 0$, where c is an undetermined constant, Eq. (3.10) becomes

$$m^2 cx^{a-1} - \frac{g_N^2}{\pi} \int_0^1 dy \frac{\phi(y) - cx^a}{(y-x)^2} \sim 0 \quad (3.20)$$

with

$$g_N^2 \equiv g^2 \left(\frac{N^2 - 1}{2N} \right).$$

The integral in Eq. (3.20) must introduce an extra power of $1/x$ to balance the kinetic term. This will originate in the $y \sim x$ region, where $\phi(y) \sim cy^a$. Defining the integration variable $u \equiv y/x - 1$ in the region $y \in [0, x - \epsilon]$ gives, to leading order in x

$$\int_0^{x-\epsilon} dy \frac{y^a - x^a}{(y-x)^2} = x^{a-1} \int_{-1}^{-\epsilon/x} du \frac{(1+u)^a - 1}{u^2},$$

which possesses the appropriate power of x . Repeating for $y \in [x + \epsilon, 1]$ and taking $\epsilon \rightarrow 0$ prior to x gives for Eq. (3.20)

$$\int_{-1}^{\infty} du \frac{(1+u)^a - 1}{u^2} = \frac{\pi m^2}{g_N^2}. \quad (3.21)$$

The integral is evaluated in Appendix B, reproducing the equation in Ref. [21] (for large N)

$$1 - (a\pi) \cot(a\pi) = \frac{\pi m^2}{g_N^2}, \quad (3.22)$$

with $a \in (0, 1)$. Note that this determines, up to a coefficient, the same asymptotic small- x behavior for all $q\bar{q}$ wavefunctions, including excited states. It depends on the parameter m/g but is independent of each state's mass. The coefficient c , however, may vary from state to state.

The exponent a determined implicitly by Eq. (3.22) monotonically increases from 0 to 1 as m/g runs from 0 to ∞ . For strong coupling (small mass)

$$a_{(m/g \sim 0)} \sim \left(\frac{3}{\pi}\right)^{1/2} \left(\frac{m}{g_N}\right), \quad (3.23)$$

while for weak coupling (large mass)

$$a_{(g/m \sim 0)} \sim 1 - \frac{1}{\pi} \left(\frac{g_N}{m}\right)^2. \quad (3.24)$$

The reasonable approximation for the lightest meson wavefunction,

$$\phi(x) \propto x^a(1-x)^a, \quad (3.25)$$

provides a fairly accurate mass expectation value at strong coupling. As $m/g \rightarrow 0$, the exponent a approaches zero, and $\phi(x) \sim 1$ everywhere except for an increasingly narrow region near the endpoints, where it decreases sharply to zero. This behavior will make accurate numerical calculations based on a regular grid increasingly difficult. For weaker coupling the wavefunction grows less drastically from zero at its endpoints, while the peak at $x = 1/2$ becomes more prominent. Finally, it should be mentioned that there do exist other possible asymptotic forms for $x \sim 0$ which may be generated from those above by taking n derivatives with respect to a . These go as $x^a \log^n x$, where a is the same function of m/g as before. Expectation values for M^2 which have been computed with $\phi(x) \propto x^a(1-x)^a \log^n[x(1-x)]$ lie consistently higher than for those discussed above, and the previous form will be assumed.

3.4. BARYON WAVEFUNCTION ENDPOINT BEHAVIOR

Just as for the meson, the asymptotic behavior of the baryon wavefunction in the valence approximation as one argument approaches zero may be extracted from the continuum Eq. (3.19). The case where $N = 3$ will be considered; again, the extension to general N is simple.

In the limit where $x_1 \rightarrow 0$ while the other x_i are fixed, the form for $\tilde{\phi}_B$

$$\phi_B(x) \sim x_1^a \tilde{\phi}_B(x_2, x_3) \quad (3.26)$$

is taken as an ansatz. The kinetic term is then

$$H_0\phi_B \sim m^2 x_1^{a-1} \tilde{\phi}_B. \quad (3.27)$$

Also, the first integral in Eq. (3.19), after the change of variables $s = -x_1 u$, gives, to leading order in x , $(N - 1)$ copies of

$$-\frac{g^2}{\pi} \left(\frac{N+1}{2N} \right) x_1^{a-1} \tilde{\phi}_B \int_{-1}^0 \frac{du}{u^2} [(1+u)^a - 1]. \quad (3.28)$$

The remaining integrals contain $(N - 1)$ terms, one from each integral, in which momentum is exchanged with the first quark; that is, x_1 appears in the combination $x_1 + s$. Defining $s = x_1 u$, these produce

$$(N - 1) \left[\frac{-g^2}{\pi} \left(\frac{N+1}{2N} \right) x_1^{a-1} \tilde{\phi}_B \int_0^\infty \frac{du}{u^2} (1+u)^a \right], \quad (3.29)$$

while those remaining partially cancel and contribute a term of the same form but with $(1+u)^a$ replaced by -1 .

The net result is that as $x_1 \rightarrow 0$, a must satisfy

$$\int_{-1}^\infty \frac{du}{u^2} [(1+u)^a - 1] = 1 - (a\pi) \cot(a\pi) = \frac{\pi m^2}{g_N^2}. \quad (3.30)$$

This is the same equation as for the meson wavefunction in the same limit. The asymptotic small- x behavior of wavefunctions appears to be universal; this equation is valid for mesons and for baryons with any number N of quarks. This result is unaffected by permitting higher-Fock states in at least the meson wavefunction, as will be shown, and is probably true in general.

Finally, this limit was defined such that all but one argument are held fixed. If more than one x_i is taken to zero simultaneously, the behavior is more complicated. For example, for Eq. (3.19), letting x_1 and x_2 approach zero holding $x_2/x_1 = \sigma$ fixed and assuming

$$\phi_B \sim x_1^a x_2^b \tilde{\phi}_B$$

gives the condition

$$\begin{aligned} \left[m^2 - \gamma(1 - (a\pi) \cot(a\pi)) \right] + \frac{1}{\sigma} \left[m^2 - \gamma(1 - (b\pi) \cot(b\pi)) \right] \\ - \gamma \int_{-1}^{\sigma} \frac{du}{u^2} \left[(1+u)^a (1-u/\sigma)^b - 1 \right] = 0 \quad , \end{aligned} \quad (3.31)$$

with

$$\gamma \equiv \frac{g^2}{\pi} \left(\frac{N+1}{2N} \right).$$

The general behavior of wavefunctions when one argument approaches one and the rest approach zero would be particularly useful for determining the behavior of form factors at large momentum transfer; this will not be attempted here. The specific case of the large- N valence meson is discussed in Ref. [18].

3.5. ESTIMATING NUMERICAL ERRORS

In the continuum limit, the problem of diagonalizing P^- may be cast in the form of an infinite set of coupled integral equations. From the derivation of these equations in the previous sections, it is clear that diagonalizing P^- in the discrete, denumerable Fock space specified by imposing antiperiodic boundary conditions is

equivalent to solving these equations numerically, with the integrals evaluated on a regularly spaced grid. For example, in the valence meson equation. Eq. (3.10),

$$\sum_{\substack{n=\frac{1}{2}, \frac{3}{2}, \dots \\ n \neq \ell}}^{K-\frac{1}{2}} \frac{\phi_n - \phi_\ell}{K(n/K - \ell/K)^2} \xrightarrow{K \rightarrow \infty} \int_0^1 dy \frac{\phi(y) - \phi(x)}{(y-x)^2} . \quad (3.32)$$

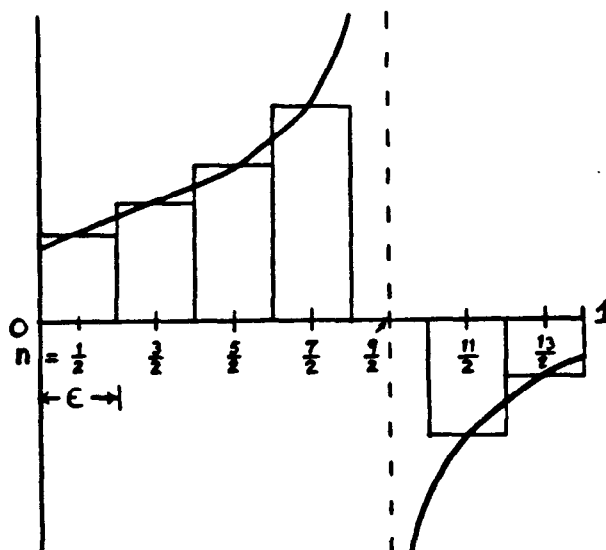


Figure 26. Numerical Approximation of Principal-Value-Regulated Integral.

For finite K , the sum approximates the integral by summing rectangles of width $\epsilon = 1/K$ as in Fig. 26. The contribution from $n = \ell$ ($= 9/2$ in this figure) is excluded. The error typically induced by approximating the integral of $f(y)$ from $y = a$ to b in this way is

$$\frac{\epsilon^2}{12} [f'(b) - f'(a)] + \mathcal{O}(\epsilon^3) . \quad (3.33)$$

This is normally not a good scheme for approximating an integral, and much faster methods exist. The case considered above, however, is not even normal.

First, because $\phi(x) \propto x^a$ as $x \sim 0$, with $a \in (0, 1)$, the derivative of the integrand appearing in the error estimate contains terms which diverge at the endpoints as x^{a-1} . Second, the singularity regulated by the principal value induces an additional error when discretized.

To determine the discretization error in the valence meson integral, consider the regions $[0, \epsilon]$, and $[1 - \epsilon, 1]$ about the endpoints, and $[\epsilon, x - \epsilon/2]$, and $[x + \epsilon/2, 1 - \epsilon]$ near x , separately; x will be assumed as fixed and finite.

First, computing the integral (with $\phi(y) \sim cy^a$)

$$\int_0^{2\epsilon} dy \frac{cy^a}{(y-x)^2} \quad (3.34)$$

and subtracting that approximated by sampling at the first grid point at $y = \epsilon/2$, produces a leading error of

$$\frac{2c}{x^2} \left[\frac{2^a}{1+a} - 1 \right] \epsilon^{1+a} \quad (3.35)$$

with higher terms of order ϵ^{n+a} , with $n > 1$. The contribution from the term with $-\phi(x)$ in the numerator produces errors of order ϵ^n with $n \geq 3$ in this region. The region near $y \sim 1$ should produce the same order errors. In $[\epsilon, x - \epsilon/2]$ and $[x + \epsilon/2, 1 - \epsilon]$ the integrand and its derivatives are finite and the usual error estimate applies. The endpoints neighboring the excluded region around $y = x$ contribute errors of order ϵ^n , $n \geq 3$ to Eq. (3.33). Those near $y = 0$ and 1 yield errors of order ϵ^{n+a} and ϵ^{n+1} , with $n \geq 1$.

Finally, eliminating the point from the sum in Eq. (3.32) where $n = \ell$ (that is, $y = x$) effectively excludes the region $[x - \epsilon, x + \epsilon]$ from the integration over y ; (cf.

Fig. (26)). The error induced is

$$\int_{x-\epsilon}^{x+\epsilon} dy \frac{\phi(y) - \phi(x)}{(y-x)^2}, \quad (3.36)$$

where ϵ is fixed at $1/K$ while the principal value limit is taken. Assuming $\phi(y)$ is sufficiently smooth and expanding around x gives for Eq. (3.36)

$$\phi''(x)\epsilon + \frac{1}{36}\phi'''(x)\epsilon^3 + \dots \quad (3.37)$$

Although in the limit $K \rightarrow \infty$ ($\epsilon \rightarrow 0$) the discrete infrared regularization employed reduces to a well-defined principal value prescription, it reduces at a leisurely pace; for finite K it is the source of the leading $\mathcal{O}(\epsilon)$ error.

Combining contributions from these various terms gives a series in ϵ for the total error in Eq. (3.32) of

$$c_1\epsilon + c_2\epsilon^{1+a} + c_3\epsilon^2 + c_4\epsilon^{2+a} + \dots, \quad (3.38)$$

in contrast with terms of order ϵ^n , $n \geq 2$ which would occur were the integrand analytic.

Because the endpoint behavior a is apparently general, physical quantities M , such as meson and baryon masses, measured at finite but sufficiently large K , should behave as

$$M(1/K) = M(0) + \frac{c_1}{K} + \frac{c_2}{K^{1+a}} + \frac{c_3}{K^2} + \frac{c_4}{K^{2+a}} + \dots, \quad (3.39)$$

with $M(0)$ the continuum limit. The leading error is of order $1/K$, so that $M(1/K)$ converges painfully slowly. The discretization scheme used to quantize this theory then ends up effectively evaluating integrals in a way which is simple but

inefficient. However, knowing Eq. (3.39), this may be turned to advantage, and convergence may be improved significantly by Richardson extrapolation. In this method, $M(1/K)$ is computed at n different finite values of K , to which the first n coefficients of the series are fit. This technique is commonly applied to improve numerical calculations of integrals, although the dependence of the series behavior on the coupling and mass through the exponent a is peculiar to this case. The error to the fit of $M(0)$ is of the order of the term $n + 1$. A rough estimate of the error in this procedure is given by the last term retained. This technique was used in the results previously quoted to allow for a meaningful comparison with other techniques, and to give some idea of their uncertainties.

3.6. ESTIMATE OF NECESSARY RESOLUTION

In order to know when this extrapolation procedure may be reliably applied, it is useful to know how large K must be before results begin to exhibit the behavior in Eq. (3.39).

The approximate valence wavefunction for the lightest meson

$$\phi(x) \propto x^a (1-x)^a,$$

where a is defined in Eq. (3.22), provides a model for estimating the size of K needed for reasonable numerical results. This is especially important to know in the case of strong coupling (small quark mass). As has been seen, a becomes small and $\phi(x)$ turns over sharply at its endpoints. K will most likely be large enough when it allows these regions to be adequately sampled.

When discretized, $x_k = k/K$, where k is the numerical quark momentum. If the first point in x is required to be small enough to sample $\phi(x)$ before the point where $\phi(x)$ reaches half its maximum, then

$$K \gtrsim \frac{1}{2x_{hmax}} ,$$

with

$$x_{hmax} = \frac{1}{2} - \frac{1}{2} \left(1 - \frac{1}{2^{1/a}} \right)^{1/2} .$$

The minimum K estimated in this way is listed in Table [8] as a function of λ for N from 2 to 4.

Table [8]

λ	m/g	$K_{min} :$		
		$N = 2$	3	4
.3325	1.6	8	8	10
.5763	.8	10	12	15
.8158	.4	20	30	50
.9425	.2	90	250	500
.9847	.1	2000	15000	7×10^4
.9961	.05	10^6	5×10^7	10^9

These estimates are probably overly conservative for computations of quantities which are not sensitive to the endpoint behavior of the wavefunctions. It does, however, indicate that numerical precision becomes increasingly difficult as the coupling strength grows; the K considered in actual computations are generally below 50, so results for $\lambda > .9425$ should be eyed suspiciously.

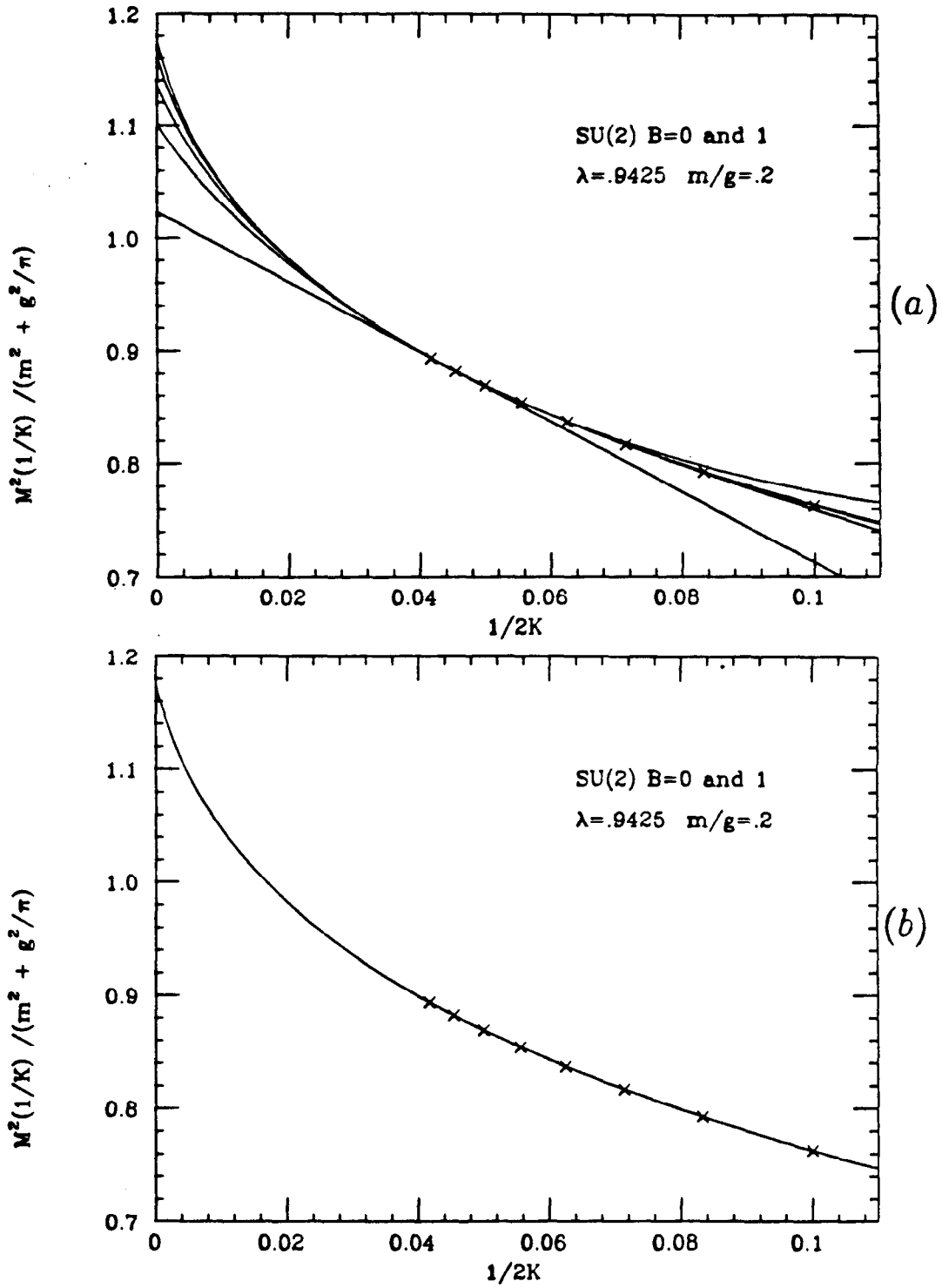


Figure 27. Extrapolation Fit to $SU(2)$ Lightest Meson Mass. (a) Fits from Last Two to Last Six Points; (b) Fit to Last Six Points, Isolated.

Fig. (27) provides an example of a fit of this kind. Eight values for the lightest meson mass-squared M_0^2 in units of $m^2 + g^2/\pi$ are plotted versus $1/2K$, where $2K$ ranges from 10 to 24. Here $N = 2$ and $\lambda = .9425$, corresponding to $m/g = .2$. For $SU(2)$, the lightest meson and baryon masses are identical at all values of K , so these apply as well to the baryon. Also, the Fock space was restricted to four quarks; the resulting error is negligible for this case.

These points are used to determine the coefficients in the series expected to describe the behavior of M_0^2 as a function of $1/2K$, as in Eq. (3.39). For this case, $a = .222$ for $\lambda = .9425$. This function is plotted in Fig. (27a) for the cases where the left-most n points are used to determine the first n coefficients in Eq. (3.39), and n ranges from two to six. Fig. (27b) isolates the six-term series. The vertical intercept is $M_0^2(0)$.

From these plots, it is clear that extrapolation substantially improves, or at least alters, the best measured value for M_0^2 at $2K = 24$. In fact, the λ in this case is probably close to the upper limit for which computations at this K are reliable. In spite of the rather large extrapolation, the curves are both smooth, that is devoid of oscillations between points, and stable as the number of included points increases. Also, the curve in Fig. (27b) is fit to only the six points nearest the continuum, but nevertheless runs through the next two points to the right. These suggest that this fit is reasonably reliable.

The value of the last term retained in the series (computed at the smallest value of K used in the fit) provides an indication of the error. For $n = 2$ to 6, these are .14, .42, .080, .39, and .078, respectively. These error estimates are admittedly crude; a much better method could certainly be devised. This would probably be

warranted if these calculations were being compared with actual physical (that is, four-dimensional) quantities.

3.7. HIGHER-FOCK EQUATIONS: ENDPOINTS AND ERRORS

Because the endpoint behavior of meson and baryon wavefunctions, derived above from integral equations in the valence approximation, play an important role in both analytic and numerical results, it is important to know what effect the inclusion of higher-Fock components might have.

Just as in the valence approximation, integral equations which incorporate higher-Fock wavefunctions may be derived from the discretized Hamiltonian by contracting the Schrodinger equation with appropriate color singlets. For example, for $B = 0$, contracting Eq. (3.17) on the left with a $q\bar{q}$ singlet at fixed momentum and taking K (or L) to infinity produces an integral equation which incorporates the $q\bar{q}$ and $q\bar{q}q\bar{q}$ meson wavefunctions. Because H can change particle number by at most two, no others are involved in this case.

The result is the complete equation for $\phi_2(x) \equiv \phi_2(x, 1 - x)$:

$$\begin{aligned}
M^2 \phi_2(x) &= m^2 \left(\frac{1}{x_1} + \frac{1}{x_2} \right) \phi_2(x) \\
&- \frac{g^2}{\pi} \left(\frac{N^2 - \alpha}{2N} \right) \int_0^1 dy \frac{\phi_2(y) - \phi_2(x)}{(y - x_1)^2} + \frac{g^2}{\pi} \left(\frac{1 - \alpha}{2} \right) \int_0^1 dy \phi_2(y) \\
&- 4 \frac{g^2}{\pi} \int_0^1 [dy] \phi_4(x_1, y_2; y_3, y_4) \left[\left(\frac{N^2 - \alpha}{2N} \right) \frac{1}{(x_2 - y_4)^2} - \left(\frac{1 - \alpha}{2} \right) \frac{1}{(x_2 - y_2)^2} \right] \\
&+ 4 \frac{g^2}{\pi} \int_0^1 [dy] \phi_4(y_1, x_2; y_3, y_4) \left[\left(\frac{N^2 - \alpha}{2N} \right) \frac{1}{(x_1 - y_3)^2} - \left(\frac{1 - \alpha}{2} \right) \frac{1}{(x_1 - y_1)^2} \right].
\end{aligned} \tag{3.40}$$

Here $[dy]$ is short-hand for $\prod_i dy_i$, with the y_i those appearing in ϕ_4 , multiplied by a delta function which restricts all the arguments of ϕ_4 to sum to one. The variables x_1 and x_2 are the fractional momenta of the q and \bar{q} which contracted Eq. (3.17), with $x_1 + x_2 = 1$. Finally, the continuum n -particle wavefunctions $\phi_n(x_i)$ are constructed from the discrete $\phi_n(l_i)$ according to

$$\phi_n(x_i) = K^{\frac{n-1}{2}} \phi_n(l_i) = K^{\frac{n-1}{2}} \phi_n(x_i K). \tag{3.41}$$

Eq. (3.40) is the first of an infinite set of coupled integral equations. The next may be derived by contracting Eq. (3.17) on the left with two $q\bar{q}$ pairs with fractional momenta of x_1 to x_4 . This equation will couple ϕ_2 , ϕ_4 , and ϕ_6 . Neglecting ϕ_6 , it is

$$\begin{aligned}
M^2 \left[N\phi_4(x) - \phi_4(\tilde{x}) \right] &= m^2 \left(\sum_{i=1}^4 \frac{1}{x_i} \right) \left[N\phi_4(x) - \phi_4(\tilde{x}) \right] \\
&- \frac{1}{2} \frac{g^2}{\pi} \left(\frac{N^2 - \alpha}{2N} \right) \left[\frac{\phi_2(x_1) - \phi_2(x_4)}{(1 - x_1 - x_4)^2} + \frac{\phi_2(x_1) - \phi_2(x_4)}{(1 - x_1 - x_4)^2} \right] \\
&+ \frac{1}{2} \frac{g^2}{\pi} \left(\frac{1 - \alpha}{2} \right) \left[\frac{\phi_2(x_1) - \phi_2(x_2)}{(1 - x_1 - x_2)^2} + \frac{\phi_2(x_3) - \phi_2(x_4)}{(1 - x_3 - x_4)^2} \right] \\
&- \frac{g^2}{\pi} \left(\frac{N^2 - \alpha}{2} \right) \int [dy] \left[\frac{\phi_4(y_1, y_2; x_3, x_4) - \phi_4(x)}{(x_1 - y_1)^2} + \frac{\phi_4(x_1, x_2; y_3, y_4) - \phi_4(x)}{(x_3 - y_3)^2} \right] \\
&+ \frac{g^2}{\pi} \left(\frac{N^2 - \alpha}{2N} \right) \int [dy] \left[\frac{\phi_4(y_1, x_2; x_3, y_4)}{(x_1 + x_4)^2} + \frac{\phi_4(x_1, y_2; y_3, x_4)}{(x_2 + x_3)^2} \right. \\
&\quad + \frac{\phi_4(y_1, y_2; x_1, x_4) - \phi_4(\tilde{x})}{(x_3 - y_1)^2} + \frac{\phi_4(x_3, x_2; y_3, y_4) - \phi_4(\tilde{x})}{(x_1 - y_3)^2} \\
&\quad + \frac{\phi_4(y_1, x_2; x_1, y_4) - \phi_4(\tilde{x})}{(x_3 - y_1)^2} + \frac{\phi_4(x_3, y_2; y_3, x_4) - \phi_4(\tilde{x})}{(x_1 - y_3)^2} \\
&\quad \left. - \frac{\phi_4(x_1, y_2; x_3, y_4) - \phi_4(\tilde{x})}{(x_2 - y_4)^2} - \frac{\phi_4(y_1, x_2; y_3, x_4) - \phi_4(\tilde{x})}{(x_1 - y_3)^2} \right] \\
&+ \frac{g^2}{\pi} \left(\frac{1 - \alpha}{2} \right) \int [dy] \left[\frac{\phi_4(y_1, y_2; x_3, x_4) - \phi_4(y_1, x_4; x_3, y_2)}{(x_1 + x_2)^2} \right. \\
&\quad + \frac{\phi_4(x_1, x_2; y_3, y_4) - \phi_4(x_1, y_2; y_3, x_4)}{(x_3 + x_4)^2} \\
&\quad - \frac{\phi_4(x_3, x_2; y_3, y_4)}{(x_1 + x_4)^2} - \frac{\phi_4(x_1, x_4; y_3, y_4)}{(x_2 + x_3)^2} \\
&\quad + \frac{\phi_4(y_1, x_2; y_3, x_4) - \phi_4(y_1, x_2; x_3, y_4)}{(x_1 - y_1)^2} \\
&\quad \left. + \frac{\phi_4(x_1, y_2; x_3, y_4) - \phi_4(x_1, y_2; y_3, x_4)}{(x_2 - y_2)^2} \right], \tag{3.42}
\end{aligned}$$

with the wavefunctions defined such that $\phi_2(x_i) \equiv \phi_2(x_i, 1-x_i)$, $\phi_4(x) \equiv \phi_4(x_1, x_2; x_3, x_4)$, $\phi_4(\tilde{x}) \equiv \phi_4(x_3, x_2; x_1, x_4)$, and $\sum x_i = 1$. Repeating this procedure would produce equations which relate the infinite set of wavefunctions.

Having continuum integral equations which include higher-Fock wavefunctions, it is possible to determine if in accounting for these, conclusions drawn from the valence wavefunctions are altered. From Eq. (3.40), ϕ_4 could affect the small- x behavior of ϕ_2 .

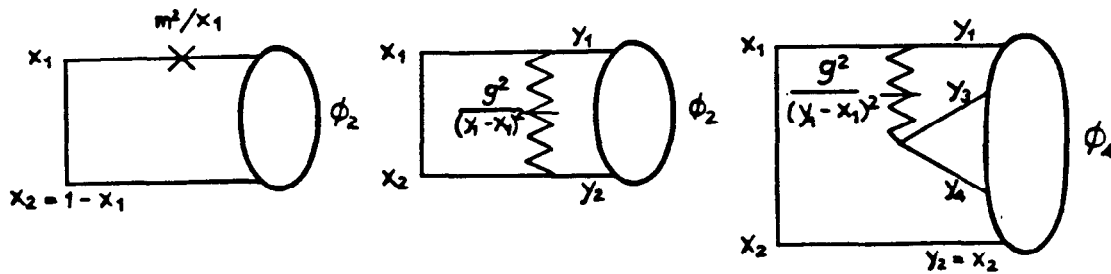


Figure 28. Typical Diagrams which Contribute to the Integral Equation for $\phi_2(x)$.

That the endpoint behavior of the valence wavefunction is unmodified by including higher-Fock states may be understood by tracing the source of the leading term. For $x_1 \sim 0$, the leading kinetic term, Fig. (28a) goes as m^2/x_1 . (The modification from the endpoint behavior of $\phi_2(x)$ may be ignored for now.) This must be matched by the leading term from the exchange of an instantaneous gluon, Fig. (28b). The dominant contribution from the y_1 integration comes from the region where y_1 is near x_1 . Taking $\Delta y_1 \sim x_1$, and g^2/x_1^2 from the gluon suggests a leading contribution which goes as g^2/x_1 , matching the kinetic term. The variable y_2 is fixed by momentum conservation, and so contributes nothing further.

Higher-Fock wavefunctions will appear in interactions of which Fig. (28c) is typical. Again, the y_1 integral is dominated by the region $y_1 \sim x_1$, and with the propagator contributes g^2/x_1 . Because $y_2 = x_2 = 1 - x_1$, the integration variable y_3 is restricted to be less than x_1 by $\sum y_i = 1$, contributing another factor of x_1 . This diagram will be of order zero in x_1 and as a consequence, ϕ_4 does not affect the leading behavior of ϕ_2 .

This may be seen explicitly in Eq. (3.40) (for $SU(N)$). The valence terms have already been discussed. The ϕ_4 term,

$$-4 \frac{g_N^2}{\pi} \int_0^{1-x_1-\epsilon} dy_4 \int_0^{1-x_1-y_4} dy_3 \frac{\phi_4(x_1, 1-x_1-y_3-y_4; y_3, y_4)}{(1-x_1-y_4)^2}, \quad (3.43)$$

(with ϕ_4 approximated by one) would contribute $+4(g_N^2/\pi)\ln(\epsilon/(\sigma-1)x_1)$ from the region $y \in [1-\sigma x_1, 1-x_1-\epsilon]$, while the second ϕ_4 term would add $-4(g_N^2/\pi)\ln(\epsilon/x_1)$. The combination is finite in ϵ and order zero in x_1 , as anticipated. As long as ϕ_4 does not in reality diverge for small x_1 , allowing it non-trivial behavior does not alter the conclusion.

There is nothing in this discussion which is specific to two and four particle wavefunctions. In general, the leading endpoint behavior is determined by two-to-two quark interactions, regardless of the presence of spectators. This has already been observed for baryon valence wavefunctions, which were shown to possess the same asymptotic small- x behavior as the valence meson.

Furthermore, this also appears to hold for higher-Fock wavefunctions. Consider Eq. (3.42) for ϕ_4 . As argued above, ϕ_6 does not influence the behavior of ϕ_4 as $x_1 \rightarrow 0$. Also, the momenta appearing in terms with ϕ_2 are fixed and cannot

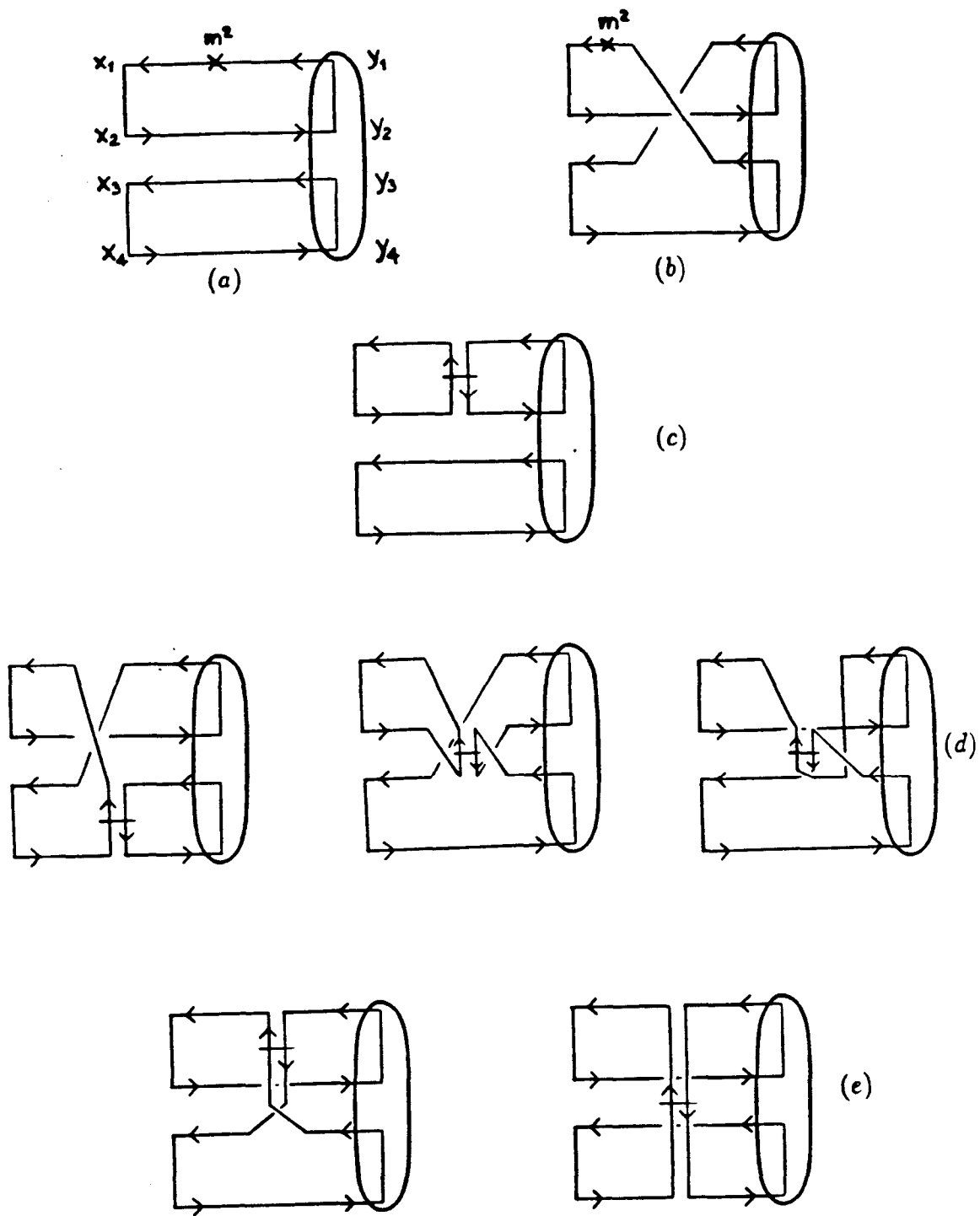


Figure 29. Terms in the Integral Equation for ϕ_4 which Contribute to the Leading Small- x Behavior. (a) Order 1; (b) Order $1/N$; (c) Order $g^2 N$; (d) Order g^2 ; (e) Order g^2 Only Appearing for $U(N)$.

match the kinetic term singularity of m^2/x_1 . The terms which do contribute are illustrated diagrammatically in Fig. (29). Color flow is explicitly indicated.

Only gluon exchange terms involving x_1 are relevant. Of these, two of the order- g^2 interactions cancel, as do the $U(N)$ terms. As a result, as $x_1 \rightarrow 0$ with the other x_i fixed, $\phi_4 \sim x_1^a f(x_2, x_3, x_4)$ with the same exponent a as for the valence meson and baryon.

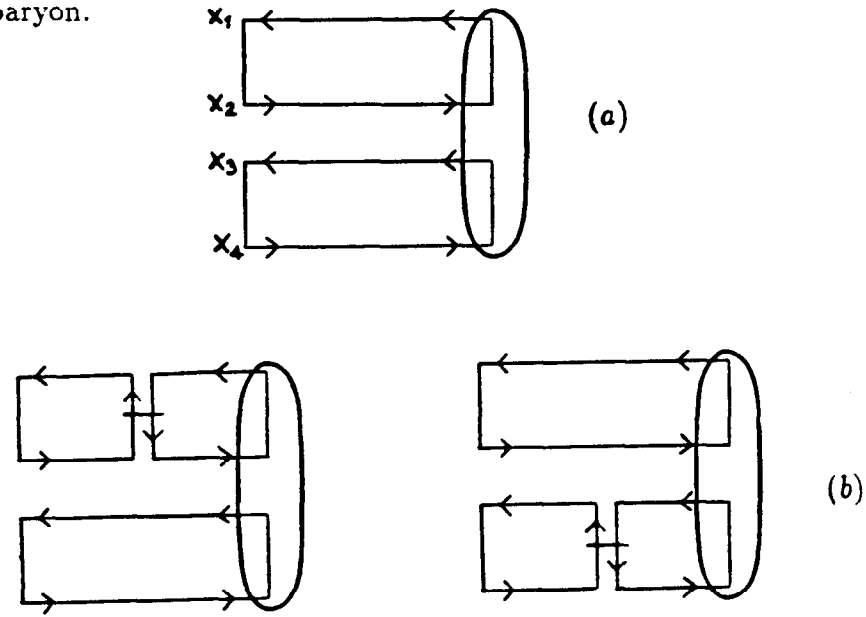


Figure 30. Leading Terms in Large- N Limit for the ϕ_4 Integral Equation. (a) Diagonal Terms, Including Normalization; (b) Interactions.

Eqs. (3.42) and (3.40) may be used to demonstrate explicitly how $q\bar{q}$ meson decouple in the large- N limit. From Eq. (3.42), only the terms which correspond to planar diagrams illustrated in Fig. (30) contribute to leading order. Note that the pairs of color singlets act independently to this order, even in the wavefunction normalization, and it is reasonable to expect a product of ϕ_2 wavefunctions to form a solution for ϕ_4 . For example, consider the case where momentum is equally shared, $x_1 + x_2 = x_3 + x_4 = 1/2$. Define new momenta u_1, u_2, v_1, v_2 as twice x_1, x_2, x_3, x_4

respectively, so as to range from zero to one. Substituting $\phi_2(u_1, u_2)\phi_2(v_1, v_2)$ for $\phi_4(x_1, x_2; x_3, x_4)$ factorizes Eq. (3.42) to leading order in N :

$$\begin{aligned}
M^2 \phi_2(u)\phi_2(v) = & \\
& 2 \left[m^2 \left(\frac{1}{u_1} + \frac{1}{u_2} \right) \phi_2(u) - \frac{g^2 N}{2\pi} \int_0^1 dy \frac{\phi_2(y) - \phi_2(y)}{(y-u)^2} \right] \phi_2(v) \\
& + 2 \left[m^2 \left(\frac{1}{v_1} + \frac{1}{v_2} \right) \phi_2(v) - \frac{g^2 N}{2\pi} \int_0^1 dy \frac{\phi_2(y) - \phi_2(y)}{(y-v)^2} \right] \phi_2(v).
\end{aligned} \tag{3.44}$$

Evidently, if ϕ_2 is an eigenstate of the large- N $q\bar{q}$ equation with mass squared of μ^2 , then M^2 for ϕ_4 is just $4\mu^2$; that is, the mass of two non-interacting mesons at zero relative momentum.

Note that in Eq. (3.40), ϕ_4 appears coupled to ϕ_2 even to leading order in N . However, for the particular case where $\phi_4 = \phi_2 \times \phi_2$, these terms cancel, and ϕ_2 satisfies the large- N valence Fock state equation, uncoupled to either higher-Fock wavefunctions or meson pairs.

Meson and baryon wavefunctions in the valence approximation exhibit a universal asymptotic behavior as a single variable approaches zero while the others remain fixed,

$$\phi(x) \propto x_1^a,$$

with a given in Eq. (3.22). This holds for all N . Furthermore, mesonic integral equations which incorporate the four-quark Fock state show both that its inclusion does not alter this property for the valence wavefunction, and that it shares the same small- x form. This holds whether this four-quark state represents a pair

of valence mesons, in which case the behavior is required for consistency, or the higher-Fock contribution to a single meson.

The interaction that provides the g^2/x to match the kinetic m^2/x term as $x \rightarrow 0$, two-quark to two-quark instantaneous gluon exchange, preserves quark number. Because this interaction appears in essentially the same way in all integral equations, it is likely that Eq. (3.22) holds for all wavefunctions, whether valence or higher-Fock, and that this behavior is unaffected by interaction with states of higher or lower quark number.

Numerical errors are due to both the endpoint behavior and the principal value prescription for the gluon propagator, as well as those usually associated with numerical integration. The principal value prescription provides the same order $1/K$ error in all cases. If the endpoint wavefunction behavior is also universal, then for a given g/m , the errors for all quantities computed will behave in the same manner as that described for the valence meson, Eq. (3.39). In any case, it has been shown to be true generally enough to make Richardson extrapolation applicable in most cases of interest. In particular, the lightest meson and baryon are dominated by their valence wavefunctions up to fairly strong coupling, and it is certainly applicable there.

3.8. HEAVY-QUARK LIMIT FOR MESONS

In order to understand the large quark mass limit of low-lying meson masses and wavefunctions, the large mass limit of the meson integral equation

$$m^2 \left(\frac{1}{x_a} + \frac{1}{x_b} \right) \phi(x_a, x_b) - \frac{g_N^2}{\pi} \int_0^1 dy \frac{\phi(y) - \phi(x)}{(y-x)^2} = M^2 \phi(x), \quad (3.45)$$

with

$$g_N^2 \equiv g^2 \left(\frac{N^2 - 1}{2N} \right) \quad \text{and} \quad x_a + x_b = 1,$$

may be taken directly. In this limit, higher-Fock components may be neglected, as they contain a larger number of the very massive quarks. Were there physical, propagating gluons, higher states containing arbitrary numbers of gluons in addition to the heavy quark pair would either be included explicitly or incorporated into an effective $q\bar{q}$ potential. Unlike the formulation in the infinite momentum frame, no special frame has been selected, and a nonrelativistic limit of Eq. (3.45) is perfectly sensible.

Furthermore, such a reduction should help to clarify the connection between wavefunctions in nonrelativistic quantum mechanics and those on the light cone. Following Ref. [24], the expansion may be performed by counting powers of quark velocity (small) and mass (large). Let k_a and k_b be the equal-time momentum in the x^1 direction, of order mv . Then

$$\begin{aligned} k_a^\pm &= (m^2 + k_a^2)^{1/2} \pm k_a \\ &\sim m \pm k_a + \frac{k_a^2}{2m} + \dots, \end{aligned} \tag{3.46}$$

with terms of order m , mv and mv^2 , respectively. After dividing Eq. (3.45) through by the total light-cone momentum P^+ to convert x_a and x_b to k_a^+ and k_b^+ from $k^+ = xP^+$, then, in terms of the equal-time momentum sum and difference,

$$k \equiv k_a + k_b \quad \text{and} \quad q \equiv k_a - k_b, \tag{3.47}$$

the expanded kinetic term is

$$m^2 \left(\frac{1}{k_a^+} + \frac{1}{k_b^+} \right) \sim 2m - k + \frac{1}{4m} (k^2 + q^2) + \dots \quad (3.48)$$

Defining the binding energy E by

$$E \equiv M - 2m = \mathcal{O}(mv^2), \quad (3.49)$$

the right-hand side of Eq. (3.45) reduces to

$$\begin{aligned} \frac{M^2}{P^+} \phi(x) &= \frac{(2m + E)^2}{k_a^+ + k_b^+} \phi(x) \\ &\sim \left(2m - K + 2E + \frac{(k^2 - q^2)}{4m} + \dots \right) \phi(x). \end{aligned} \quad (3.50)$$

Note that the arguments of $\phi(x)$ in this limit, x_a and x_b , become

$$\begin{aligned} x_a &\sim \frac{1}{2} + \frac{q}{4m} + \dots, \\ x_b &\sim \frac{1}{2} - \frac{q}{4m} + \dots. \end{aligned} \quad (3.51)$$

As discussed in Ref. [24], light-cone wavefunctions involving n heavy quarks will be strongly peaked around $x \sim 1/n$, or $1/2$ in this case. The nonrelativistic wavefunction is then

$$\phi(q) \equiv \phi \left(\frac{1}{2} + \frac{q}{4m}, \frac{1}{2} - \frac{q}{4m} \right). \quad (3.52)$$

Finally, the potential term becomes, after replacing y with $1/2 + q'/4m$ and

letting $p = q' - q$,

$$-\frac{4g_N^2 m}{\pi P^+} \int_{-2m}^{2m} \frac{dp}{p^2} [\phi(p+q) - \phi(q)]. \quad (3.53)$$

Keeping the leading term from P^+ , and assuming that the wavefunctions fall off quickly enough to extend the integration to infinity, Eq. (3.45) is finally

$$\frac{q^2}{4m} \phi(q) - \frac{g_N^2}{\pi} \int_{-\infty}^{\infty} \frac{dp}{p^2} [\phi(p+q) - \phi(q)] = E\phi(q). \quad (3.54)$$

In terms of the position-space wavefunction

$$\phi(z) = \frac{1}{(2\pi)^{1/2}} \int_{-\infty}^{\infty} dq e^{-iqz} \phi(q), \quad (3.55)$$

the interaction term transforms into the local potential

$$V(z) \equiv \int_{-\infty}^{\infty} \frac{dp}{p^2} [e^{-ipz} - 1] = -\pi|z|. \quad (3.56)$$

Note that this principal value prescription does not generate an additional finite renormalization of the quark mass. Eq. (3.54) becomes the Schrodinger equation

$$\left[-\frac{1}{4m} \partial_z^2 + g_N^2 |z| \right] \phi(z) = E\phi(z). \quad (3.57)$$

This derivation required the relevant momenta in the wavefunction to be much less than twice the quark mass; for example, it was used to obtain Eq. (3.54) from Eq. (3.53). In other words, the position-space wavefunction is sensible as long as distances as small as the Compton wavelength of the quarks are not probed, where, for example, pair production would foil a probabilistic interpretation of $\phi(z)$.

This equation and its solutions are discussed in Ref. [37]. Introducing dimensionless variables

$$u \equiv (4g_N^2 m)^{1/3} z \quad \text{and} \quad \lambda \equiv \left(\frac{4m}{g_N^4} \right)^{1/3} E, \quad (3.58)$$

the equation becomes

$$[-\partial_u^2 + |u|] \phi(u) = \lambda \phi(u). \quad (3.59)$$

The solutions are Airy functions,

$$\phi_n(u) = A_i(u - \lambda_n), \quad (3.60)$$

with eigenvalues given by

$$A_i'(-\lambda_n) = 0 \quad (3.61)$$

for symmetric (parity odd) states, and

$$A_i(-\lambda_n) = 0 \quad (3.62)$$

when antisymmetric (parity even).

The lowest meson mass

$$\frac{M_1}{g} = \frac{2m}{g} + \left(\frac{g}{4m} \right)^{1/3} \left(\frac{N^2 - 1}{2N} \right)^{2/3} \lambda_1 \quad (3.63)$$

is plotted in Fig. [31] for $N = 2, 3$ and 4 and compared with the actual output. Note that in all cases, the binding energy E is positive. The actual data asymptotically approaches the nonrelativistic limit from below, reaching to within about 5% for $m/g = 1.6$.

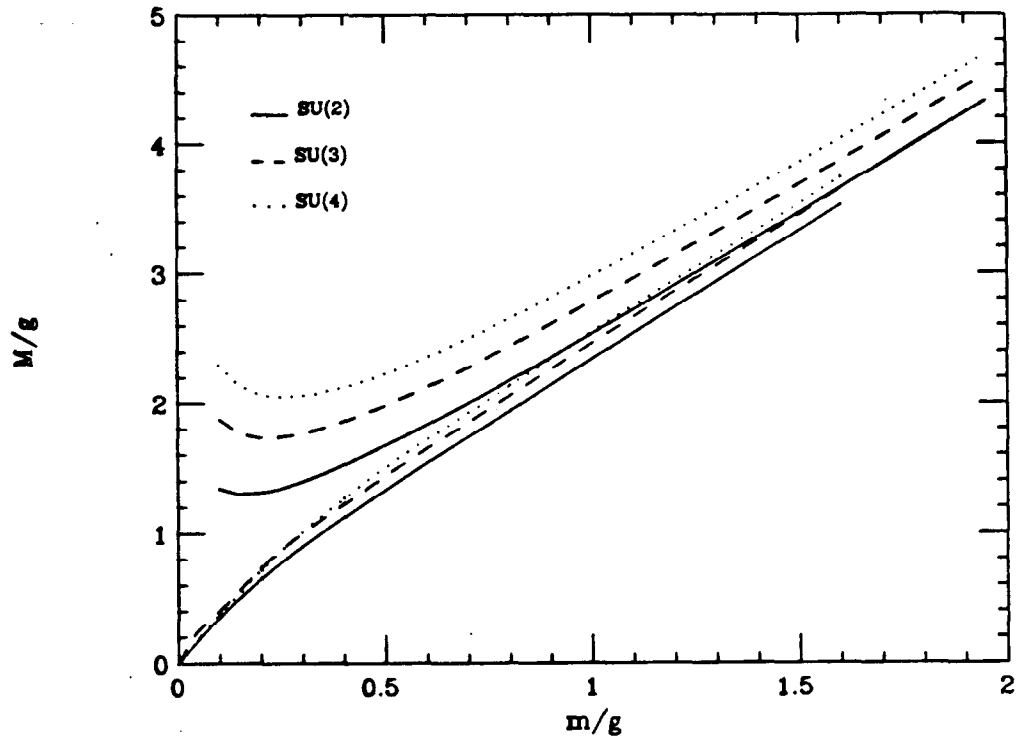


Figure 31. Comparison of Lightest Meson Mass for $N = 2, 3,$ and 4 with Nonrelativistic Solutions.

3.9. HEAVY-QUARK LIMIT FOR BARYONS

The same nonrelativistic reduction may be applied to the minimum Fock state equation for the baryon. Three colors will be considered here, although the extension of the nonrelativistic Schrodinger equation to baryons of larger N will be evident. As a consequence, the confining potential for three (or more) very massive quarks may be derived from first principles.

The light-cone eigenvalue equation for the $N = 3$ baryon restricted to three quarks is

$$\begin{aligned}
& m^2 \left(\frac{1}{x_a} + \frac{1}{x_b} + \frac{1}{x_c} \right) \phi(x) - \frac{g^2}{\pi} \left(\frac{N+1}{2N} \right) \left[\right. \\
& \quad \int_{\epsilon}^{x_a} \frac{ds}{s^2} [\phi(x_a - s, x_b, x_c + s) + \phi(x_a - s, x_b + s, x_c) - (N-1)\phi(x)] \\
& \quad + \int_{\epsilon}^{x_b} \frac{ds}{s^2} [\phi(x_a + s, x_b - s, x_c) + \phi(x_a, x_b - s, x_c + s) - (N-1)\phi(x)] \\
& \quad \left. + \int_{\epsilon}^{x_c} \frac{ds}{s^2} [\phi(x_a, x_b + s, x_c - s) + \phi(x_a + s, x_b, x_c - s) - (N-1)\phi(x)] \right] \\
& = M^2 \phi(x) ,
\end{aligned} \tag{3.64}$$

where $x_a + x_b + x_c = 1$. Proceeding as for the meson, the equation is divided through by P^+ , the k_i^+ are expanded in powers of velocity over mass, and the binding energy is defined to be

$$E \equiv M - 3m . \tag{3.65}$$

In terms of the relative momenta

$$\begin{aligned}
K &= k_a + k_b + k_c, \\
p &= k_a - k_b, \\
q &= k_b - k_c, \\
p + q &= k_a - k_c,
\end{aligned} \tag{3.66}$$

where the k_i are the equal-time spatial momenta, Eq. (3.64) reduces to

$$\frac{1}{3m} [p^2 + q^2 + (p+q)^2] \phi(x) + V\phi(x) = 2E \phi(x) , \tag{3.67}$$

with the potential V still to be computed. As before, the total momentum K has dropped out.

The arguments of the wavefunction, x_i , to leading nontrivial order in p and q , become

$$\begin{aligned} x_a &\sim \frac{1}{3} + \frac{2p+q}{3m}, \\ x_b &\sim \frac{1}{3} + \frac{q-p}{3m}, \\ x_c &\sim \frac{1}{3} - \frac{(2q+p)}{3m}. \end{aligned} \tag{3.68}$$

The nonrelativistic momentum-space wavefunction is then determined from the light-cone wavefunction by

$$\begin{aligned} \phi(x_a, x_b, x_c) &\sim \phi\left(\frac{1}{3} + \frac{2p+q}{3m}, \frac{1}{3} + \frac{q-p}{3m}, \frac{1}{3} - \frac{(2q+p)}{3m}\right) \\ &\equiv \phi(p, q). \end{aligned} \tag{3.69}$$

To compute the potential V , consider the first potential term of Eq. (3.64). Expanding the arguments of $\phi(x)$ as in Eq. (3.69), and defining a new integration variable $t = ms$, the leading contribution from this integral is

$$m \int_{\epsilon}^{m/3} \frac{dt}{t^2} \phi(p-t, q-t). \tag{3.70}$$

Including the term where s appears with the opposite sign, as well as the terms necessary to keep the integral well-defined gives an interaction of the form

$$m \int_{-m/3}^{m/3} \frac{dt}{t^2} [\phi(p-t, q-t) - \phi(p, q)]. \tag{3.71}$$

To develop a position-space equation, define z_a, z_b , and z_c to be the variables con-

jugate to k^a, k^b , and k^c . Then the variables conjugate to K, p , and q , respectively, are

$$\begin{aligned}\bar{z} &= \frac{1}{3}(z_a + z_b + z_c), \\ z_p &= \frac{1}{3}(2z_a - z_b - z_c), \\ z_q &= \frac{1}{3}(z_a + z_b - 2z_c).\end{aligned}\tag{3.72}$$

Defining the position-space wavefunction by

$$\phi(p, q) = \int_{-\infty}^{\infty} \frac{dz_p dz_q}{(2\pi)} e^{-i(pz_p + qz_q)} \phi(z_p, z_q)\tag{3.73}$$

and converting Eq. (3.71) into a position-space potential, the Schrodinger equation for $\phi(z)$ is

$$\begin{aligned}\left[-\frac{1}{6m^2} \left(\partial_{z_p}^2 + \partial_{z_q}^2 + (\partial_{z_p} + \partial_{z_q})^2 \right) \right. \\ \left. + \frac{g^2}{6} \left(\frac{N+1}{2N} \right) \left(|z_a - z_b| + |z_a - z_c| + |z_b - z_c| \right) \right] \phi(z) \\ = E \phi(z).\end{aligned}\tag{3.74}$$

The variables z_a, z_b , and z_c are understood to be functions of z_p and z_q . The extension of this equation to N other than three is now straightforward.

To sketch the method for solving Eq. (3.74), rewrite it in terms of the variables

$$r = \frac{1}{3}(z_p + z_q) \quad \text{and} \quad t = z_p - z_q.\tag{3.75}$$

These diagonalize the derivatives, and Eq. (3.74) is now

$$\left[-\frac{1}{3m} \left(\frac{1}{9} \partial_r^2 + \partial_t^2 \right) + \frac{g^2}{4} \left(\frac{N+1}{2N} \right) \left(|r+t| + 2|r| + |r-t| \right) \right] \phi(r,t) = E \phi(r,t) \quad (3.76)$$

This may be solved by separation of variables

$$\phi(r,t) = R(r)T(t), \quad (3.77)$$

yielding the equations

$$\begin{aligned} -\frac{1}{27m} R'' + \alpha \frac{g^2}{2} \left(\frac{N+1}{2N} \right) r R &= \lambda R \\ -\frac{1}{3m} T'' + \beta \frac{g^2}{2} \left(\frac{N+1}{2N} \right) t T &= (E - \lambda) T, \end{aligned} \quad (3.78)$$

where $\beta = 0, \pm 1$ and $\alpha = \pm 1, \pm 2$ depending on the region of r and t . The solutions are again Airy functions, except when $\beta = 0$, and eigenvalue conditions may be derived by matching solutions at the various boundaries of r and t .

3.10. MASSLESS MESONS AND BARYONS AT STRONG COUPLING

As discussed previously, the momentum space transforms of the $SU(N)$ currents (at $x^+ = 0$)

$$V_k^a = \frac{1}{2} \int_{-L}^L dx^- e^{-i \frac{kx^-}{L}} j^{+a}(x^-) \quad (3.79)$$

satisfy the algebra of Eq. (1.140). This may be extended to include the $U(1)$

current

$$j^{+(0)} = 2 : \psi_R^\dagger T^0 \psi_R : \quad (3.80)$$

with $T^0 = \frac{1}{\sqrt{2N}} \mathbf{1}$. The transformed operator V_k^0 commutes with the other $SU(N)$ elements, and satisfies

$$[V_k^0, V_\ell^0] = \frac{1}{2} \ell \delta_{k+\ell, 0}. \quad (3.81)$$

Noting that $V_k^{a\dagger} = V_{-k}^a$, this may be rewritten

$$[V_k^{0\dagger}, V_\ell^0] = \frac{1}{2} \ell \delta_{k, \ell}. \quad (3.82)$$

The interacting part of the Hamiltonian is greatly simplified when expressed in terms of these operators:

$$P_I^- = -\frac{g^2}{16} \int_{-L}^L dx^- dy^- j^{+a}(x^-) |x^- - y^-| j^{+a}(y^-) \quad (3.83)$$

becomes

$$\frac{L}{\pi} \frac{g^2}{4\pi} \sum_{k=-\infty}^{\infty} \frac{1}{k^2} V_k^a V_{-k}^a. \quad (3.84)$$

Because $V_0^a = Q^a$, the contribution at $k = 0$ is proportional to the total charge $Q^a Q^a$ and so may be discarded.

The V_k^0 are color-singlet bilinears in ψ_R , and so may be used to create mesonic-like states. Specifically, the related operators (for $k > 0$ by definition)

$$a_k^\dagger \equiv \left(\frac{2}{k}\right)^{\frac{1}{2}} V_k^0, \quad a_k \equiv -\left(\frac{2}{k}\right)^{\frac{1}{2}} V_k^{0\dagger} = -\left(\frac{2}{k}\right)^{\frac{1}{2}} V_{-k}^0 \quad (3.85)$$

satisfy standard free boson commutation relations

$$[a_k, a_l^\dagger] = \delta_{k,l} \quad (3.86)$$

and so V_k^0 creates a boson with momentum $P^+ = 2\pi k/L$. In the limit where m/g is zero, the entire Hamiltonian is given by Eq. (3.84). Because the V_k^0 commute with the V_k^a which appear in P_I^- ,

$$M^2 V_k^0 |0\rangle = \frac{2\pi k}{L} [P^-, V_k^0] |0\rangle = 0. \quad (3.87)$$

Not only is the state created by acting with V_k^0 on the vacuum an exactly massless eigenstate in this limit, but states formed by repeated applications are also exactly massless. Furthermore, acting with V_k^0 on an eigenstate of non-zero mass produces a degenerate state of opposite parity, as will be demonstrated. This argument is independent of the value of the numerical momentum K and so gives an exact continuum result.^[38]

The finiteness of K becomes relevant, however, when counting the number of massless mesons which can be produced. Massless mesonic states of total numerical momentum K of $10/2$, for example, may be constructed by from one to five applications of V_k^0 on the vacuum, with momentum distributed as (5), (1, 4), (2, 3), (1, 1, 3), (1, 1, 2), (1, 1, 1, 2) and (1, 1, 1, 1, 1). Comparing with Fig. (4a), these account for all seven of the states whose masses vanish in this limit. Increasing K permits an increasing number of massless states, which becomes infinite in the continuum limit.

Just as the existence and number of massless states is most simply discussed in terms of the V_K^0 , so also are the wavefunctions of these states. Applying one V_K^0

to the vacuum

$$V_K^0 |0\rangle = \frac{1}{\sqrt{2N}} \sum_{n=\frac{1}{2}, \frac{3}{2}, \dots}^{K-\frac{1}{2}} b_{K-n}^{\dagger c} d_{n,c}^{\dagger} |0\rangle \quad (3.88)$$

yields a continuum wavefunction of $\phi(x) = 1$; in the continuum, n/K becomes x . Because ϕ is even under the interchange of x and $1-x$, this state is a pseudoscalar. The wavefunctions of momentum K created by applying V^0 twice are, for any $\ell < K$,

$$V_{K-\ell}^0 V_{\ell}^0 |0\rangle = \frac{1}{2N} \left[\sum_{n=\frac{1}{2}}^{\ell-\frac{1}{2}} \left(b_{K-n}^{\dagger c} d_{n,c}^{\dagger} - b_n^{\dagger c} d_{K-n,c}^{\dagger} \right) + \sum_{m=\frac{1}{2}}^{K-\ell-\frac{1}{2}} \sum_{n=\frac{1}{2}}^{\ell-\frac{1}{2}} b_{K-\ell+m}^{\dagger c_2} d_{m,c_2}^{\dagger} b_{\ell-n}^{\dagger c_1} d_{n,c_1}^{\dagger} \right] |0\rangle . \quad (3.89)$$

The $q\bar{q}$ piece is odd and so this state is a scalar, as a product of pseudoscalars must be. All the massless meson wavefunctions for a given K may be constructed in this manner, and parity will alternate with each additional V^0 .

Two further comments should be made. First, each additional V^0 increases the particle number of the highest Fock state, which has a coefficient of order one, by one $q\bar{q}$ pair. Because these states are degenerate as $m/g \rightarrow 0$, it is possible that a great deal of mixing occurs, and Fock states with any number of quanta might be expected to appear with arbitrary strength in any wavefunction. In fact, for finite but small m/g , the lower states are approximately ordered according to the number of V^0 's. The first state is almost entirely composed of $V_K^0 |0\rangle$, the second by $V_{K/2}^0 V_{K/2}^0 |0\rangle$, and so on. There is however a small but persistent four-quark

component for the lightest meson which is given in Table [5]. This component drops rapidly with N , decreasing by a factor of ten from $N = 2$ to 3, and again to $N = 4$, as in Fig. (19a).

Second, these states are massless and described in terms of the bosonic operators V_k^0 only when m/g is identically zero. For small but finite m/g , the free Hamiltonian contains terms like m^2/x_i , and so is singular when constituent i carries zero momentum. Wavefunctions must therefore vanish at these endpoints, whereas those described above for m/g identically zero do not; $m/g \rightarrow 0$ is evidently a singular point in this formalism and perhaps in the theory.^[39] Although it need not have been the case, it will be shown that m/g finite but approaching zero, the solutions for $m/g = 0$ provide an accurate description of both the spectrum and the wavefunctions, apart from small regions around $x_i = 0$, where the wavefunctions must vanish.

If the gauge group were $U(N)$ rather than $SU(N)$ ^[40] the additional term associated with the extra $U(1)$,

$$\frac{L}{\pi} \frac{g^2}{4\pi} \sum_{k=-\infty}^{\infty} \frac{1}{k^2} V_k^0 V_{-k}^0 = \frac{L}{\pi} \frac{g^2}{4\pi} \sum_{k=1}^{\infty} \frac{1}{k} a_k^\dagger a_k + \text{constant} \quad (3.90)$$

appears in P^- . The a_k satisfy free bosonic commutation relations, and this additional interaction is therefore the discrete light-cone Hamiltonian for free bosons of mass squared $g^2/2\pi$. These formerly massless states created by the a_k^\dagger are promoted to the free massive bosons found in the Schwinger model and discussed Refs. [23] and [20]. The wavefunctions for these states however are unchanged.

Note that while the entire $U(1)$ spectrum may be built up from these non-interacting bosons,^[20] for $U(N)$ or $SU(N)$ they describe only part of the spectrum;

these are the massless mesons for $SU(N)$. In addition there are massive states composed predominantly of excited $q\bar{q}$ pairs.

The $U(1)$ (Schwinger) model has been solved exactly by establishing a correspondence between the current $j^{\mu(0)}$ and a scalar field^[41]

$$j^{\mu(0)}(x) \equiv \frac{1}{\sqrt{2\pi}} \epsilon^{\mu\nu} \partial_\nu \phi^0(x). \quad (3.91)$$

By means of the axial anomaly, this field may be shown to satisfy the equation of motion for a free massive scalar field, with a mass squared of $g^2/2\pi$. Not surprisingly, the operators a_k^\dagger and a_k discussed above are the creation and annihilation operators which result from quantizing $\phi^0(x)$ on the light cone with periodic boundary conditions in x^- . The scalar $\phi^0(x)$ expanded in these operators,

$$\phi^0(x^-) = \frac{i}{\sqrt{2\pi}} \sum_{\ell>0} \left(\frac{1}{2\ell}\right)^{\frac{1}{2}} \left[a_\ell e^{-i\frac{\ell\pi}{L}x^-} + a_\ell^\dagger e^{i\frac{\ell\pi}{L}x^-} \right] \quad (3.92)$$

satisfies the standard light-cone commutation relation

$$[\phi^0(x), \partial_- \phi^0(y)]_{x^+=y^+=0} = -\frac{i}{2} \delta(x^- - y^-). \quad (3.93)$$

For a discussion of bosonization for the non-Abelian currents, see Ref. [42].

A similar argument may be advanced to show that in this limit there are massless baryons as well. The commutator of the V_k^a which appear in the interacting part of the Hamiltonian, and N products of the field $\psi_L^\dagger(x)$ at the point $(0, x^-)$ is

$$\begin{aligned} [V_k^a, \psi_R^{\dagger c_1}(x^-) \cdots \psi_R^{\dagger c_N}(x^-)] = \\ e^{-i\frac{k\pi}{L}x^-} ([T^a]_d^{c_1} \psi_R^{\dagger d}(x^-) \cdots \psi_R^{\dagger c_N}(x^-) + \\ \cdots + [T^a]_d^{c_N} \psi_R^{\dagger c_1}(x^-) \cdots \psi_R^{\dagger d}(x^-)) . \end{aligned} \quad (3.94)$$

The fields multiplied at the same point are all adjoints, and singularities which are regulated by point splitting should be absent.

The entire k dependence appears in the overall factor $e^{-i\frac{k\pi}{L}x^-}$. Consequently, noting that V_k^a at $k = 0$ is the charge operator Q^a ,

$$[V_k^a, \psi_R^{\dagger c_1} \cdots \psi_R^{\dagger c_N}] = e^{-i\frac{k\pi}{L}x^-} [Q^a, \psi_R^{\dagger c_1} \cdots \psi_R^{\dagger c_N}]. \quad (3.95)$$

If the fields are contracted with $\epsilon_{c_1 \cdots c_N}$ to form an $SU(N)$ singlet, this commutator will vanish.

In particular, the composite baryon field

$$B_k \equiv \frac{1}{2} \int_{-L}^L dx^- e^{-i\frac{k\pi}{L}x^-} \epsilon_{c_1 \cdots c_N} \psi_R^{\dagger c_1}(x^-) \cdots \psi_R^{\dagger c_N}(x^-) \quad (3.96)$$

commutes with the V_k^a , and, in the limit $m/g \rightarrow 0$, with the Hamiltonian P^- . As in the case for mesons, this field creates an identically massless baryon. Repeated applications on the vacuum produce a massless state with arbitrarily desired baryon number. Furthermore, degenerate states with the same baryon number may be created by acting with the massless mesonic operators V_k^0 in conjunction with B_k . Again, these results are independent of K and are true in the continuum limit.

The (unnormalized) wavefunction associated with this massless baryon is

$$B_k |0\rangle = \frac{1}{2(2L)^{\frac{N-1}{2}}} \sum_{\mathbf{n}_i} \delta_{K, \Sigma n_i} \epsilon_{c_1 \cdots c_N} b_{n_1}^{\dagger c_1} \cdots b_{n_N}^{\dagger c_N} |0\rangle. \quad (3.97)$$

Whether this state is a fermion or boson depends on N being odd or even.

As an illustration, the normalized state for $N = 3$ obtained from $B_k |0\rangle$ is

$$\frac{\epsilon_{c_1 c_2 c_3}}{[18(K + \frac{1}{2})(K - \frac{1}{2})]^{\frac{1}{2}}} \sum_{n_1, n_2} b_{n_1}^{\dagger c_1} b_{n_2}^{\dagger c_2} b_{K-n_1-n_2}^{\dagger c_3} |0\rangle . \quad (3.98)$$

The quark structure function derived from this wavefunction,

$$q(x_\ell) \equiv K \langle B | b_\ell^{\dagger c} b_{\ell, c} | B \rangle = \frac{6(1 - \ell/K)}{(1 + 1/2K)(1 + 1/2K)} , \quad (3.99)$$

becomes $6(1 - x)$ in the continuum limit. This is the x dependence clearly evident in Fig. (10). Note that this satisfies the baryon number sum rule

$$\int_0^1 dx \, 6(1 - x) = 3 . \quad (3.100)$$

The general expression for the quark structure function for a single baryon in the $m/g \rightarrow 0$ limit is

$$q(x) = N(N - 1)(1 - x)^{N-2} . \quad (3.101)$$

For $N = 2$, $q(x) = 2$, which apart from the normalization, is identical to the meson structure function for all N .

3.11. EXCITED MESON STATES AT STRONG COUPLING

In the limit of vanishing quark mass, the presence of massless decoupled mesons allows the lightest sector of the meson spectrum to be interpreted simply, but it enormously complicates the excited states. For weakly interacting states, the separation of the spectrum into states with several mesons, as opposed to single excited $q\bar{q}$ states was obvious. Excited meson wavefunctions are composed predominantly

of two quarks, while meson-pair wavefunctions, by contrast, are products of two single meson wavefunctions which are also individually present in the spectrum. Meson-pair wavefunctions contain predominantly two quark and antiquark pairs, and their masses begin at the sum of the single meson masses and increase with relative velocity, and so are easy to discriminate.

The situation is quite different as the quark, (and meson) mass vanishes. In two dimensions, two massless particles may be combined while leaving the total invariant mass zero, even when they possess a nonzero relative momentum. One consequence discussed earlier was the large number of massless states, limited only by the ability to subdivide a finite momentum K , created by repeatedly acting on the vacuum with the composite pseudoscalar field V_k^0 which commutes with the Hamiltonian.

Furthermore, excited, finite-mass states will occur in clusters of nearly equal mass and alternating parity as the quark mass vanishes. The same pseudoscalar fields which create the cluster of massless mesons can also be added to excited $q\bar{q}$ states. As k vanishes, their masses become degenerate. It is, in general, difficult and perhaps not meaningful to try to distinguish an excited quark-antiquark state from one with additional massless mesons, or from pairs of mesons. As the quark mass diminishes there is, in general, a large degree of mixing, and Fock states with all number of quarks give non-negligible contributions to almost all wavefunctions.

It is possible, however, to present a fairly simple picture of the total spectrum in this limit, even while difficult to characterize individual states by their wavefunctions. Consider first the spectrum of states when the Fock space is restricted

to a $q\bar{q}$ pair. The wavefunctions for the first four states are pictured in Fig. (9e) for very strong coupling or small mass, $m/g = .1$.

These states $\phi_n(x)$ are clearly well described, except at the endpoints, by

$$\phi_n(x) \sim \cos n\pi x . \quad (3.102)$$

An argument from Refs. [36] and [30] which applies to excited states at moderate couplings may be adapted to explain why a wavefunction of the form in Eq. (3.102) might be expected. The variable x in the $q\bar{q}$ equation for $\phi(x)$,

$$\frac{m^2}{x(1-x)} \phi(x) - \frac{g_N^2}{\pi} \int_0^1 dy \frac{\phi(y) - \phi(x)}{(y-x)^2} = M^2 \phi(x) , \quad (3.103)$$

may be reinterpreted as a position variable restricted to $x \in [0, 1]$, and $m^2/[x(1-x)]$ as a confining potential. The convolution integral would be roughly equivalent to $g_N^2 |\hat{p}| \phi(x)$ if y were integrated to infinity, with \hat{p} acting as the momentum operator conjugate to x . 't Hooft and Coleman argue that for highly excited states the (pseudo)potential $m^2/x(1-x)$ could be ignored, apart from requiring that $\phi(x)$ vanish at the endpoints. The eigenstates are then

$$\phi_n(x) \sim \sin n\pi x , \quad (3.104)$$

with

$$M^2 \approx g_N^2 \pi n . \quad (3.105)$$

However, for the strong coupling case above, while $\phi(x)$ must vanish at the endpoints for any finite m , to understand the wavefunctions and eigenvalues, it is apparently more appropriate to ignore the extreme endpoint behavior and to require

instead that $\phi'(x)$ vanish there. To see why this is the case, consider computing M^2 by taking the expectation value of the Hamiltonian in an eigenstate $\phi(x)$. The kinetic term endpoint singularities will be shown to cancel one power of m , and M^2 for a massless meson will go to zero as approximately a single power of m . However, since this kinetic contribution still vanishes with m , both the wavefunction, apart from the very ends, and the mass M for massive states are governed by the interaction term proportional to g^2 . The endpoint contributions to this integral are potentially singular. It is energetically favorable, then, for $\phi(x)$ to go to a constant in this region to cancel one power of the denominator; that is, for $\phi'(x)$ to vanish. Eigenstates are then given by cosines rather than sines.

An estimate of M^2 based on this picture may be obtained by computing the expectation value numerically, using $\phi(x) = \sqrt{2} \cos n\pi x$. The estimates for the first few states, given in Table [9], describe the spectrum to within about 10%.

Table [9]

n	M^2/g_N^2
0	0
1	5.9
2	14.3
3	23.4
4	32.7

This $q\bar{q}$ spectrum, augmented by clusters of nearly equal-mass states by the addition of massless, low-momentum, mesons, provides a fairly accurate characterization of the full strong-coupling spectrum.

3.12. HADRON MASSES AT SMALL QUARK MASS

In the limit of vanishing quark mass, a great deal of information about the dependence of the meson and baryon masses as a function of the quark mass can be extracted from the small- x behavior of their wavefunctions. Consider first the meson wavefunction $\phi(x)$ in the valence, or equivalently, the large- N approximation, which obeys the eigenvalue equation

$$M^2 \phi(x) = m^2 \left(\frac{1}{x} + \frac{1}{1-x} \right) \phi(x) - \frac{g_N^2}{\pi} \int_0^1 dy \frac{\phi(y) - \phi(x)}{(y-x)^2}. \quad (3.106)$$

The wavefunction $\phi(x)$ is normalized to one, and therefore

$$M^2 = m^2 \int_0^1 dx \frac{\phi^2(x)}{x(1-x)} - \frac{g_N^2}{\pi} \int_0^1 dx \int_0^1 dy \frac{\phi(x)[\phi(y) - \phi(x)]}{(y-x)^2}. \quad (3.107)$$

The form of $\phi(x)$ at small x is understood, and this can be exploited by examining quantities which are sensitive to this region, as in Refs. [22], [18] and [43]. A particularly useful trick is to express the dependence of M^2 on the quark mass m^2 in terms of the free Hamiltonian. By the Hellmann-Feynman theorem,

$$\partial_{m^2} M^2 = \partial_{m^2} \langle M^2 \rangle = \langle \partial_{m^2} M^2 \rangle, \quad (3.108)$$

and since

$$M^2 = m^2 H_0 + g^2 H_I, \quad (3.109)$$

then

$$\partial_{m^2} M^2 = \langle H_0 \rangle. \quad (3.110)$$

The brackets here indicate the expectation value within the meson. This is espe-

cially useful, as it relates $\partial_{m^2} M^2$ to the expectation value of a simple, diagonal operator. In the valence approximation,

$$\partial_{m^2} M^2 = \int_0^1 dx \frac{\phi^2(x)}{x(1-x)}. \quad (3.111)$$

Though generally true, it is useful in the $m/g \rightarrow 0$ limit. For $x \rightarrow 0$ (or 1), $\phi(x) \rightarrow cx^a$ (or $c(1-x)^a$), with c independent of x and equal in magnitude at both endpoints by parity. As $m \rightarrow 0$, $a \rightarrow (3/\pi)^{1/2}(m/g_N)$. In this limit, $\phi(x)$ in Eq. (3.111) is approaching a constant at the endpoints and these regions then dominate the integral. In this limit

$$\partial_{m^2} M^2 \rightarrow \frac{c^2}{a} = c^2 \left(\frac{\pi}{3}\right)^{\frac{1}{2}} \left(\frac{g_N}{m}\right), \quad (3.112)$$

or, integrating,

$$M^2 = M_{(m=0)}^2 + 2c^2 \left(\frac{\pi}{3}\right)^{\frac{1}{2}} g_N m \quad (3.113)$$

to leading order in m . The mass $M_{(m=0)}^2$ is independent of m , and so must be proportional to g^2 , if not zero. For lightest meson, $M_{(m=0)}^2$ is known to be zero. In the valence approximation, $\phi(x)$, and therefore c , approaches one as $m/g \rightarrow 0$, and therefore the leading term for the lightest meson is

$$M^2 = 2 \left(\frac{\pi}{3}\right)^{\frac{1}{2}} g_N m. \quad (3.114)$$

Also, it might be noted that because in general

$$m^2 \langle H_0 \rangle = c^2 \left(\frac{\pi}{3}\right)^{\frac{1}{2}} g_N m = \frac{1}{2} M^2, \quad (3.115)$$

then in this limit

$$m^2 \langle H_0 \rangle = g^2 \langle H_I \rangle = \frac{1}{2} M^2 .$$

The same argument may be advanced for $U(N)$, except that g_N^2 is replaced by $g(N/2)^{1/2}$. For the lightest meson, $M_{(m=0)}^2 = g^2/2\pi$, and $c = 1$. This is true even without restricting to the valence wavefunction, as this occurs dynamically. Then, for $U(N)$

$$M^2 = \frac{g^2}{2\pi} + 2 \left(\frac{\pi}{3}\right)^{\frac{1}{2}} \left(\frac{N}{2}\right)^{\frac{1}{2}} g m + \dots . \quad (3.116)$$

This discussion applies to the $SU(N)$ baryon as well as to the meson as $m/g \rightarrow 0$, since the wavefunction behaves in the same way as each argument $x_i \sim 0$. For each x_i there is a term m^2/x_i in H_0 which picks it out in the region near zero. As a result,

$$M_B^2 = M_{B(m=0)}^2 + 2 c_B^2 \left(\frac{\pi}{3}\right)^{\frac{1}{2}} \left(\frac{N}{2}\right)^{\frac{1}{2}} g m + \dots . \quad (3.117)$$

for valence $B = 1$ states. The coefficient c_B^2 here is given by the integral

$$\int dx_2 \cdots dx_N \delta(1 - \sum_{i \neq 1} x_i) \tilde{\phi}_B^2(x_2 \cdots x_N) , \quad (3.118)$$

where

$$\phi_B(x)_{x_1 \rightarrow 0} \rightarrow x_1^a \tilde{\phi}_B(x_2 \cdots x_N) . \quad (3.119)$$

For the lightest state, $M_{B(m=0)}^2 = 0$, and $c_B = 1$, so the baryon mass-squared, like the meson, goes to zero as a single power of m , but with a different N dependence.

Because this discussion relies only on the small- x behavior of the wavefunctions, and because H_0 is diagonal, it is simple to extend it to the case where higher-Fock states are included. Each n -particle state contributes a term $2c_n^2 \left(\frac{\pi}{3}\right)^{\frac{1}{2}} \left(\frac{N}{2}\right) g_N m$, with c_n defined as for the baryon. A great deal of interesting physics for finite N is tucked away into the coefficients c_n , which may at least be extracted numerically, although with some effort, and possibly analytically.

3.13. COMPARISON WITH RESULTS FROM BOSONIZATION

As has been seen, the dependence of the mass of the lightest meson and baryon states on the quark mass and coupling in the limit $m/g \rightarrow 0$ may be related to the asymptotic small- x behavior of wavefunctions. This behavior is shared by both the valence and higher-Fock states of mesons and baryons, lowest-lying and excited. As a result, all hadron masses obey

$$\partial_{m^2} M^2 = \left[\sum_n (n/2) c_n^2 \right] \left(\frac{\pi}{3}\right)^{\frac{1}{2}} \frac{g_N}{m}, \quad (3.120)$$

where n runs over the particle number of each wavefunction. That is, $n = 2, 4, 6, \dots$ for a meson, and $n = N, N + 2, N + 4, \dots$ for a baryon. The coefficients c_n^2 are defined as in the previous section.

In the valence or large- N approximation, only the leading c_n^2 is retained, which, for the lowest-lying meson or baryon, approaches one as $m/g \rightarrow 0$. The result for the lightest meson at large N , Eq. (3.114), has been derived by several methods, beginning with 't Hooft.^[21,36]

Accurate measurements of meson and baryon masses as functions of m and g in the $m/g \rightarrow 0$ limit for arbitrary N are of particular value in checking analytic

results obtained by several authors by means of bosonization.^[44,45] These yield a mass for both the lightest baryon and meson (for one flavor) which goes to zero with m as

$$M^2 \propto [m^2]^{\frac{1}{2}+\delta} [g^2]^{\frac{1}{2}-\delta} ,$$

with

$$\delta = \frac{1}{2(2N-1)} . \quad (3.121)$$

Clearly in the large- N limit, δ vanishes, consistent with the results above. However, for N finite, δ can be checked numerically.

The valence approximation produces the large- N result $\delta = 0$ for all hadrons; therefore, non-zero δ must be due to the presence of higher-Fock states. Furthermore, Eq. (3.120) depends only on the universal small- x behavior of wavefunctions and is true in general. To produce a relation such as Eq. (3.121) upon integrating Eq. (3.120), the coefficients c_n , which are independent of x , must however depend on m/g according to

$$c_n^2 \propto (m/g)^\delta ; \quad (3.122)$$

that is, as $x \rightarrow 0$, the leading dependence of $\phi(x)$ on both x and m/g must be such that

$$\phi(x_i)_{\substack{x_i \rightarrow 0 \\ m \rightarrow 0}} \propto (m/g)^\delta x_i^{(3/\pi)^{\frac{1}{2}}(m/gN)} , \quad (3.123)$$

where only the leading behavior of the power of x_i is retained. The suppression by the factor $(m/g)^\delta$ for small m is extremely mild, and is not significant until $m/g \sim e^{-1/\delta}$. If δ is given by Eq. (3.121), then $e^{-1/\delta} = e^{-2(2N-1)}$ which decreases rapidly with N , going from 2×10^{-1} at $N = 2$, to 8×10^{-5} at $N = 4$.

Certain qualitative features should be observed in the wavefunctions if δ is given by Eq. (3.121). First, including higher-Fock states should suppress the valence wavefunction $\phi_v(x)$ near $x \sim 0$, $m \sim 0$ by roughly a factor of $(m/g)^\delta$ relative to the valence approximation. In Table [10], the decrease of the $q\bar{q}$ wavefunction for the $N = 2$ meson at $2K = 24$, after including $q\bar{q}q\bar{q}$ higher-Fock states, is given for several m/g and x in this region, qualitatively confirming this. For $N = 2$, Eq. (3.121) gives $\delta = 1/6$.

Table [10]

m/g	$(m/g)^{\delta=1/6}$	x	$\phi_2(x)/\phi_2(x)_{val\ approx}$
.4	.86	5/24	.98
		3/24	.96
		1/24	.91
.2	.76	5/24	.99
		3/24	.95
		1/24	.89

Second, this suppression and the importance of higher-Fock states should diminish for larger N . As is evident in Fig. (19b), the magnitude of the $q\bar{q}q\bar{q}$ higher-Fock state decreases by two orders of magnitude from $N = 2$ to 4. The concurrent loss of probability from the ends of the valence wavefunction diminishes comparably.

The exponent β for the general case $M^2 \propto m^\beta$ as $m \rightarrow 0$ can be extracted numerically by measuring $\beta = M^{-2}m\partial_m M^2$. Attempts at this have produced results which, although consistent, have large errors, and a realistic check on β ,

while worthwhile, will require much larger values of K .

Another general bosonization result for the lightest meson and baryon masses as $m/g \rightarrow 0$,⁽⁴⁵⁾

$$M_{meson}/M_{baryon} = 2 \sin \left[\frac{\pi}{2(2N-1)} \right], \quad (3.124)$$

has been checked with slightly greater success. In particular, M_{mes}/M_{bar} was computed for N from 2 to 4 at several values of $2K$ up to about 20 and then extrapolated. Computing the ratio at each K prior to extrapolation proved more accurate than extrapolating the baryon and meson masses independently.

Table [11]

N	$2 \sin(\frac{\pi}{2(2N-1)})$	$2/N$
2	1	1
3	.6180	.6667
4	.4450	.5

For $N = 2$, the ratio is exactly one at all K and m/g , while the results for $N = 3$ and 4 are presented in Table [12]. These are clearly consistent, although with large errors, with those of Eq. (3.124) (Table [11]), approaching it from the nonrelativistic value of $2/N$ obtained by adding quark masses. The numbers in parentheses are the uncertainties in the final digit, estimated by the last term retained in the extrapolation series.

Table [12]

m/g	M_{mes}/M_{bar}	
	$N = 3$	$N = 4$
∞	$2/3$	$1/2$
1.6	.656(5)	.48(1)
.8	.647(3)	.477(6)
.4	.639(7)	.468(3)
.2	.64(7)	.46(2)
.1	.63(4)	.46(4)
.05	.62(5)	.46(4)

3.14. MATRIX ELEMENTS FOR SMALL QUARK MASS

Once having computed the full set of wavefunctions, not only masses but any other quantity desired (and well-defined) can be obtained simply by computing integrals. In this section, several analytic results for matrix elements, mainly vacuum-to-one-meson, will be presented, specifically for small quark mass, as an illustration.

The small-mass limit is of particular interest because several exact (mainly large- N) results become accessible, while numerical accuracy becomes increasingly difficult. Furthermore, certain anxieties about this region potentially provoked by previous discussions may be addressed First, for finite quark mass, boundary terms are neglected, and

$$\psi_L(0, x^-) = -\frac{im}{4} \int_{-L}^L dy^- \epsilon(x^- - y^-) \psi_R(0, y^-). \quad (3.125)$$

Only ψ_R is treated as a dynamical degree of freedom, and for vanishing quark mass, ψ_L apparently decouples, leading to an unacceptable loss of degrees of freedom. Second, mesons and baryons become massless simultaneously, giving conflicting suggestions about chiral symmetry.

Using the continuum forms for the fields, wavefunctions, and commutation relations, the matrix elements

$$\langle 0 | \psi_L^{\dagger c_2}(z^-) \psi_R^{c_2}(z^-) | \phi(k^+) \rangle = -m \delta_{c_1}^{c_2} e^{-\frac{i}{2} k^+ z^-} \int_0^1 \frac{dx}{(4\pi N)^{\frac{1}{2}}} \frac{\phi_2(x)}{x}, \quad (3.126)$$

$$\langle 0 | \psi_R^{\dagger c_2}(z^-) \psi_L^{c_2}(z^-) | \phi(k^+) \rangle = m \delta_{c_1}^{c_2} e^{-\frac{i}{2} k^+ z^-} \int_0^1 \frac{dx}{(4\pi N)^{\frac{1}{2}}} \frac{\phi_2(x)}{1-x}, \quad (3.127)$$

and

$$\langle 0 | \psi_R^{\dagger c_2}(z^-) \psi_R^{c_2}(z^-) | \phi(k^+) \rangle = \delta_{c_1}^{c_2} k^+ e^{-\frac{i}{2} k^+ z^-} \int_0^1 \frac{dx}{(4\pi N)^{\frac{1}{2}}} \phi_2(x) \quad (3.128)$$

Directly from these, the scalar, pseudoscalar, and gauge-current matrix elements are

$$\langle 0 | \bar{\psi}(z^-) \psi(z^-) | \phi(k^+) \rangle = -m \delta_{c_1}^{c_2} e^{-\frac{i}{2} k^+ z^-} \int_0^1 \frac{dx}{(4\pi)^{\frac{1}{2}}} \phi_2(x) \left[\frac{1}{x} - \frac{1}{1-x} \right], \quad (3.129)$$

$$\langle 0 | \bar{\psi}(z^-) \gamma^5 \psi(z^-) | \phi(k^+) \rangle = -m \delta_{c_1}^{c_2} e^{-\frac{i}{2} k^+ z^-} \int_0^1 \frac{dx}{(4\pi)^{\frac{1}{2}}} \phi_2(x) \left[\frac{1}{x} + \frac{1}{1-x} \right], \quad (3.130)$$

and

$$\langle 0 | j^{+a}(z^-) | \phi(k^+) \rangle = 2 \text{Tr}[T^a] k^+ e^{-\frac{i}{2} k^+ z^-} \int_0^1 \frac{dx}{(4\pi N)^{\frac{1}{2}}} \phi_2(x). \quad (3.131)$$

The last vanishes, except for the $U(1)$ current for which $\text{Tr}[T^0] = (N/2)^{1/2}$. In accordance with the discussion on parity, only pseudoscalar states (ϕ_2 odd under $x \leftrightarrow 1-x$) couple to $\bar{\psi}\gamma^5\psi$, and scalar states (even under $x \leftrightarrow 1-x$) to $\bar{\psi}\psi$, as would be expected.^[22]

ψ_L is proportional to the quark mass m , and is responsible for the m in front of Eqs. (3.129) and (3.130). These matrix elements appear to vanish with m , and were this the case, it would be an unwelcome symptom that ψ_L decouples. However, as discussed previously, as $m \rightarrow 0$, the integrals over $\phi_2(x)$ are dominated by the endpoints, where $\phi_2(x)_{x \rightarrow 0} \sim cx^a$, and similarly for $1-x \sim 0$.

A factor of $1/m$ from the integral exactly cancels the m from ψ_L . The result is a well-defined limit,

$$\langle 0 | \bar{\psi}(z^-) \gamma^5 \psi(z^-) | \phi(k^+) \rangle \rightarrow c(N/3)^{\frac{1}{2}} g_N e^{-\frac{i}{2} k^+ z^-} \quad (3.132)$$

when $|\phi(k^+)\rangle$ is a pseudoscalar, with the same result for $\bar{\psi}\psi$ and a scalar state. Apparently, the asymmetric treatment of ψ_L and ψ_R in quantization is exactly compensated for dynamically. In particular, the singular $1/p^+$ in the expansion for ψ_L prevents it from vanishing with m in matrix elements.

This provides fairly convincing evidence that the standard light-cone quantization is adequate for finite quark mass, and that the limit $m \rightarrow 0$ is sensible,

but also that for $m = 0$ identically, special care is required during quantization to retain ψ_L .

The singular m/p^+ in ψ_L , as in Eq. (1.105), and the corresponding kinetic term m^2/x in the Hamiltonian, while potentially ticklish, have actually proven advantageous in extracting the small- x behavior of wavefunctions and understanding the theory for small quark mass. Also, as discussed in Ref. [18], the leading behavior for the large- N meson form factor is also governed by this region of the wavefunction. Numerical and analytic results for form factors at finite N , including counting rules at large Q^2 , will be presented in subsequent work.

The behavior of the lightest meson as the quark mass vanishes is of particular interest and has been studied in the large- N limit extensively.^[36,22,18,39,46,43] It has already been noted that this particle is a pseudoscalar whose mass squared goes to zero with the quark mass as

$$M^2 \sim 2c^2 \left(\frac{\pi}{3}\right)^{\frac{1}{2}} g_N m , \quad (3.133)$$

with $c \sim 1$ in the large- N or valence approximation. This is all suspiciously suggestive of a two-dimensional pion; that is, the Goldstone boson associated with the spontaneous breakdown of chiral symmetry. Furthermore, from Eq. (3.117) and Fig. (10), if N is taken to infinity before m is allowed to vanish, the mass of the lowest-lying baryon is infinite, another indication of symmetry breaking. As frequently pointed out,^[36,39,43] the order of limits is important. Finally, repeating the standard derivation for the chiral condensate $\langle \bar{\psi}\psi \rangle$, beginning with a pion interpolating field ϕ_π from the divergence of the $U(1)$ axial current

$$\partial_\mu j_5^\mu \equiv \sqrt{2} f_\pi m_\pi^2 \phi_\pi \quad (3.134)$$

and using Eq. (3.132) with $c = 1$ yields^[43]

$$f_\pi = (N/2\pi)^{\frac{1}{2}} , \quad (3.135)$$

and

$$\langle 0 | : \bar{\psi} \psi : | 0 \rangle = -\frac{N}{(12\pi)^{\frac{1}{2}}} g_N . \quad (3.136)$$

This is very curious. By the nature of the light-cone formalism, no non-trivial vacuum behavior is permitted with any non-zero quark mass. Nevertheless, formal arguments in the large- N limit which depend only on the nature of the pseudoscalar meson wavefunction at small x yield a non-zero (in fact, infinite for $N \rightarrow \infty$) value for $\langle \bar{\psi} \psi \rangle$ as m vanishes.^[47]

This seems to directly conflict with Coleman's theorem^[7] that Goldstone bosons cannot exist in two dimensions, due to the severe infrared divergences from the ill-defined delta function $\delta(k^2) = \delta(k^+k^-)$ associated with massless scalars. An allowed exception in Ref. [7] is one which decouples, such as a scalar constructed from a pair of non-interacting massless fermions.

The scalar $\bar{\psi} \psi$, for example, does have zero probability to create such a pair; that is (ignoring color)

$$\langle 0 | \bar{\psi} \psi(z) b_{(1-x)p^+}^\dagger d_{xp^+}^\dagger | 0 \rangle = m e^{-ip \cdot z} \left[\left(\frac{x}{1-x} \right)^{\frac{1}{2}} - \left(\frac{1-x}{x} \right)^{\frac{1}{2}} \right] , \quad (3.137)$$

which vanishes as $m \rightarrow 0$. However, the large- N pseudoscalar does not decouple in this manner, as evidenced by Eq. (3.132) (with $c = 1$). On the other hand, the operators which create this pion have been shown to satisfy free commutation

relations, and they commute with the operators in the Hamiltonian. Finally, in at least one case where a term which couples to these operators is added to P_I by introducing an extra $U(1)$ interaction, these pions acquire a mass, $g/(2\pi)^{1/2}$, obviating this dilemma.

As a final curiosity which illustrates the importance of the order of limits, note that for $U(N)$, the $U(1)$ chiral anomaly produces an additional contribution of $g^2/(8\pi m)$ for $\langle\bar{\psi}\psi\rangle$. In the large- N limit this vanishes, while for finite N , it diverges as $m \rightarrow 0$.

For finite values of N , the situation is somewhat clearer. When $m \rightarrow 0$, the lightest baryon mass also vanishes. Also, acting on existing states with the operator V_k^0 , which creates the massless pseudoscalar meson, can flip parity without altering mass if k is zero. As a result, parity doublets are trivial to generate. These would seem to indicate that chiral symmetry is restored as the quark mass vanishes.

Furthermore, bosonization results imply that the asymptotic coefficients c which appears in, for example Eqs. (3.132) and (3.133), vanish slowly with quark mass as $(m/g)^\delta$, with $\delta = 1/[2(2N - 1)]$. Numerical results have been presented which indicate that this is likely the case. As a consequence, even though the meson mass still vanishes, it vanishes proportionally with $m^{1+\delta}$ rather than m . If this is correct, operators such as $\bar{\psi}\gamma^5\psi$ do indeed have zero probability of creating a massless meson from the vacuum, although the probability vanishes extremely slowly in m for any sizable N .

CONCLUSIONS

In this work, QCD in 1+1 dimensions was quantized on the light-cone, and the role of boundary terms clarified. By imposing antiperiodic boundary conditions in x^- , a discretized Hamiltonian was constructed and diagonalized for several numbers of color N and one quark flavor. At relatively little cost in computer time, the full spectra and wavefunctions were produced, and these were in agreement with results from other calculations when available. Finally, the nature of solutions in the limits of both strong and weak coupling was discussed.

Even in two dimensions, there is still a great deal that might be done to extend these results. By studying systems with higher baryon number, the nuclear potential that results from the linear interquark potential could be determined. Form factors for baryons and higher-Fock states could be computed and counting rules at large momentum transfer derived. Finally, the inclusion of several flavors would bring the model closer to reality. It would allow for a more general study of chiral symmetry and for the calculation of such things as the strangeness content of the proton, at least in two dimensions.

Of course, physics is conducted in (at least) four dimensions, where this numerical quantization scheme may or may not provide a successful approach to QCD . It was, however, the way to solve it in two dimensions, and there is as yet no reason to be discouraged.

APPENDIX A

MATRIX ELEMENTS AND COLOR CONTRACTIONS

A typical matrix element of creation and annihilation operators which must be computed both for normalization and for evaluating the Hamiltonian is (for $N = 3$)

$$\epsilon_{c_1 c_2 c_3} \epsilon^{a_1 a_2 a_3} \delta_{c_4}^{c_5} \delta_{a_5}^{a_4} f(k, \ell) \times \quad (A.1)$$

$$\langle 0 | b_{\ell_1, a_1} b_{\ell_2, a_2} b_{\ell_3, a_3} b_{\ell_4, a_4} d_{\ell_5}^{a_5} d_{k_5, c_5}^\dagger b_{k_4}^{\dagger c_4} b_{k_3}^{\dagger c_3} b_{k_2}^{\dagger c_2} b_{k_1}^{\dagger c_1} | 0 \rangle,$$

where c_i and a_i are color indices, k_i and ℓ_i are momenta, with f some function of these such as the photon propagator. Baryonic and mesonic singlets are formed by contraction of color indices with epsilon and delta tensors. In all matrix elements color indices will be completely contracted, since the Hamiltonian as well as the Fock space are color singlets. A small amount of reflection indicates (and many minutes of wasted CPU confirm) that it would be advantageous to compute the contribution from contracting color indices diagrammatically rather than iteratively, especially for large N . That is, to follow the flow of color through the epsilon and delta tensors, count closed loops, and assign factors of N rather than assign specific numbers to color indices and then sum.

The operators which carry color indices also depend on momentum. Before computing color factors, particular values for momenta are assigned, and the vacuum expectation of these operators converted into products of delta functions in color. In this appendix, the algorithm used by the program to evaluate general matrix elements and color sums is presented.

A.1. A SIMPLE ALGORITHM FOR THE EVALUATION OF CREATION AND ANNIHILATION MATRIX ELEMENTS

Matrix elements such as

$$\langle 0 | b_{i_{10}} b_{i_9} b^{\dagger i_8} b_{i_7} b_{i_6} b^{\dagger i_5} b_{i_4} b^{\dagger i_3} b^{\dagger i_2} b^{\dagger i_1} | 0 \rangle, \quad (\text{A.2})$$

where i_1 to i_{10} may incorporate a set of indices such as color, momentum, or spin, may be computed using Wick's theorem. A recipe which is more efficient and compact for both mechanical and human computers takes advantage of the symmetries due to the anticommutation of the operators to generate all the possible contractions with appropriate signs from one initial product of delta functions. To compute an element such as Eq. (A.2):

Construction of Initial Term

Proceeding from right to left, skip creation operators and stop at the first annihilation operator. Pair this with the creation operator to its immediate right to form a delta ($\delta_{i_4}^{i_3}$ in this case) and remove these from the matrix element. Continue left, pairing and removing operators until only the product

$$\delta_{i_4}^{i_3} \delta_{i_6}^{i_5} \delta_{i_7}^{i_2} \delta_{i_9}^{i_8} \delta_{i_{10}}^{i_1} \quad (\text{A.3})$$

remains. The overall sign of this term is positive since no operators were permuted.

Construction of Permutation Operators

Beginning again with the matrix element Eq. (A.2), proceed left until hitting the first annihilation operator. The first permutation operator

$$1 - P_{3,2} - P_{3,1} , \quad (\text{A.4})$$

which will permute indices in Eq. (A.3), is built by subtracting from $\mathbf{1}$ operators which independently swap the index of the creation operator to the immediate right of the current annihilation operator with each subsequent creation operator index to its right. Remove from Eq. (A.2) this annihilation operator and the creation operator to its immediate right and proceed left to the next annihilation operator, repeating the procedure. The next permutation is

$$1 - P_{5,2} - P_{5,1} .$$

This second operator is placed to the right of operator Eq. (A.4). Continue left until all annihilation operators are exhausted. The final result is

$$[1 - P_{3,2} - P_{3,1}][1 - P_{5,2} - P_{5,1}][1 - P_{2,1}][1 - P_{8,1}] , \quad (\text{A.5})$$

which then acts upon the indices of the initial term Eq. (A.3), giving the 36 terms with appropriate signs:

$$\begin{aligned} & + \delta_{i_4}^{i_3} \delta_{i_6}^{i_5} \delta_{i_7}^{i_2} \delta_{i_9}^{i_8} \delta_{i_{10}}^{i_1} - \delta_{i_4}^{i_3} \delta_{i_6}^{i_5} \delta_{i_7}^{i_2} \delta_{i_9}^{i_1} \delta_{i_{10}}^{i_8} \\ & - \delta_{i_4}^{i_3} \delta_{i_6}^{i_5} \delta_{i_7}^{i_1} \delta_{i_9}^{i_8} \delta_{i_{10}}^{i_2} + \delta_{i_4}^{i_3} \delta_{i_6}^{i_5} \delta_{i_7}^{i_1} \delta_{i_9}^{i_2} \delta_{i_{10}}^{i_8} \\ & + \dots \end{aligned} \quad (\text{A.6})$$

One of the advantages of this procedure is that all the information is contained

compactly in the operator Eq. (A.5) acting on Eq. (A.3) with the symmetries manifest. In cases, for example, when operators are contracted into epsilon tensors, many of the permutations are clearly redundant and may be converted into numerical factors.

Finally, matrix elements in general will include creation operators and annihilation operators which cannot be contracted with one another, as for example, antiquark versus quark, or operators where some types of indices such as flavor are fixed and different. In these cases, an overall sign is computed by determining the operator interchanges needed to construct an initial term such as in Eq. (A.3).

A.2. COLOR SUMS

The vacuum expectation value of creation and annihilation operators has been converted into a sum of products of kronicker deltas in color indices. In each term these deltas are entirely contracted with the delta and epsilon tensors used to form the color singlet Fock states, and the deltas which appear contracted with the operators in the Hamiltonian, of the form $\delta_{c_2}^{c_1} \delta_{c_4}^{c_3} - (1/N)\delta_{c_4}^{c_1} \delta_{c_2}^{c_3}$ in H_I , and $\delta_{c_2}^{c_1}$ in H_0 .

Computing the color factor has now been reduced to contracting a product of an arbitrary number of epsilon and delta tensors. For the case with only deltas, it is necessary only to associate a factor of N with each closed color loop. Loops are formed by products of deltas such as $\delta_{c_3}^{c_1} \delta_{c_1}^{c_2} \delta_{c_2}^{c_3}$.

This is implemented in the program by constructing a vector $V(n)$ where each

$\delta_{c_m}^{c_n}$ is represented by an m in the n^{th} location. A closed loop is traced by moving from location n to $V(n) = m$ and so on until finally returning to n .

For contractions which include epsilons, any deltas present are first traced through and eliminated. The fully contracted products of epsilons which remain are then converted into a sum of products of deltas by the identity (for N colors)

$$\epsilon_{c_1 c_2 \dots c_N} \epsilon^{c_1 b_2 \dots b_N} = \delta_{c_2}^{b_2} \delta_{c_3}^{b_3} \dots \delta_{c_N}^{b_N} - \delta_{c_2}^{b_3} \delta_{c_3}^{b_2} \dots \delta_{c_N}^{b_N} + \dots \quad (\text{A.7})$$

where the ellipses include permutations of the b_i with appropriate signs. The resulting deltas are then contracted as before. For a general discussion on computing color factors diagrammatically, see Ref. [48].

APPENDIX B

EVALUATION OF INTEGRAL IN SECTION 3.3

This appendix presents a calculation of the integral

$$\int_{-1}^{\infty} du \frac{(1+u)^a - 1}{u^2} \quad (\text{B.1})$$

which appears in Eq. (3.21).

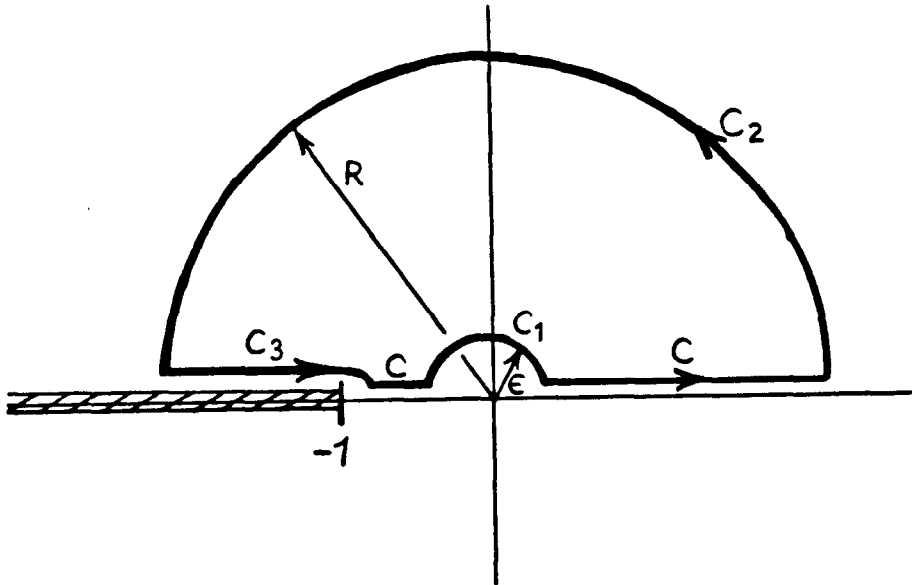


Figure 32. Integration Contour.

Consider the closed contour of Fig. (32). As no poles are enclosed, the integral along contours C_1 , C_2 and C_3 plus the desired integral along C sum to zero. The leading contribution from C_2 is proportional to $(1/R)^{1-a}$, which vanishes for $a \in (0, 1)$. From C_1 , $-ia\pi$ survives when ϵ is taken to zero. Finally, the integral

along C_3 is

$$\int_{C_3} du \frac{(1+u)^a - 1}{u^2} = \int_0^\infty dt \frac{t^a e^{ia\pi} - 1}{(1+t)^2} . \quad (\text{B.2})$$

The second term in the integrand contributes -1 , while, by defining $s = 1/(1+t)$, the first term may be rewritten as

$$e^{ia\pi} \int_0^1 ds s^{-a} (1-s)^a . \quad (\text{B.3})$$

By the Γ function relations^[49]

$$\int_0^1 dx x^\alpha (1-x)^\beta = \frac{\Gamma(1+\alpha)\Gamma(1+\beta)}{\Gamma(2+\alpha+\beta)} \quad (\text{B.4})$$

and

$$\Gamma(z)\Gamma(1-z) = \pi \csc(\pi z) , \quad (\text{B.5})$$

the total for contour C_3 is

$$-[1 + e^{ia\pi} a\pi \csc(a\pi)] . \quad (\text{B.6})$$

Next, the same analysis is applied to the closed contour which reflects the contour in Fig. (32) across the real axis. Adding the two, the contribution from C_1 is cancelled, the reflection of C_3 gives

$$-[1 - e^{-ia\pi} a\pi \csc(a\pi)] , \quad (\text{B.7})$$

and the final result by Cauchy's theorem is

$$\int_{-1}^{\infty} du \frac{(1+u)^a - 1}{u^2} = 1 - a\pi \cot(a\pi) . \quad (\text{B.8})$$

REFERENCES

1. This introduction is based on material appearing in Hornbostel, K., Brodsky, S. J., and Pauli, H. C., *Proceedings of the Ohio State Workshop on Relativistic Many-Body Physics*, World Scientific, 1988.
2. Pauli, H. C., and Brodsky, S. J., Phys. Rev. **D32**, 1993 (1985); **D32**, 2001 (1985).
3. For an introduction to light-cone quantization, cf. Yan, T.-M., Phys. Rev. **D7**, 1780 (1972) and references therein.
4. Weinberg, S., Phys. Rev. **150**, 1313 (1966).
5. This is not strictly true if there are quanta for which p^+ is zero. See for example Harindranath, A., and Vary, J., Phys. Rev. **D37**, 3010 (1988). There are other subtleties which will be addressed in future work.
6. Pauli, H. C., and Brodsky, S. J., Phys. Rev. **D32**, 1993; **D32**, 2001 (1988).
7. Coleman, S., Comm. Math. Phys., **31**, 259 (1973).
8. Bassetto, A., Lazzizzera, I., Soldati, R., Nucl. Phys. **B236**, 319 (1984).
9. Halpern, M. B., and Senjanovic, P., Phys. Rev. **D15**, 3629 (1977).
10. Bars, I., and Green, M. B., Phys. Rev. **D17**, 537 (1978).
11. McCartor, G., Mission Research Corp. Preprint, 1988, and private communications.
12. Mathews, J., and Walker, R. L., *Mathematical Methods of Physics*, Benjamin/Cummings, N.Y., 1970.

13. Rohrlich, F., *Acta Phys. Austr.* **32**, 87 (1970).
14. Steinhardt, P., *Ann. Phys.*, **128**, 425 (1980).
15. I would like to thank A. Tang for discussions on this point.
16. Kogut, J., and Susskind, L., *Phys. Rev.* **D10**, 3468 (1974).
17. Coleman, S., Jackiw, R., and Susskind, L., *Ann. Phys. (N.Y.)* **93**, 267 (1975);
Coleman, S., *Ann. Phys. (N.Y.)* **101**, 239 (1976).
18. Einhorn, M. B., *Phys. Rev.* **D14**, 3451 (1976).
19. See Ref. [41], and also the comment by Coleman referenced in Ref. [10]. In discussions involving $U(N)$ which follow, the effect of this background field will be ignored.
20. Eller, T., Pauli, H. C., and Brodsky, S. J., *Phys. Rev.* **D35**, 1493 (1987).
The notation of this paper will be followed as much as possible in this section.
21. 't Hooft, G., *Nucl. Phys.* **B75**, 461 (1974).
22. Callan, C. G., Coote, N., and Gross, D. J., *Phys. Rev.* **D13**, 1649 (1976).
23. Bergknoff, H., *Nucl. Phys.* **B122**, 215 (1977).
24. For an excellent review of wavefunctions in QCD, including a discussion of normalizations, cf. Lepage, G. P., Brodsky, S. J., Huang, T., and Mackenzie, P. B., CLNS-82/522, published in Banff Summer Institute 81 (1981); also, Lepage, G. P., Brodsky, S. J., *Phys. Rev.* **D22**, 2157 (1980).
25. Bardeen, W. A., and Zumino, B., *Nucl. Phys.* **B244**, 421 (1984).
26. See for example, Goddard, P. and Olive, D., *Int. J. Mod. Phys.* **A1**, 303 (1986).

27. Press, W. H., Flannery, B. P., Teukolsky, S. A., Vetterling, W. T., *Numerical Recipes*, Cambridge Univ. Press, Cambridge, 1986.
28. Hamer, C. J., Nucl. Phys. **B195**, 503 (1982).
29. Witten, E., Nucl. Phys. **B160**, 57 (1979).
30. Coleman, S., in *Pointlike Structures Inside and Outside Hadrons*, Proceedings of the 1979 Intl. School of Subnuclear Physics, A. Zichichi, ed. Plenum Press, N.Y., 1982.
31. Blankenbecler, R., private communication.
32. Eller, T., thesis; unpublished.
33. Durgut, M., Nucl. Phys. **B116**, 233 (1976).
34. Bars, I., Nucl. Phys. **B111**, 413 (1976).
35. Webber, B. R., Nucl. Phys. **B153**, 455 (1979).
36. Ref. [21]; see also, 't Hooft, G., in *New Phenomena in Subnuclear Physics*, Proceedings of the 1975 Intl. School of Subnuclear Physics, A. Zichichi, ed. Plenum Press, N.Y., 1977.
37. Hamer, C. J., Nucl. Phys. **B121**, 159 (1977); **B132**, 542 (1978).
38. The massless state obtained by acting once on the vacuum with V_k^a has been discussed in
Buchmuller, W., Love, S. T., and Peccei, R. D., Phys. Lett. **108B**, 426
(1982).
39. Frishman, Y., Nucl. Phys. **B148**, 74 (1979).

40. This is the group considered by 't Hooft in Ref. [21]; the two are equivalent in the large- N limit. In general the extra $U(1)$ introduced need not be associated with the same coupling constant as $SU(N)$, but this is sufficient for this discussion
41. Coleman, S., Jackiw, R., and Susskind, L., *Ann. Phys. (N.Y.)* **93**, 267 (1975); Coleman, S., *Ann. Phys. (N.Y.)* **101**, 239 (1976).
42. Witten, E., *Comm. Math. Phys.* **92**, 455 (1984).
43. Zhitnitskii, A. P., *Sov. J. Nucl. Phys.* **43**, 999 (1986).
44. Steinhardt, P., *Nucl. Phys.* **B176**, 100 (1980).
45. Date, G. D., Frishman, Y., and Sonnenschein, J., *Nucl. Phys.* **B283**, 365 (1987), and Sonnenschein, J., private communication.
46. Amati, D., and Rabinovici, E. *Phys. Lett.* **101B**, 407 (1981).
47. A lattice calculation of this chiral condensate in this model is presented in Grandou, T., Cho, H. T., and Fried, H. M., *Phys. Rev.* **D37**, 946 (1988).
48. Cvitanovic, P., *Group Theory*, Nordita Notes, 1984; Cvitanovic, P., *Phys. Rev.* **D14**, 1536, (1976).
49. Abramowitz, M., and Stegun, I. A., *Handbook of Mathematical Functions*, Dover Publications, N.Y., 1972.